Distribution Agreement

In presenting this thesis or dissertation as a partial fulfilment of the requirements for an advanced degree from Emory University, I hereby grant to Emory University and its agents the non-exclusive license to archive, make accessible, and display my thesis or dissertation in whole or in part in all forms of media, now or hereafter known, including display on the world wide web. I understand that I may select some access restrictions as part of the online submission of this thesis or dissertation. I retain all ownership rights to the copyright of the thesis or dissertation. I also retain the right to use in future works (such as articles or books) all or part of this thesis or dissertation.

Signature: _____ _____

Jasmine Miller-Kleinhenz Date

Receptor Targeted Theranostic Nanoparticles for Treatment of Drug-Resistant Triple-negative breast cancer

By

Jasmine M. Miller-Kleinhenz
Doctor of Philosophy

Graduate Division of Biological and Biomedical Science
Cancer Biology

_____

Lily Yang, M.D., Ph.D.
Advisor

_____

Haian Fu, Ph.D.
Committee Member

_____

Larry Boise, Ph.D.
Committee Member

_____

Carlos Moreno, Ph.D.
Committee Member

_____

Jack Arbiser, M.D., Ph.D.
Committee Member

Accepted:

_____

Lisa A. Tedesco, Ph.D.
Dean of the James T. Laney School of Graduate Studies

Receptor Targeted Theranostic Nanoparticles for Treatment of Drug-Resistant Triple-negative breast cancer

By

Jasmine M. Miller-Kleinhenz
B.S., M.S., University of North Carolina at Chapel Hill, 2010

Advisor: Lily Yang, M.D., Ph.D.

An abstract of
A dissertation submitted to the Faculty of the
James T. Laney School of Graduate Studies of Emory University
in partial fulfillment of the requirements for the degree of
Doctor of Philosophy
in
Graduate Division of Biological and Biomedical Sciences
Cancer Biology
2017

Abstract

Receptor Targeted Theranostic Nanoparticles for Treatment of Drug-Resistant Triple-negative breast cancer

By Jasmine M. Miller-Kleinhenz

Breast cancer is the most common cancer in women world-wide. About 20% of women with breast cancer are negative for estrogen receptor, progesterone receptor, and HER-2/neu receptor and are diagnosed with triple negative breast cancer (TNBC). TNBC occurs more frequently in young women and African-Americans and presents as an aggressive disease with a poor prognosis. Since those with TNBC do not express the receptors and pathways for which targeted therapies have been developed, the only therapeutic options are chemotherapy and surgery. Unfortunately, the majority of women with TNBC are resistant to chemotherapeutic treatment. Given the poor survival and lack of effective therapeutics for TNBC, the development of new therapeutic approaches for patients with drug-resistant TNBC is essential**.**

Drug resistance in TNBC has been associated with the presence of a high level of cancer stem-like cells (CSCs). This dissertation, through investigation of the heterogeneity of response to chemotherapy drug, Doxorubicin (Dox) or uPAR-targeted nanoparticle carrying Dox in a human patient derived xenograft (PDX) models of TNBC, identified the Wnt/β-catenin CSC pathway as being overexpressed in drug-resistant tumors compared to tumors that were sensitive to treatment. Based on the overexpression of Wnt co-receptor LRP5/6, we developed a novel Wnt-targeted therapy to effectively treat drug resistant TNBC.

Our results demonstrate that dual targeting of the Wnt and uPAR leads to decreasing of Wnt/β-catenin signaling, inhibition of the CSC phenotype, and epithelial to mesenchymal transition (EMT) *in vitro*. Systemic delivery of our dual targeted nanoparticles led to nanoparticle-drug delivery into PDX tumors, resulting in stronger tumor growth inhibition compared to non-targeted or single-targeted nanoparticle carrying Dox in a human breast cancer PDX model *in vivo*.

Altogether, this work confirms the relationship of the Wnt/β-catenin pathway to drug-resistance in TNBC. Our results provide a foundation for the long-term goal of developing targeted therapies for drug-resistant TNBC. Enhanced delivery of chemotherapeutics into breast cancer stem-like cells using dual Wnt receptor and uPAR-targeted theranostic nanoparticles will significantly impact development of novel therapy for drug-resistant TNBC tumors and thereby improve prognoses for TNBC patients.

Receptor Targeted Theranostic Nanoparticles for Treatment of Drug-Resistant Triple-negative breast cancer

By

Jasmine M. Miller-Kleinhenz
B.S., M.S., University of North Carolina at Chapel Hill, 2010

Advisor: Lily Yang, M.D., Ph.D.

A dissertation submitted to the Faculty of the
James T. Laney School of Graduate Studies of Emory University
in partial fulfillment of the requirements for the degree of
Doctor of Philosophy
in
Graduate Division of Biological and Biomedical Sciences
Cancer Biology
2017

Acknowledgements

I would like to thank all of my family, friends, community, and co-workers who have supported me during the course of my education which has lead me towards the path of earning my PhD degree. I have a deeper understanding of the phrase 'It takes a village' and I am grateful that I have such a loving, nurturing, and encouraging "village' to support me.

Thank you to my advisor, Lily Yang, who has always been very encouraging and supportive of any initiative I have taken both within and outside of the lab. Your interest in my development as a scientist, scholar, and as a human-being has had profound impact on the person I am today. I thank my dissertation committee members, Carlos Moreno, Haian Fu, Jack Arbiser, and Larry Boise for their expertise and guidance throughout the years. I thank my lab members Erica Bozeman, Hongyu Zhou, Wei Chen, Zhiyang Zhou, Ning Gao, Xiangxue Guo, Lei Zhu, Tongrui Liu, Weiping Qian, Christina Ward, Claudia Baumann, and Raheel Jajja. Thank you for making lab an environment of scientific inquiry and of joy.

I thank everyone at Emory who has supported me during this journey including individuals within the graduate program, the administration, and fellow graduate students. These last six years have been made better by knowing that I was surrounded by so many people who wanted to see me succeed and were always willing to lend a helping hand, a listening ear, and their friendship.

Lastly, I thank God for loving network of family, friends, and community I have in my life. To my sister and first friend, Tenea, who has paved the way for me in the sciences and has inspired me in more ways than I can count. Thank you to my dearest husband, Nabil, who has been my partner through this entire journey and whose warmth, thoughtfulness, and encouragement has been a needed constant in my life. To my son, Badi, who has made the last year of my dissertation work so much sweeter. I am eternally thankful to my parents, Curtis and TeAndra, who have always encouraged me to strive academically even when others did not. Finally, I thank my grandmother, Delores Martin, who is a triple-negative breast cancer survivor and is the reason I pursued a PhD in Cancer Biology. Her fortitude, love, and elegance are awe-inspiring.

Table of Contents

List of Figures

List of Tables

Chapter 1: Introduction

This chapter is adapted from a review submitted by J Miller-Kleinhenz JM, EN Bozeman, and L Yang. *Targeted Nanoparticles for Image-guided Treatment of Triple Negative Breast Cancer: Clinical Significance and Technological Advances.* Accepted to WIREs Nanomedicine and Nanobiotechnology, 2015.

1.1 Introduction

Despite extensive research and clinical strides being made, about 40,000 women in the U.S. alone are expected to die annually of breast cancer [1]. While mortality rates have decreased by 14% since 2008, the incidence of breast cancer worldwide has increased by more than 20% with nearly 1.5 million new cases each year [2,3]. Molecular analysis of breast cancer tissues revealed the presence of four breast cancer subtypes, including hormone receptor (estrogen (ER) and progesterone (PR)) positive, human epidermal growth factor receptor 2 (HER-2) positive, triple negative (ER, PR and HER-2 negative), and normal breast [4–6]. At present, targeted therapies for hormone and HER-2 receptor positive cancers, such as the estrogen receptor antagonist (Tamoxifen) and anti-HER-2 antibodies (Trastuzumab and Pertuzumab), have been used in the clinic for breast cancer treatment [7,8]. However, for triple negative breast cancer (TNBC) there are no such targeted treatments currently available, highlighting not only the disparity in therapeutic options for these patients, but also demonstrating an urgent clinical need towards the development of more personalized therapeutics.

TNBC, which accounts for 15-20% of all breast cancer cases, is among the most aggressive forms of breast cancer and is diagnosed more frequently in young African-American and Hispanic women [9,10], and those with BRCA-1 mutations [11]. TNBC is diagnosed based on the absence of the ER and PR receptors and the lack of HER-2 overexpression of biopsied tumor samples by immunohistochemical (IHC) and fluorescence *in situ* hybridization (FISH) analyses. Due to its highly aggressive biology, the standard methods of detection, mammograms, magnetic resonance imaging (MRI) and ultrasound, typically

detect TNBCs at later stages with large tumor lesions (>2.5 cm) and locally advanced disease [12].

1.2 Current Treatment for TNBC

Current treatment options for TNBC remain limited to chemotherapy, surgery, and radiotherapy [13]. In order to reduce large tumor burden, thus mediating complete surgical resection of the tumor, and to treat potentially disseminated tumor cells in distant organs, TNBC patients usually receive preoperative neoadjuvant chemotherapy, typically consisting of taxanes, anthracyclines, and cyclophosphamide [14]. However, over 30% of those TNBC patients develop local and distant recurrent tumors in visceral sites including the lungs, liver and brain and have a worse survival rate compared to non-TNBC, particularly within the first 5 years of diagnosis [15–17]. While TNBC patients have a poorer distant metastasis-free rate (67%) compared with non-TNBC patients (82%) during the first 5 years post diagnosis [18], the risk for recurrence after five years is decreased in TNBC patients compared with non-TNBC patients [15].

While generally successful at reducing the size of primary TNBC tumors, neoadjuvant chemotherapy provides an opportunity to determine the chemosensitivity of the tumors, which serves not only as a potential guide for future treatment of recurrent tumors but may also provide insight into overall survival benefit[16]. Results of clinical studies showed that TNBC patients have differential responses to chemotherapeutics and a population of TNBC patients (20 to 30%) tends to have increased pathological complete responses (pCR) relative to non-TNBC patients following neoadjuvant therapy and a better overall survival

[16]. Following neoadjuvant chemotherapy, TNBC patients with a pCR typically have a decrease in tumor recurrence and an increase in overall survival compared patients without a pCR [19]. Unfortunately, ~60% of TNBC patients have tumors highly resistant to chemotherapy.

Recent clinical trials have been conducted to determine whether adding additional agents, such as platinum based carboplatin or anti-angiogenesis inhibitor bevacizumab, would assist in increasing a pathological complete response (pCR) in TNBC patients [20,21]. Previous studies have shown that TNBC patients with BRCA1 mutations are sensitive to platinum agents and relatively less sensitive to taxanes [22,23]. Results indicated that adding either agent or the combination of agents to the standard chemotherapy regimen increased pCR compared to patients with just the standard chemotherapy, resulting in a decrease in recurrence and an increase in overall survival [20].

There is also interest in investigating the use of immunotherapy in TNBC, especially TNBCs with a more immunomodulatory phenotype. A recent Phase Ib trial was conducted using the anti-programmed cell death protein-1 (PD-1) agent pembrolizumab in TNBC patients. The results showed that around 58% of the patients expressed PDL-1 and there was a response rate of close to 20% [24]. Another Phase II trial using the androgen receptor (AR) inhibitor, enzalutamide, has been conducted in AR positive TNBCs, which has shown promising benefits in patients with high expression of AR [25]. These results are encouraging that there may be an expansion in treatment options that can increase overall pCR in TNBC patients.

1.3 TNBC Subtypes and Biomarkers for Characterization

Currently, there is no predictive biomarker to distinguish between the patients who will have good therapeutic responses and those patients who will not benefit from neoadjuvant therapy. The presence of large, drug-resistant residual tumors after neoadjuvant therapy has been associated with higher tumor recurrence and poorer survival [16]. Histological analysis of tumors of chemo-resistant patients revealed that a high level of drug resistant tumor cells express breast cancer stem-like cell biomarkers, $CD44^{hi}/CD24^{lo}$ [26]. Overall, TNBC patients who fail to achieve a pCR following neoadjuvant therapy have a worse prognosis compared to the patients with pCR [16,27]. Therefore, the development of novel approaches to address timely monitoring of therapeutic responses and effective treatment of drug resistant tumor cells should have significant impact on the improvement of survival of TNBC patients.

The biology of TNBC and the clinical responses observed among TNBC patients is further complicated by the high degree of intratumoral (heterogeneity within a tumor) and intertumoral (heterogeneity between given tumors) heterogeneity. While the majority of TNBC has a molecular gene signature associated with the basal-like subtype of breast cancer (BLBC), the remaining 20-30% of TNBCs are classified as other subtypes [28]. Lehmann *et al* [29] identified seven subtypes of TNBC based on global gene expression analysis: basal 1 (BL1), basal 2 (BL2), immunomodulatory (IM), luminal androgen receptor (LAR), mesenchymal (M), mesenchymal stem cell (MSL) and unstable (UNS). Each subtype has distinct characteristics which not only make them more sensitive to

specific classes of drugs and inhibitors (**Table 1.1**) but is being found to serve as potential predictors of clinical responses following current therapy.

Table 1.1. TNBC subtypes and treatment responsiveness [29]

	Subtype	Characteristics	Treatment Sensitivity	Cell line derivative
Basal-like	Basal-like 1 (BL1)	Highly proliferative, DNA damage and cell cycle genes	Cisplatin; taxanes	HCC1806 and MDA-MB-468
	Basal-like 2 (BL2)	Growth factor signaling pathways	----	
	Immunomodulatory (IM)	Immune cell processes and signaling pathways	----	HCC1187 and DU4475
	Luminal androgen receptor (LAR)	Steroid synthesis, androgen/estrogen metabolism	mTOR inhibition; AR agonist bicalutamide	MDA-MB-453, SUM185PE, HCC2185, CAL-148, and MFM-223
	Mesenchymal (M)	Cell motility and differentiation pathways	PI3K/mTOR inhibitor (NVP-BEZ235)	----
	Mesenchymal-like (MSL)	Cell motility and differentiation pathways; growth factor signaling pathways, low levels of proliferation genes	PI3K/mTOR inhibitor (NVP-BEZ235); Chemoresistant	CAL-51 and SUM159PT

Abbreviations: mTOR: mammalian target of rapamycin, AR: androgen receptor, PI3K: phosphatidylinositol-3-kinase

Retrospective studies are revealing that the differential chemotherapy responses are correlative with the six TNBC subtypes. Masuda *et al* [30] reported that among 130 TNBC patients who had received standard neodjuvant chemotherapy (doxorubicin/ cyclophosphamide/paclitaxel), the BL1 subtype had the highest pCR (52%) whereas LAR and BL2 had the lowest pCR with 10% and 0% respectively. Importantly, their findings

indicated that TNBC subtype is an independent predictor of pCR status. They hypothesize that the differential responses between the BL1 and BL2 subtypes could be due to the enhanced gene signature of EGFR and IGF1-R pathways among the BL2 subtype which could in turn be utilized for the development of targeted therapies.

These classifications further demonstrate the advantages of stratifying/grouping patients based not solely on subtype but also by a defined set of biomarkers. Prat *et al* [31] recently identified that complete pathological responses (pCR) and improved survival after chemotherapy was associated with a proliferation signature or low expression of the luminal A signature among BLBC, not TNBC as a whole **(Table 1.2).** As more knowledge is gleaned about the various subtypes, more appropriate, personally tailored therapies can be developed and evaluated clinically.

The unique differential response to chemotherapy within the TNBC patient population makes it crucial to assess early tumor response to a given chemotherapy so that the patient will receive the most effective chemotherapeutics while avoiding unnecessary toxicity from an ineffective drug. Recent advances in the development of multifunctional nanoparticles with the ability of targeted drug delivery and non-invasive imaging of biomarker expression, drug delivery and tumor responses (theranostic nanoparticles) offer great opportunities for novel, precision nanomedicine protocols to address the clinical challenges observed in TNBC treatment.

The development of targeted theranostic nanoparticles is highly significant for overcoming drug resistance of TNBC by: 1) targeted delivery of large doses of one or multiple drugs

into cancer cells to maximize therapeutic effects while reducing systemic toxicity; 2) receptor targeted nanoparticles that promote intracellular drug delivery and release, and bypass multi-drug resistant protein (p-glycoprotein), located near the cell membrane, mediated efflux of drug molecules [32,33] 3) capability of non-invasive imaging of

Table 1.2: Biomarkers for better characterization of TNBC

Biomarker	Stage	Finding	Reference
Proliferation signature/low luminal A signature	Clinical	Association with better survival among BLBC	Prat et al 2014 [31]
BRCA1 gene	Clinical	BRCA1 loss of function relates to treatment sensitivity	Kennedy et al 2004 [34]
Androgen receptor (AR)	Clinical	AR^+ BC less responsive to NAC	Masuda et al 2013 [30]
CD73	Preclinical	Poor prognosis, increased resistance to anthracyclines	Loi et al 2013 [35]

intratumoral drug delivery and response could allow timely replacement of ineffective drugs to increase the pCR rate and overcome drug resistance; 4) systemic delivery of targeted theranostic nanoparticles that enables targeted therapy of locally disseminated tumor cells and distant tumor metastases, and 5) multimodal imaging ability of theranostic nanoparticles that provides imaging signals for intraoperative image-guided detection and removal of small drug resistant tumors to reduce local tumor recurrence.

Although non-targeted nanoparticles have been used in the clinic for cancer therapy, delivery of those nanoparticles is mediated by the enhanced permeability and retention (EPR) effect, which is primarily dependent on the tumor's leaky vasculature for entry and retention into the tumor bed [36,37]. The EPR effect is often inefficient and provides minimal tumor specificity relative to normal organs. Identification of cell surface targets

that are highly expressed in TNBC tissues should provide means for the development of targeted theranostic nanoparticles for effective treatment of TNBC patients.

1.4 Potential cellular targets for the development of TNBC targeted theranostic nanoparticles

Based on the biology of TNBCs, potential molecular targets are being identified to mediate more efficient drug delivery as well as image-guided treatment. In comparison with other breast cancer subtypes, TNBC has unique pathological characteristics that need to be considered for the development of cancer therapeutics. There are very few cases of TNBC patients diagnosed at the early ductal carcinoma *in situ* stage [38]. The majority of TNBC tumors demonstrate aggressive behavior with high-grade tumour cells and a high percentage of proliferating tumor cells (Ki67 positive cells). The presence of extensive tumor stroma and infiltrating inflammatory cells is a marked pathological feature in TNBC tissues. A clinical study showed that 68% of TNBCs have tumors with over 50% consisting of intra-tumoral stroma and those patients have significantly higher tumor recurrent incidence and shorter survival time compared with the patients without enriched stroma [39]. It is well known that tumor stroma is one of the major barriers for drug delivery, especially for nanoparticle drug carriers. Therefore, it is important to consider the stromal affect when developing effective nanotherapeutics, for both targeted and non-targeted nanoparticles. It is likely that tumor targeting strategies enabling the nanoparticle carriers to efficiently extravasate and migrate through tumor stroma to reach tumor cells should offer promising targeted drug delivery approaches. Nanoparticles targeted to tumor cell surface targets alone can only be delivered into the tumor interstitial space by "leaky" tumor vasculatures mediated by the enhanced permeability and retention (EPR) effect

[40,41]. Lack of mechanisms to overcome tumor stromal barriers will reduce the efficiency of tumor cell targeted nanoparticles to deliver the drug payload into tumor cells. Therefore, strategies that allow for active targeting to the tumor endothelial cell layer, tumor stroma as well as tumor cells should facilitate the drug-nanoparticles crossing the endothelial layer, in addition to the EPR effect of tumor vessels, thus increasing the overall efficiency of nanoparticle delivery into the tumor cells [42]. There are a number of molecules that are currently being investigated for the development of targeted therapies for TNBC based on their roles in tumorigenesis as well as their overexpression among breast cancer subtypes which are summarized in **Table 1.3**. Delivery mechanisms of different receptor targeted nanoparticles are shown in **Figure 1.1**. Although expression of these cellular surface targets is not specific for TNBC, a high level of the receptor expression in TNBC tissues support the development of targeted nanoparticle drug carriers for effective treatment of TNBC.

Table 1.3. Potential cell surface targets for enhanced drug delivery in TNBC

Protein	Cellular distribution	Role in TNBC tumorigenesis
uPAR	Tumor cells, tumor endothelial cells, stromal fibroblasts and macrophages	Motility, invasiveness, angiogenesis.
EGFR	Tumor cells	Cell proliferation, survival, EMT
IGF-1R	Tumor cells, stromal macrophages and fibroblasts	Cell growth, migration, survival
MUC1	Tumor cells	Confers resistance to apoptosis
Folate Receptor	Tumor cells, tumor endothelial cells, stromal cells	Cell proliferation
CXCR4	Invasive tumor cells, tumor endothelial cells, stromal cells	Metastasis, stromal cell infiltration
Wnt receptor	Tumor cells, cancer stem cells (CSCs)	Cell proliferation, survival, differentiation, motility

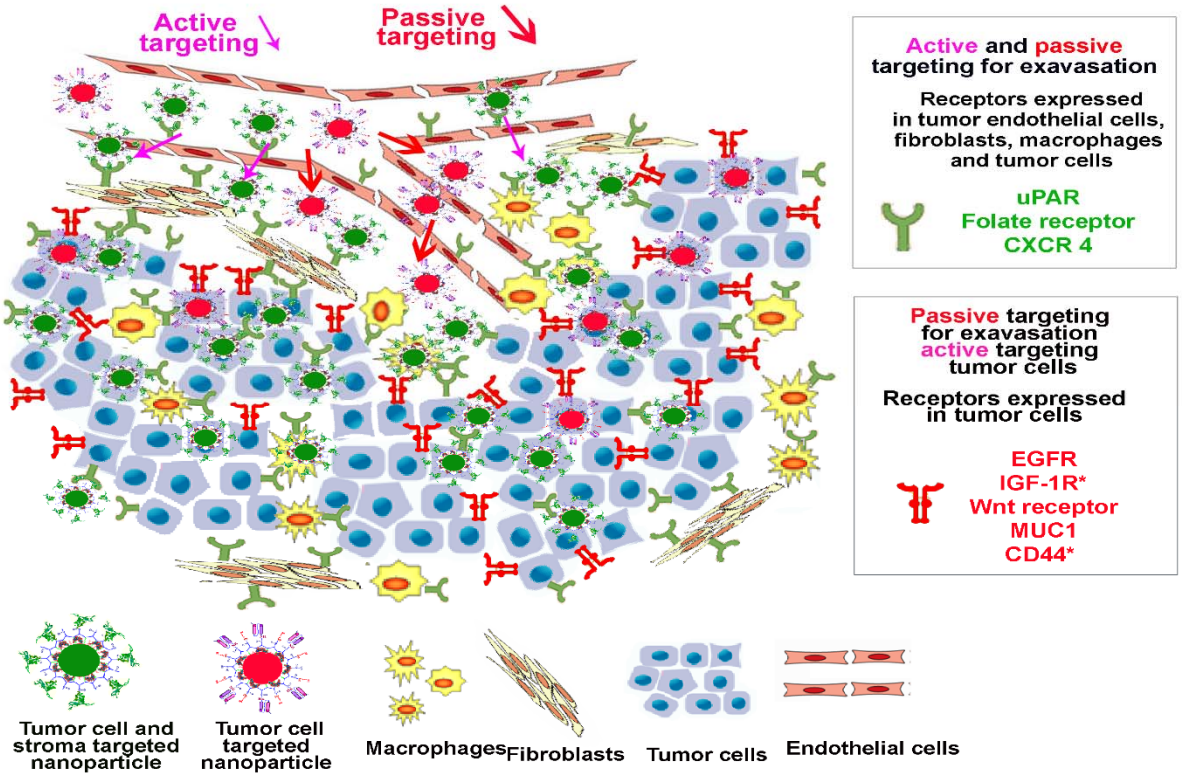

Figure 1.1 Cellular receptor highly expressed in TNBC tissues for the development of targeted theranostic nanoparticles

Cellular receptors upregulated in TNBC tissues have differential levels in tumor cells and stromal cells. uPAR, folate receptor and CXCR4 are expressed in tumor cells, angiogenic endothelial cells, and stromal fibroblasts and macrophages. EGFR, Wnt receptor and MUC1 are found in tumor cells. IGF-1R and CD44 are highly expressed in tumor cells and some stromal cells. Tumor endothelial cell targeted theranostic nanoparticles are delivered into TNBC tissues by both active targeting and passive targeting (or EPR effect). Theranostic nanoparticles targeting to tumor cells alone are delivered by passive targeting into the tumor interstitial space. Receptor targeted theranostic nanoparticles with cellular targets expressed in tumor cells and stromal fibroblasts and macrophages, but lack the expression in tumor endothelial cells, will also be delivered into the tumor interstitial space by passive targeting. The binding of the targeted theranostic nanoparticles to stromal fibroblast, macrophages, and tumor cells enhances retention of the nanoparticles in the tumor. Receptor-mediated internalization of nanoparticle drug carriers increases intratumoral cell drug delivery and therapeutic effect.

1.4.1 Urokinase plasminogen activator receptor (uPAR)

In efforts to more effectively treat TNBC patients, targeting cell types found in the tumor microenvironment that contribute to the aggressive biology of this disease will likely prove most efficacious. uPAR, which plays a critical role in cell growth, motility and invasiveness [43], is overexpressed on the surface of many cellular components found within the tumor microenvironment including angiogenic tumor endothelial cells, stromal fibroblasts, and macrophages [44]. uPAR is detected in stromal macrophages of early breast lesions, which provides the opportunity for targeted delivery of imaging and therapeutic agents into small tumors [44]. The highest level of uPAR is usually found in the invasive edge of tumor cells and extensive tumor associated macrophages and fibroblasts [45]. The level of uPAR has been associated with a poor prognosis among breast cancer patients [46]. Therefore, uPAR targeted nanoparticle-drug delivery makes it possible to treat aggressive and invasive tumor cells as well as the stromal environment that promotes the invasiveness of TNBC tumor cells. Upon ligand binding, uPAR is internalized thus facilitating the uptake of the desired therapeutics. Several groups have developed uPAR or uPA targeted nanoparticle imaging probes or drug carriers for tumor imaging and targeted therapy using TNBC animal tumor models. uPAR targeted, dual optical and MR imaging probes have been shown to target primary and metastatic tumors following systemic delivery in the 4T1 TNBC mouse model and human TNBC tumor xenografts in nude mice [47,48]. Radiolabelled antagonist antibodies targeting uPAR have proven successful in the reduction of TNBC tumor burden [49]. In addition to its attractive cellular distribution, uPAR expression has been shown to be correlative with a drug-

resistant phenotype [50] which is highly prevalent among TNBC patients. LeBeau *et al* recently demonstrated successful targeting and imaging of uPAR by multiple imaging modalities including near-infrared (NIR) and single-photon emission computed tomography (SPECT) among drug-resistant TNBC xenografts [51].

1.4.2 Epidermal growth factor receptor (EGFR)

EGFR is a well-studied cell surface molecule that is overexpressed by TNBCs, which is generally more prevalent among TNBCs compared with non-TNBCs, with up to 50% positivity [52,53]. EGFR overexpression is associated with more aggressive, poorly differentiated tumors and is associated with a poorer clinical prognosis [54]. Phase II clinical trials indicated that EGFR-targeted monoclonal antibody cetuximab with the chemotherapeutic cisplatin extended progression-free survival and overall responses rates among TNBC patients with metastatic disease [55]. However, clinical investigation with small molecule EGFR inhibitor, erlotinib, has been disappointing with only 2 partial responses and no complete responses [56], which could be attributable to the lack of specificity of this class of tyrosine kinases and intrinsic resistance of TNBC cells [54]. However, overexpression of EGFR in TNBC tissues supports the potential development of EGFR targeted nanoparticles, imaging probes, and drug carriers that selectively deliver nanoparticles into EGFR expressing tumor cells to enhance imaging specificity and the effectiveness of cancer therapeutics. One drawback of EGFR targeted delivery of nanoparticles is that it relies on passive targeting to extravasate into the tumor interstitial space. However, due to the high level of expression, at a range of $7e^5$-$1e^6$ on the surface of

each tumor cell [57,58], EGFR is a viable target for nanoparticle delivery of therapeutics into tumor cells by receptor-mediated endocytosis.

1.4.3 Insulin growth factor 1 receptor (IGF-1R)

IGF-1R mediated signaling facilitates tumor cell growth, migration, invasion and survival [59] and is expressed at elevated levels on TNBC tissues relative to normal breast tissues [60] while being highly expressed in all subtypes of breast cancer [61,62]. Results of preclinical studies demonstrated that IGF-1R targeting of TNBC lesions with dual-acting IGF-1R inhibitor BMS-754807 sensitized TNBC xenografts to chemotherapeutic apoptosis [63]. The use of IGF-1 for tumor targeting offers a natural ligand with high binding affinity and low immunogenicity. Due to receptor-mediated endocytosis, IGF-1 conjugated nanoparticles are less likely to deliver a stimulatory signal to IGF-1R expressing tumor cells. Lastly, IGF-1R is also highly expressed in drug-resistant TNBC [64], which further makes IGF-1R an appropriate target for TNBC.

1.4.4 Mucin 1 (MUC1)

The overexpression of the heterodimeric glycoprotein MUC1 is observed in over 90% of breast cancers with 67% of early-stage TNBC showing moderate to strong MUC1 expression [65]. While critical to the survival of normal epithelial cells, MUC1 overexpression protects tumor cells from stress-induced apoptosis [66]. The C-terminal subunit, MUC1-C, interacts and forms complexes with receptor tyrosine kinases such as EGFR and HER-2 and contributes to their activation [67]. Direct targeting of MUC1 using the MUC1 inhibitors GO-201/203 was shown to markedly reduce the tumorigenicity of

MDA-MB-231 [68] and MDA-MB-468 xenograft models of TNBC [69], thus making it an attractive target for nanoparticle-mediated delivery of therapeutic and imaging agents.

1.4.5 Folate receptor

The folate receptor is an ideal and widely used protein for active targeting of drug delivery due to its overexpression by tumor tissues, with 86% of metastatic TNBC patients expressing this protein [70], as well as its limited normal tissue distribution on the apical surface of epithelial cells making it inaccessible to intravenously administered agents [71]. Similar to the before mentioned molecules, its expression is associated with a poor clinical prognosis among TNBC patients [72]. It has been shown that the folate receptor is expressed in inflammatory cells, tumor endothelial cells, and tumor cells and therefore, is a good candidate for the development of targeted therapeutics for TNBC. A number of folate receptor targeted imaging and therapeutic approaches have been developed and tested in pre-clinical and clinical trials [73].

1.4.6 CXCR4

Tumor expression of the chemokine receptor CXCR4 is associated with an aggressive phenotype, is up-regulated on metastatic tumors, and is correlative with a worse clinical outcome [74]. CXCR4 is also expressed at a high level in TNBC tissues [75]. Thus, active targeting of CXCR4 has the potential to enhance delivery of therapeutics to invasive and metastatic TNBC cells. Another appealing feature of targeting CXCR4 for the treatment of stroma-rich TNBC is that the receptor is also found in tumor-associated fibroblasts and macrophages [76]. Active tumor fibroblasts produce the ligand for CXCR4, stromal cell-

derived factor1 (SDF-1), in order to promote tumor cell invasion and angiogenesis [77]. A small molecule CXCR4 antagonist (MSX-122) has been developed and its ability to specifically target primary and metastatic TNBC lesions has been demonstrated *in vitro* and *in vivo* in the MDA-MB-231 tumor xenograft model [78]. Such a small molecule ligand can be used for the development of targeted nanoparticle imaging probes and drug carriers.

1.4.7 Wnt/β-catenin pathway

The Wnt/β-catenin pathway is of interest as a target because it is involved in the regulation of proliferation and migration of tumor cells, the epithelial-mesenchymal transition, and the stemness maintenance of cancer stem cells [79–82]. Upon Wnt ligand binding to co-receptors LRP5/6 and Frizzled, the Wnt/ β-catenin pathway is activated and β-catenin is freed from the APC destruction complex and accumulates in the nucleus where it binds to transcription factors to activate Wnt target gene transcription. In the absence of Wnt ligand binding or blocking of Wnt ligand by a Wnt/β-catenin pathway inhibitor, such as Dickkopf-1 (Dkk1), the Wnt/β-catenin pathway becomes inactive. When the Wnt/β-catenin pathway is inactive, excess cytosolic β-catenin is modified by the APC destruction complex consisting of adenomatous polyposis coli (APC) and Axin, which promotes phosphorylation of β-catenin by casein kinase-1 (CK1) and glycogen synthase kinase 3 (GSK3). Phosphorylated β-catenin is then ubiquitinated and degraded [83] and transcription of Wnt target genes are repressed.

Wnt signaling has been associated with stem cells and cancer stem-like cells. Activation of Wnt signaling enhances breast cancer cell motility and components of this pathway are up-regulated in TNBC [29,84], whereas blockage of the Wnt pathway has been shown to inhibit cellular migration and induce apoptosis in TNBC cells [85]. Wnt signaling has also been associated with TNBC metastatic disease [86] and a lower disease-free survival rate [87]. Cellular receptors for Wnt ligands, such as Frizzled and lipoprotein receptor-related protein (LRP)-5/6, have been shown to mediate endocytosis [88]. Therefore, targeting Wnt receptors for efficient drug delivery into TNBC lesions can potentially enhance therapeutic responses specifically among drug-resistant, cancer stem-like cells.

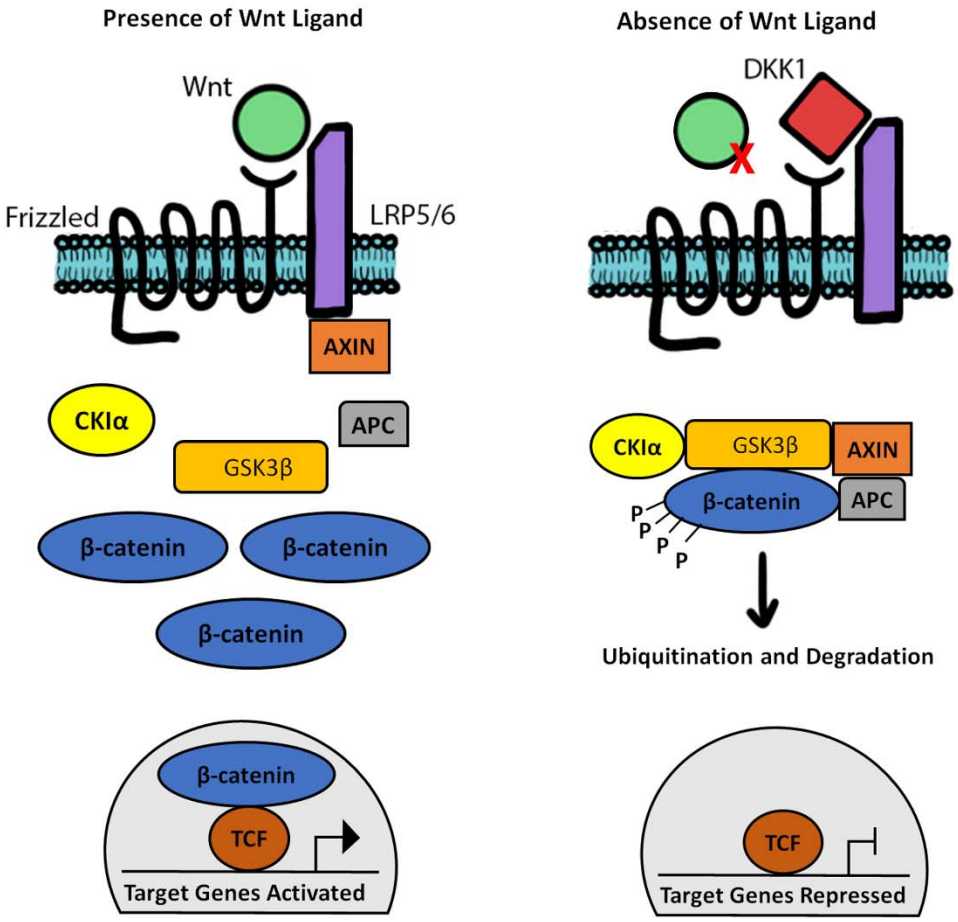

Figure 1. 2: Wnt/β-catenin Signaling Pathway

A. Following Wnt ligand binds to co-receptors LRP5/6 and Frizzled, the Wnt/ β-catenin pathway is activated and β-catenin is freed from the APC/Axin destruction complex and translocates to the nucleus where it activates Wnt-target gene transcription. **B**. When Wnt ligand is absent or blocked by a Wnt/ β-catenin pathway inhibitor like DKK1, β-catenin is phosphorylated by the APC/Axin destruction complex, ubiquitinated, and degraded. This leads to a repression in Wnt target gene transcription.

1.5 Targeting Cancer Stem Cells in TNBC

Cancer progenitor cells or stem-like cells (CSCs) are important cell populations to investigate when determining drug resistance in TNBC [89,90]. In breast cancer, the markers that are used to identify breast cancer stem-like cells are $CD44^{hi}/CD24^{lo}$ [91]. Breast cancer tissues enriched in breast CSCs appear to be more drug resistant and have a poorer prognosis [92]. Likewise, these cells are found in a greater abundance in TNBC tissues relative to non-TNBC and are associated with a poorer prognosis [93]. The adhesion/homing molecule CD44 is the primary surface receptor for hyaluronic acid (HA), a major component found in the extracellular matrix of most tissues but is overexpressed in tumor tissues [94]. HA synthesized by tumor and stromal cells is correlative with CD44 and HA synthase protein expression and is associated with more aggressive tumor behavior and poorer patient outcome [95]. Because of their self-renewal capacity, it is believed that if CSCs are not eliminated during treatment then the CSCs can generate more tumor cells and can cause the patient to relapse (**Figure 1.3**). Also, these recurrent tumors could be resistant to initial treatment and could have a more aggressive phenotype than the original tumor. For these reasons, it will be of critical importance to develop therapies that will also target the CSC population when attempting to overcome drug resistance in TNBC.

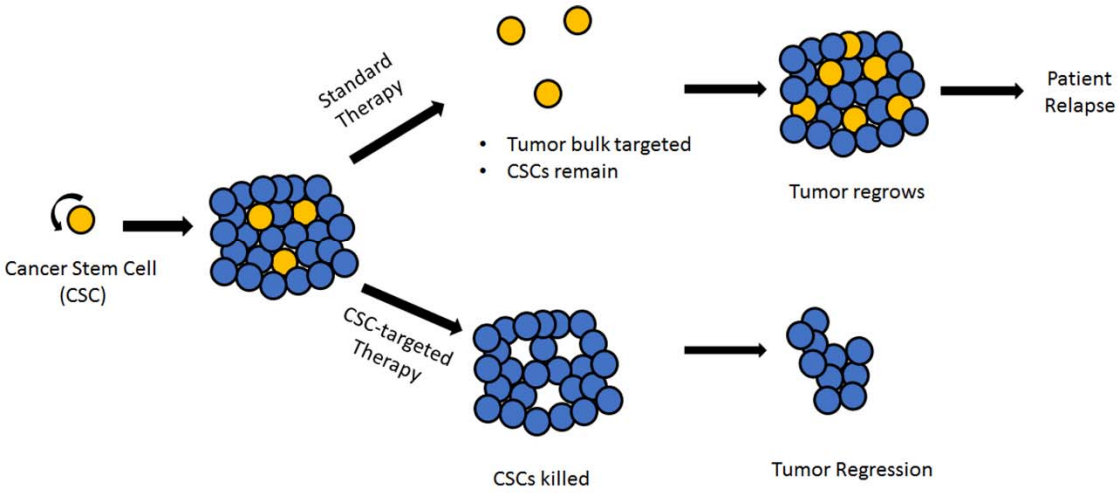

Figure 1.3: Cancer Stem-Cells Following Standard and Cancer-Stem Targeted Therapies

Cancer stem cells are a sub-population of tumor cells with the capacity for self-renewal. The capacity of self-renewal allows for CSCs to recapitulate the heterogeneity of cells within a tumor and maintain the CSC population which non-CSCs are not capable of. Studies have shown that recurrent tumors are enriched with CSCs suggesting that standard therapy are unable to eliminate the CSC population, allowing for the tumor to regrow and the patient to relapse. Efforts are being made to develop CSC-targeted therapy so that CSCs can be eliminated leading to tumor regression and overall better prognosis for patients.

1.6 Current Advances in Cancer Nanotechnology for TNBC

During the last decade, investigators in the nanomedicine field have developed various nanomaterials for the detection and treatment of breast cancer. Nanoparticles, typically between 1-1000 nm in size, can be made up of a variety of materials including lipids, polymers, silica, protein/peptides, oligonucleotides, and metals, such as gold, silver, and iron. Different types of nanoparticles provide unique chemical and physical properties for carrying therapeutic agents, intratumoral drug delivery, and tumor imaging [96].

At present, two nanoparticle formulated drugs have been used clinically for breast cancer treatment. The polyethyl glycosylated (PEG) liposome-encapsulated doxorubicin (Doxil) was determined to be more effective and less toxic when compared to conventional doxorubicin (Dox) [97,98]. In 2005, the second nanoparticle drug was approved, nanoparticle albumin bound (nab)-paclitaxel (Abraxane) [99]. Nab-paclitaxel improved the anti-tumor activity and decreased toxicity when compared to solvent based paclitaxel in several types of human cancers, including breast cancer [100,101].

The increased efficacy of both nanoparticle drugs is dependent on the principles that nanoparticle formulated drugs increase circulation time of the drug and can selectively deliver drugs into tumors by the EPR effect. Tumors undergo rapid vascularization which leads to impaired tumor vascular structures with “leaky” vessels and allows for nanoparticles smaller than 400 nm to accumulate in the tumor [40,41]. Relatively large nanoparticle size compared to small molecule drugs minimizes the delivery of drugs into

normal organs and tissues and therefore reduces systemic toxicity so that a higher drug dose can be administrated to cancer patients.

To overcome the clinical challenges for TNBC treatment, a broad range of nanoplatforms are under investigation as potential therapeutic options. Unique clinical and pathological properties of TNBC support the potential development of novel targeted and image-guided therapeutic approaches for the effective treatment of this aggressive type of breast cancer. To improve delivery efficiency of therapeutic agents into breast tumors, various nanoparticle drug carriers have been developed to target tumor cells, tumor vasculature, and the tumor microenvironment. The investigation of nanoparticles with the capacity for targeted drug delivery as an approach to treat metastatic disease, is of critical importance in TNBCs. Due to the increased likelihood of distant recurrence among TNBC patients, targeted theranostic nanoparticles have the unique potential to effectively detect metastatic lesions and deliver chemotherapeutics to them following systemic administration, based on the expression of the before-mentioned cellular receptors, especially receptors associated with tumor invasion and metastasis, such as uPAR and CXCR4. The effectiveness of these targeted drug carriers and imaging probes on drug delivery and tumor imaging have been demonstrated in multiple TNBC breast cancer cell lines and human xenograft tumor models as discussed herein.

1.6.1 Liposome Nanoparticles

Liposomal nanoparticles were the first nanoparticle drug carrier composed of a phospholipid bilayer. Liposomes possess a hydrophobic core which is ideal for

encapsulating high concentrations of hydrophobic drugs and allows for controlled drug release [102]. Liposomes coated with polyethylene glycol (PEG) decrease nonspecific uptake by macrophages in the reticuloendothelial system (RES), resulting in an increased blood half-life and bioavailability to tumors. Several non-targeted liposomal drug carriers have been developed for investigation in the treatment of TNBC in preclinical studies.

Systemic delivery of PEGylated liposome carrying a chemotherapeutic agent, arsenic oxide (AS_2O_3), referred to as arsenic nanobins, resulted in 3 to 5 fold increases in arsenic accumulation in tumors and enhanced antitumor effect relative to tumors treated with free AS_2O_3 in the MDA-MB-231 human breast cancer xenograft model [103]. Another non-targeted approach has been the development of pH sensitive liposomes that have the capacity to selectively release drug molecules into the acidic tumor environment or inside endosomes of tumor cells [104].

Endo-Tag-1 is a paclitaxel embedded liposomal nanoparticle that has been evaluated in a phase II clinical trial for advanced TNBC [105]. Its mechanism of action involves the negatively charged, newly formed tumor vasculature attracting the cationic liposome carrying the paclitaxel thus facilitating drug delivery. The paclitaxel can then attack the newly formed tumor vessels and cut off blood supply to the tumor. In a trial of 141 TNBC patients, at 16 weeks the disease free survival was 59.1% in the Endo-Tag-1/ paclitaxel combination group compared to 48% in the paclitaxel only group [105].

Liposomes which are functionalized with monoclonal antibodies to specific target proteins, or immunoliposomes, can more effectively mediate intracellular drug delivery via receptor-mediated endocytosis. Cetuximab conjugated immunoliposomes carrying Dox showed strong tumor growth inhibition in the MDA-MB-231 xenograft model [106]. An anti-CXCR4 antibody conjugated and pH sensitive immunoliposome has been developed for the delivery of gene silencing small interference RNA (siRNA) for lipocalin-2 (Lcn2), a protein that is secreted by breast cancer cells and is associated with a poor prognosis [107]. CXCR4-Lcn2 siRNA-immunoliposomes significantly reduced cell motility in human TNBC cell lines but failed to inhibit cell viability.

Liposomes can also be targeted with small molecules and peptides. For example, folate receptor targeted PEGlyated poly(l-lactide) (PLLA) and poly(l-histidine) polymeric nanoparticles loaded with Dox showed tumor growth inhibition and reduced lung metastasis in the 4T1 murine mammary tumor model [108]. Therefore, targeted-liposomes are a promising nanoparticle platform in the treatment of TNBC disease.

To produce targeted liposomes with imaging ability, various imaging agents, such as organic dyes, gadolinium (Gd), radioisotopes and magnetic iron oxide nanoparticles (IONP), are either conjugated to or encapsulated within the liposomes [109]. Combining targeting and imaging offers a more effective approach for the treatment of TNBC using the liposome nanoparticles, allowing for the increased internalization of the drug payload into cells while allowing for imaging capabilities for monitoring drug delivery and therapeutic responses.

An octopeptide (Cys-Asp-Gly-Phe (3-5-DiF)-Gly-Ay-Cys-NH2) conjugated liposome targeting to α-integrin was loaded with NIR dye and dual therapeutic agents, Dox and rapamycin, a mTOR inhibitor [110]. Systemic delivery of this α-integrin targeted liposomal carrier mediated selective accumulation of the nanoparticle-drug in MDA-MB-231 tumor xenografts, as observed by *in vivo* fluorescence imaging, and significantly decreased tumor volume compared to single agent treatment with either Dox or rapamycin [110]. Another approach that has been taken by a number of research groups is to encapsulate or conjugate radionucleotides in addition to chemotherapeutic agents. EGFR targeted immunoliposomes labeled with technetium 99m (^{99m}T) were shown to be retained in the surgical cavity, had high accumulation in the residual tumor surface of MDA-MB-231 xenografts, and in the metastatic lymph nodes of nude rats by SPECT/CT imaging [111].

1.6.2 Polymeric Nanoparticles

Polymeric nanoparticles are commonly used drug delivery vehicles that are biodegradable and have low toxicity. Many approaches have been developed to produce various polymeric nanoparticles by conjugation of multiple units of macromolecules or self-assembling of co-polymers. Therapeutic agents can be encapsulated inside the nanoparticles or conjugated to polymers. Most polymeric nanoparticles were developed based on the poly (d,l lactidecoglycolide) PLGA polymer that has been approved by the FDA for therapeutic use in humans. Non-targeted polymeric nanoparticles drug carriers have been developed for preclinical investigations in TNBC tumor models including an active metabolite of irinotecan (SN38) encapsulated in polymeric nanoparticle that showed anti-tumor efficacy in the 4T1 mouse mammary tumor model [112]. Systemic delivery of

IT-101, a camptothecin-conjugate cyclodextrin-based polymeric nanoparticle, showed a significantly stronger anti-tumor effect compared with conventional irinotecan in the human TNBC MDA-MB-231 model [113]. Currently, clinical trials are ongoing to determine the efficacy of IT-101 in cancer patients [114].

A PEGylated poly (epsilon-caprolactone)-carrying docetaxel (DTX) nanoparticle has also been shown to inhibit tumor growth and increase mouse survival compared to mice treated with conventional DTX [115]. The encapsulation of the water soluble platinum based agent, mitaplatin, in PLGA nanoparticles was also investigated and produced strong anti-tumor effects in nude mice bearing human TNBC xenografts derived from the MDA-MB-468 cell line [116]. Additionally, a cross-linked polymer cage that is sensitive to low pH was coated onto Dox-loaded liposomal nanobins and release of the payload drugs under the acidic tumor environments provided selective anti-tumor effect in the MDA-MB-231 TNBC xenograft model. Varying the degree of cross-linking in the polymer cage allows the surface potential to be fine-tuned for optimal stability, thus increasing circulation time and release properties [117]. As with liposomal nanoparticles, addition of targeting ligands and imaging agents has increased the effectiveness of polymer-based nanoparticles. Investigators have designed targeted polymeric nanoparticles with a diverse set of targets including cancer stem cell markers [118,119], newly formed vasculature [120], and cell surface receptors [119–121].

An EGFR targeted peptide conjugated PLGA PEG polymeric nanoparticle has been developed for carrying dual chemotherapy drugs paclitaxel and aerobic glycolysis

inhibitor, lonidamine. This polymeric nanoparticle showed targeted delivery into tumors and reduced systemic toxicity in an orthotopic, multidrug-resistant TNBC xenograft model [122]. Significant enhancement in therapeutic efficacy and altered multidrug resistance was observed within the EGFR-targeted nanoparticle treated group compared to the non-targeted nanoparticle treated group [123].

A hyaluronic acid (HA) conjugated, multi-layered nanoparticle targeting the CD44 receptor was developed consisting of multilayer polyelectric shell with one layer of polyanion HA and one layer of polycation L-lysine [124]. When the nanoparticle reaches an environment with a pH of 6.0, the nanoparticle expands from 17 nm to 53.2 nm, resulting in an increase in cellular uptake compared to control nanoparticles in MDA-MB-468 cell line and a 4-fold higher accumulation in MDA-MB-468 xenograft tumors compared to control non-targeted nanoparticles [124].

Various imaging agents have been incorporated onto targeted polymeric nanoparticles for monitoring drug delivery. NIR imaging has been extensively investigated due to its simplicity and capability for rapid real-time detection of nanoparticle-drug delivery and the potential for optical imaging of drug-resistant tumor cells for surgical resection. Huang *et al* designed a hyaluronic acid conjugated block copolymer (PLGA) that targets the CD44 receptor, encapsulates DTX as well as the NIR dye, DiR, into the nanoparticles [125]. Systemic delivery of CD44 targeted-PLGA-nanoparticles led to effective accumulation of the nanoparticle in tumors in the MDA-MB-231 tumor xenograft model and facilitated NIR tumor imaging. The CD44 targeted-PLGA nanoparticle treated group also showed a

marked decrease in tumor growth (92% growth inhibition) compared to the non-targeted group.

A multifunctional nanoparticle with potential for NIR imaging and phototherapy has also been developed. This nanoparticle was made from a poly (9,9—bis(4-(2-ethylhexylphenyl)-4,fluorine-alt-co-6,7-bis(4-(hexyloxy)phenyl)-4,9-di(thiophn-2-yl)-yhiadiazoloquinoxaline](PFTTQ) polymer that has a high NIR absorbance for infrared thermal images to be generated at the tumor site and upon irradiation at 808 nm for 5 min, the temperature can be raised to more than 50^0C *in vitro* in MDA-MB-231 cells, resulting in tumor cell death [126]. Beyond polymer-based nanoparticles for NIR imaging, nanoparticles for clinically relevant imaging modalities such as PET and MRI have also been developed. An amphiphilic block copolymers poly (amide-amine)-poly (L-lactide)-b-poly ethylene glycol (PAMAM-PLA-PEG) nanoparticles that contained radiolabeled ^{64}Cu was developed [127]. The nanoparticles were targeted to CD105, a protein expressed by neo-vasculature, by conjugating to the anti-CD105 antibody TR105. Serial non-invasive PET was used to measure PAMAM-PLA-b-PEG-TR105-^{64}Cu nanoparticle accumulation in the 4T1 murine mammary tumor model. Mice treated with PAMAM-PLA-b-PEG-TR105-^{64}Cu had a much higher level of nanoparticle accumulation according to PET imaging compared to non-targeted nanoparticles.

1.6.3 Carbon Nanotubes

Carbon nanotubes are cylindrical carbon nanostructures that are being investigated as drug delivery vehicles as well as imaging probes in TNBC. A PEGylated single-walled carbon

nanotube (SWNT) conjugated with paclitaxel was shown to have a higher efficiency in suppressing tumor growth compared to conventional paclitaxel in the 4T1 mouse mammary tumor model [128]. SWNTs have intrinsic NIR photoluminescence and thus can be used for NIR optical imaging [129]. SWNTs with different $^{13}C/^{12}C$ isotope compositions and Raman peaks were synthesized and conjugation of different targeting ligands into those SWNTs allowed for multiplexed Raman imaging of multiple biomarkers [130]. Strong optical absorbance of NIR light is the basis for photothermal cancer therapy. Systemic delivery of SWNTs into mice bearing 4T1 mouse mammary tumors led to NIR tumor imaging in the 1.0–1.4 μm emission region and tumor elimination based on photothermal effect at NIR 808 nm [131]. Complete tumor elimination was observed in photothermally-treated mice with no observed toxic side effects. SWNTs also produce excellent photoacoustic imaging contrasts for tumor imaging [131]. Compared to NIR optical imaging, photoacoustic imaging has a higher spatial resolution and deeper tissue imaging ability. However, to be able to translate this nanoparticle platform into future clinical translation, issues concerning long-term systemic and cellular toxicity, biodegradability, biodistribution and clearance of carbon nanotubes have yet to be investigated thoroughly.

1.6.4 Metallic Nanoparticles

Nanoparticles composed of metals or with metallic cores, such as gold and iron, have been used as drug carriers or theranostic agents.

Gold Nanoparticles:

Several types of gold nanoparticles and nanorods have been developed as thermal therapeutic, imaging and drug delivery nanoparticles. A multilayered gold nanoparticle ($Au/SiO_2/Au$), referred to as a gold nanomatryoshkas, consists of a gold core coated with silica and a thin film of gold shell. Systemic delivery of nanomatryoshkas and irradiation significantly inhibited tumor growth and some mice were tumor free for over 60 days in a MDA-MB-231 xenograft model [132]. In addition to photothermal ablation therapy, gold nanoparticles can be loaded with chemotherapeutics to enhance antitumor efficacy. To treat metastatic breast cancer, a Dox loaded DNA wrapped gold nanorod was developed which allowed for dual therapeutic functions, photothermal ablation and chemotherapy [133]. Mice bearing 4T1 mammary tumors were treated with the Dox loaded DNA wrapped gold nanorod and received 655 nm laser irradiation. A significant reduction of primary tumor growth was observed in the gold nanorod treated mice as well as a suppression in lung metastases when compared to untreated mice [133].

Another hollow gold nanosphere which is a promising theranostic nanoparticle platform has plasmon absorption in the NIR region and displays strong photothermal coupling properties suitable for photothermal ablation therapy [134]. The hollow gold nanospheres (HAuNS, ~40-nm diameter) had the capacity to carry large amounts of Dox (63% by weight) and drug release can be triggered by NIR light irradiation. The dual therapeutic effects of Dox loaded-HAuNS and laser irradiation were demonstrated through enhanced cell death of combination treated groups compared to single treatment groups in the human TNBC MDA-MB-231 cell line [134].

The results from the studies described above demonstrate gold-based theranostic nanoparticles as an effective platform for the treatment of TNBC, especially in conjunction with photothermal ablation therapy. Questions still remain as to the biodegradability and clearance of gold nanoparticles in human subjects since cancer therapy requires large doses and repeated administrations, which may hinder the development of gold nanoparticles as clinically applicable theranostic agents. Further studies are required to elucidate the fate and mechanisms of degradation and clearance of gold-based nanoparticles for future clinical translation.

Magnetic Iron-Oxide Nanoparticles:

Magnetic iron oxide nanoparticle (IONP) is an attractive theranostic nanoparticle platform because of its capability as a drug carrier as well as a MRI contrast. IONPs are biocompatible and biodegradable nanoparticles with low toxicity. IONPs have unique paramagnetic properties, which generate a significant susceptibility effect resulting in strong T_2 and T^*_2 contrast, as well as T1 effect at very low concentrations [135]. Several forms of IONPs have been used in clinical settings and have proven to be safe for human use [136,137].

MRI provides 3D anatomic resolution, soft tissue contrast, and unlimited tissue penetration depth. MRI is a common clinical imaging modality that makes it feasible to translate the MRI-guided cancer therapy into clinical applications. Several groups have developed targeted IONPs as imaging probes or theranostic nanoparticles [138]. IONPs targeting

underglycosylated MUC-1 (uMUC-1) were developed by conjugation of MUC1 targeting peptides (EPPT) to NIR dye Cy5.5 labeled IONPs. This imaging IONP was used to monitor response of breast cancer to Dox treatment by MRI in a human TNBC BT20 cell line-derived xenograft model [139].

Our group has developed uPAR-targeted IONPs by conjugating a NIR dye labeled, recombinant amino terminal fragment (ATF) of mouse or human uPA to amphiphilic polymer coated IONPs [47,140]. Systemic delivery of uPAR-targeted IONPs led to an accumulation of IONPs in tumors of Balb/c mice bearing 4T1 mouse mammary tumor or nude mice bearing MDA-MB-231 tumor xenografts and generated strong MRI T_2- contrast for tumor MRI [47] . We further demonstrated targeted delivery of NIR-dye labeled IONPs into mice bearing breast tumor xenografts enabling non-invasive multimodal tumor imaging by NIR optical, T_2-weighted or ultra-short TE MRI, 3D fluorescence tomography, and photoacoustic tomography [141–143]. uPAR-targeted nanoprobes significantly enhanced photoacoustic contrast of the tumor margins compared to non-targeted groups, with imaging to depths up to 31 mm. NIR-dye labeled uPAR targeted IONP was used for intraoperative optical imaging of tumor margins, allowing for complete removal of breast tumors [47]. Further, our *in vitro* data indicates that uPAR-targeted IONP-Dox deliver high levels of Dox into 4T1 and MDA-MB 231 cells and produce a strong inhibitory effect on cell growth when compared to cells treated with free Dox or non-targeted-IONP-Dox [140]. The ability of targeted therapy and MRI of nanoparticle–drug delivery following systemic delivery of uPAR-targeted IONP-Dox theranostic IONPs were demonstrated in 4T1 mouse mammary tumor model [144]. An intracellular adhesion molecule-1 (ICAM-

1) antibody conjugated-IONP, developed by Guo *et al* [145] has been used as a MRI probe to evaluate tumor targeting in a TNBC xenograft model by MRI. The ICAM-1 targeted probe accumulated in ICAM-1 overexpressing TNBC tumor xenografts.

Due to the ability to assist in enhancing clinically relevant imaging modalities, such as MRI, a liposomal nanoparticle encapsulated with irinotecan (MM-398) in combination with an iron nanoparticle based imaging agent, ferumoxytol, has been used in a phase 1 clinical trial in TNBC patients to assess the targeted drug into tumors and its relationship with the level of intratumoral macrophages[137].

1.7 Conclusion

Although extensive preclinical studies have been carried out in the development of numerous targeted nanoparticle imaging probes and drug carriers and evaluation of the effects of targeted tumor imaging and therapy, the process of translation of targeted nanoparticle agents into clinical applications has been challenging and relatively slow, compared with non-targeted nanoparticle drug carriers. One of the major issues is that many nanoparticle drug carriers targeted to cellular receptors are expressed only by tumor cells, such as EGFR and HER-2. Those targeted nanoparticles are delivered into the tumor using the same EPR effect mechanism as non-targeted nanoparticles. Nanoparticles targeted to tumor endothelial cells, such as RGD conjugated nanoparticles, target αVβ3 integrin in angiogenic tumor vessels but only a small percentage of human tumor cells express αVβ3 integrin. Following extravasation, the majority of targeted nanoparticle drug carriers were secluded in perivascular areas due to the presence of tumor stromal cells and

extracellular matrix barriers [40]. Therefore, without novel approaches to overcome tumor stromal drug delivery barriers, current methods for targeted delivery of nanoparticle drug carriers will fail to reach their fullest therapeutic potential for targeted cancer treatment. Success in translating targeted nanoparticles into clinical applications will require innovative nanoparticle designs to break tumor stroma and efficiently deliver nanoparticle-drug into tumor cells.

In this chapter, we narrowed our scope on experimental systems and results generated from TNBC cell line-derived animal models. Other theranostic nanoparticles and imaging approaches that have been developed and tested in other tumor types also have potential for targeted and image-guided treatment of TNBC. Additionally, the vast majority of preclinical studies on TNBC use the limited number of human, MDA-MB-231, MDA-MB-468, BT20, and 4T1 mouse mammary tumor cell lines and those cell line-derived xenograft TNBC tumor models in mice. However, due to the molecular heterogeneity of TNBC, novel imaging and therapeutic agents should be tested in models that more closely recapitulate human TNBC disease, such as patient derived xenograft (PDX) models.

Despite the observed preclinical efficacy of nanoparticles in TNBC models, in order to be translated into the clinics, several challenges remain: large scale production of consistent nanoparticle–drug carriers, improved delivery efficiency, new approaches to avoid liver and spleen nonspecific uptake, evaluation of pharmacokinetics and pharmacodynamics in preclinical studies, determination of systemic toxicity of targeted theranostic nanoparticles, the establishment of sensitive imaging methods and protocols for clinically available

imaging devices as well as the development of new imaging devices for new types of theranostic nanoparticles. With the significant and promising progress in the delivery and imaging of nanocarriers to treat breast cancers, including TNBC, strides are being made toward the critically needed translational and clinical discoveries that are on the horizon.

1.8 Scope of this Dissertation

In this dissertation, we investigated the phenotypic characteristics of drug-resistant TNBCs which allowed us to identify promising receptors for developing targeted nanoparticle therapeutics for this aggressive sub-type of breast cancer. First, we tested the hypothesis that drug-resistant TNBCs are enriched with CSCs by examining the expression of breast CSC marker CD44 and components of the Wnt/ β-catenin pathway, following treatment with chemotherapeutic doxorubicin (Dox) or uPAR-targeted nanoparticles carrying Dox in PDX models of drug-resistant TNBCs. Having identified Wnt co-receptor LRP5/6 and uPAR as receptors that are overexpressed in drug-resistant TNBCs in Chapter 2 we hypothesized that specific targeting of the Wnt receptor (LRP5/6) with a novel inhibitory peptide will effectively inhibit Wnt signaling in TNBC cells and Wnt-targeted nanoparticles will deliver chemotherapeutic drugs into tumor cells to enhance the therapeutic response in drug-resistant TNBCs. In Chapter 3 we demonstrated that our dual Wnt and uPAR-targeted theranostic nanoparticles can inhibit the cancer stem cell phenotype in drug-resistant TNBCs and hormone positive breast cancer. Our findings support further evaluation of co-targeting Wnt/LRP and uPAR using theranostic nanoparticles as a promising therapeutic approach for effective drug delivery to drug-resistant TNBC.

Chapter 2: Characterization of Differential Drug Response in TNBC PDX tumors after treatment with uPAR targeted theranostic nanoparticles

Jasmine Miller-Kleinhenz, Weiping Qian, Lily Yang

2.1 Introduction

Triple-negative breast cancer is an aggressive subtype of breast cancer that is diagnosed at an advanced stage, with high recurrence rate, and a rapid progression from recurrence to death compared to other breast cancers [146–148]. Defining triple-negative breast cancer as a subtype that lacks expression of estrogen receptor (ER), progesterone receptor (PR), and human epidermal growth factor receptor 2 (HER2) is an oversimplification of a very complex disease. TNBCs are a highly heterogenous disease with at least six identified distinct subtypes each with their own particular and unique molecular biologies [149,150]. Currently, there are no specific targeted agents approved for the treatment of TNBC and the standard therapeutic option is chemotherapy. Unfortunately, following neoadjuvant chemotherapy more than 70% of TNBC do not have a response to treatment [19,151]. Interestingly, a study by Balko et al showed that through molecular analysis of residual tumors 90% of TNBC with drug-resistant tumors had a treatable target [151]. While there is no unifying molecular target in TNBC there are several overexpressed growth factors and receptors in the various TNBC subtypes that can serve as meaningful targets[152].

The urokinase plasminogen activator (uPA) system has been identified as a potential target for some TNBCs. The uPA system, which is a serine protease family, consists of the ligand, uPA, and its receptor, uPAR. There are two functions for uPAR, one is proteolytic and the other non-proteolytic. The proteolytic function of uPAR involves cleavage of inactive (pro-uPA) ligand to become active [153]. Active uPA catalyzes plasminogen into its active form, plasmin, leading to degradation of the extracellular matrix (ECM) (**Figure 2.1A**). This remodeling of the extracellular matrix leads to an increase of invasiveness in cells

with high expression of uPAR and is thought to play a role in proteolysis at the invasive front in breast cancers [154].

In addition, uPAR functions in a non-proteolytic way through its interactions with ECM protein vitronectin or integrins leading to an increase in cell adhesion or through acting as a single transducer through interactions with other cell surface receptors (**Figure 2.1B**) [155]. uPAR has been shown to interact with growth factor receptor pathways leading to increases in cell viability, migration and invasion [156]. In addition, uPAR signaling has been shown to induce cancer stem like properties in breast cancer cells leading to an increase in tumor initiation and growth *in vivo* [157]. Studies have shown that uPAR expression is higher in TNBCs and is associated with shorter progression free survival [158,159]. In a study by Hao et al serum levels of uPAR was shown to be a reliable marker for breast cancer recurrence [160]. uPAR is an attractive target because of its overexpression on drug-resistant tumor cells as well as tumor-associated macrophages in breast cancer [154],[161].

Using recombinant peptides of the amino terminal fragment (ATF) end of uPAR ligand, uPA, our lab has developed uPAR-targeted magnetic nanoparticles (IONPs). We showed that ATF-IONPs can bind and be internalized in uPAR expressing tumor cells in vivo using 4T1 mouse mammary cell-line derived model of breast cancer [47]. In addition, the ATF-IONPs accumulate in the tumors and generate a strong MRI signal. Next, we wanted to show the utility of our ATF-IONPs as an imaging probe in a human cell-line derived orthotopic TNBC model. We conjugated a near-infrared optical (NIR) imaging dye to the ATF-IONPs and after systemic delivery we detected strong optical imaging of the tumor

allowing for identification of the invasive tumor edge and in residual tumors [162]. Our data establishes uPAR as a valid target in TNBC for identification and imaging of tumor using our ATF-IONPs though we have not studied the treatment effect of uPAR-targeted nanoparticles.

To study the therapeutic effect of our uPAR-targeted IONPs we developed a patient derived xenograft (PDX) model of drug-resistant TNBC. PDX models are generated by implanting tumor fragments from patients into mice and are considered an ideal tool for cancer research because of the ability to recapitulate tumor morphology, gene expression, and drug susceptibility compared to cell-line derived models [163]. Using freshly resected tumor tissue fragments from TNBC patients following neoadjuvant chemotherapy, we implanted the tumors orthotopically into the mammary fat pad of SCID or nude immune deficient mice and utilized the resulting PDX model to study the effect of our uPAR-targeted IONPs to increase overall survival, reduce recurrence, and decrease the expression of pathways implicated in drug-resistance in TNBC.

A.

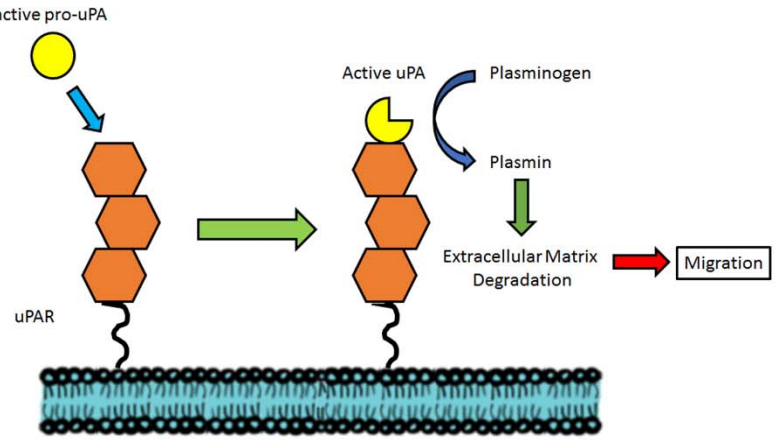
Inactive pro-uPA
Active uPA
Plasminogen
Plasmin
Extracellular Matrix Degradation
Migration
uPAR

B.

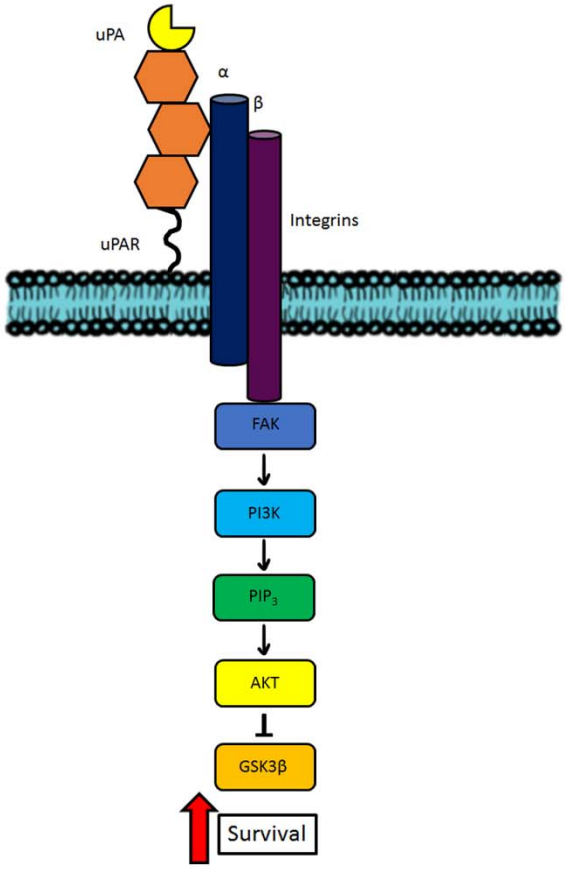
uPA
α
β
Integrins
uPAR
FAK
PI3K
PIP3
AKT
GSK3β
Survival

Figure 2.1: The urokinase plasminogen activator system

The urokinase plasminogen activator system consist of the uPA ligand and its receptor, uPAR. **A.** Prior to binding uPAR, uPA is in an inactive state (pro-uPA). Upon binding to uPAR, uPA is cleaved and becomes activated. In this active state, uPA converts plasminogen into its active form, plasmin leading to degradation of the extracellular matrix. **B**. uPAR can also bind to other receptors, such as integrins, which allows for increase in cell signaling resulting in an increase in cell survival and proliferation. Focal adhesion kinase (FAK), phosphatidylinositide 3-kinase (PI3K), phosphatidylinositol 3,4,5 trisphosphate (PIP_3), glycogen synthase kinase 3-β (GSK3β).

2.2 Materials and Methods

Production and Purification of Recombinant ATF Peptides

As described in [140], a cDNA fragment encoding amino acids 1–135 of uPA, isolated by PCR amplification, was cloned into pET101/D-TOPO expression vector (Invitrogen, Carlsbad, CA). Recombinant ATF peptides (ATF135) were expressed in E. coli BL21 (Invitrogen) and purified from bacterial extracts under native conditions using a Ni2+ NTA-agarose column (Qiagen, Valencia, CA).

Production of uPAR targeted IONPs.

Paramagnetic iron oxide nanoparticles were prepared and obtained from Ocean Nanotech, LLC as described in [164] using iron oxide powder as the iron precursor, oleic acid as the ligand, and octadecene as the solvent. The core size and hydrodynamic size of the iron oxide nanoparticles were measured using transmission electron microscopy and light scattering scan, respectively. The particles were coated with amphiphilic polymers using a similar method, as reported previously [165]. Amino-terminal fragment peptides (ATF135) were conjugated to the surface of iron oxide nanoparticles via cross-linking of carboxyl

groups to amino side groups on the amino-terminal fragment peptides. Briefly, the polymer-coated iron oxide nanoparticles were activated with ethyl-3-dimethyl amino propyl carbodimide (Pierce)and sulfo-N-hydroxysuccinimide for 15 min. After purification using Nanosep 100k OMEGA (Pall Corp.), activated iron oxide nanoparticles were reacted with amino-terminal fragment or NIR 830 dye–amino-terminal fragment peptides at a molar ratio iron oxide to amino-terminal fragment of 1:20 in PBS (pH 7.0) at 4C overnight, generating amino-terminal fragment–iron oxide or NIR 830 dye–amino-terminal fragment–iron oxide nanoparticles. The final amino-terminal fragment–iron oxide conjugates were purified using Nanosep 100k column filtration.

Prussian blue staining.

Fixed tissue was incubated with a mixture of 10% potassium ferrocyanide(II) trihydrate and 10% HCl solution for 3 hours at 37^0C. After being washed three times with distilled water, tissues were counterstained with nuclear fast red solution for 5 min. Following consecutive dehydrations with 70% and 100% EtOH and two rinses in xylene, the slides were mounted. Result of Prussian blue staining was examined under a light microscopy.

Immunofluorescence labeling.

Frozen tissue sections of tumor and normal tissues were used for immunofluorescence labeling. The following antibodies were purchased from Santa Cruz: rabbit anti-Wnt10b (G-19; no. sc6280, 1:200), rabbit anti-uPAR (FL-290; no. sc10815, 1:200), rabbit anti-Ki67, rabbit anti-CD24 (FL-80; no. sc11406, 1:500)., and goat anti-HCAM (CD44) (N-18; no.sc7051, 1:200). Alexa Fluor 555 dye (red fluorescence, dilution 1:500) and Alexa Fluor

488 dye (green fluorescence, dilution 1:500) labeled secondary antibodies (Invitrogen) were used to detect biomarker-positive cells. Images were taken using fluorescence microscopy.

Western blot analyses.

Frozen PDX tumors were placed in liquid nitrogen and then pulverized. Samples were then lysed in radioimmunoprecipitation assay buffer (Cell Signaling Technology, Danvers, MA) supplemented with protease and phosphatase inhibitors (Sigma-Aldrich). Total protein extracts were run on SDS-PAGE gel and blotted onto polyvinylidene difluoride (PVDF) membrane. Blots were probed overnight. The following antibodies were purchased from Santa Cruz: rabbit anti-Wnt1b (H-70; no. sc25524, 1:500), rabbit anti-LRP6 (H-300; no. sc15399, 1:500), rabbit anti-uPAR (FL-290; no. sc10815, 1:500), and goat anti-HCAM (CD44) (N-18; no.sc7051, 1:500). Mouse anti-β-actin was purchased from Sigma-Aldrich (AC-15, 1:10,000). All primary antibodies were diluted in Tris-buffered saline and Tween 20. Goat anti-mouse secondary IgG-HRP antibody (no. sc-2005, 1:3,000), goat anti-rabbit secondary IgG-HRP antibody (no. sc-2004, 1:3,000), and donkey anti-goat secondary IgG-HRP antibody (no. sc-2020, 1:3,000) were purchased from Santa Cruz Biotechnology (Santa Cruz, CA). Protein bands were detected using ECL.

Establishment of orthotopic human TNBC PDX tumor models in nude mice.

Fresh tumor tissues were collected from surgically resected tumors from TNBC patients who completed neoadjuvant therapy and had large residual tumors using an Emory Institutional Review Board approved protocol (IRB#00071700). TNBC patient #1 had

neoadjuvant therapy using Sorafenib in combination with Cisplatin followed by dose dense Paclitaxel. TNBC patient #6 had neoadjuvant therapy using Dox followed paclitaxel.

Within 2 hours of surgical resection, tumor tissues were cut into 1-2 mm fragments and implanted into the mammary fat pad of immune deficient SCID mice (8 to 10 weeks old, female) using a surgical procedure approved by Emory Institutional Animal Care and Use Committee (IACUC). Excess tissues were frozen in liquid nitrogen and stored for further pathological analysis. After surgery, the tumor growth in the mice was monitored by a caliper weekly. Orthotopic tumors grew to 5 to 10 mm diameter in about 8 to 10 weeks. These PDX tumors then were harvested, and tumor fragments at 1 to 2 mm sizes were then implanted into the mammary fat pad of 6- to 8-week-old female nude mice for large-scale studies.

In vivo targeting and imaging.

Tumor bearing mice were subjected to NIR optical imaging 48 hours after the tail vein injection of 800 pmol of NIR-830-labeled ATF-IONPs. NIR optical imaging was conducted using the Kodak *in vivo* FX imaging system (Carestream Health Inc., Rochester, NY, USA).). All optical images were captured using an 800 nm excitation and 850 nm emission filter set with 3 min exposure time and a gamma value of 0.2. Optical images were analyzed using the software provided by the Kodak imaging system.

In vivo effect of nanoparticle-Dox treatment.

Free Dox, IONP-Dox, and ATF-IONP-Dox was injected at 10 mg/kg Dox equivalent dose via the tail vein into the nude mice bearing the fourth passage of TNBC patient #1 PDX

tumors once per week for a total of 5 treatments. One week after final treatment, tumors were harvested and weighed. Western blot and immunofluorescence analysis were performed on tumor tissue lysates and frozen tissue sections.

2.3 Results

2.3.1 Generation of Primary Orthotopic Drug-Resistant TNBC Patient Derived Xenograft

An orthotopic patient derived xenograft (PDX) model of drug-resistant triple-negative breast cancer was established by implanting tumor fragments from surgically resected tumors from breast cancer patients that were first implanted into SCID mice and then passaged into nude mice to conduct large-scale treatment efficacy studies using our uPAR targeted theranostic nanoparticles (**Figure 2.2A**). Histological analysis was performed on frozen tissue sections of the primary tumor from patient #1 paired with PDX tumor derived from patient #1 in nude mice. As shown in **Figure 2.2B**, the PDX tumor was able to recapitulate the expression of receptors of interests including uPAR and IGF-1R, proliferation marker Ki67, as well as expression of cancer stem cell markers $CD44^{hi}/CD24^{lo}$. Our study focuses on the efficacy of our uPAR-targeted iron oxide nanoparticle (IONPs) carrying chemotherapeutic doxorubicin (Dox) *in vivo* (**Figure 2.2C**). Nanoparticles for these studies have a 10 nm iron core coated in an amphiphilic polymer with poly-ethyl glycol (PEG). To target uPAR, we used the amino terminal fragment (ATF) of uPA ligand conjugated to the surface of the IONPs. In addition, near-infared NIR-830 dye was conjugated to the IONPs for delivery studies.

A.

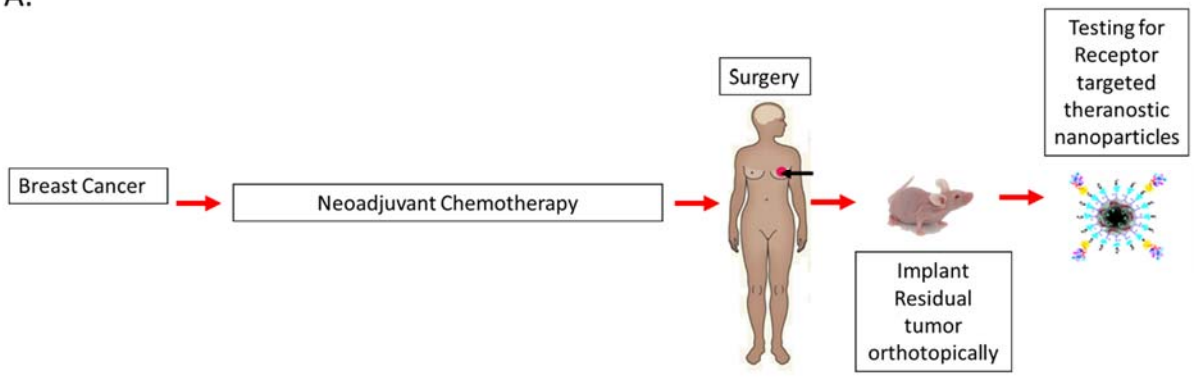
Breast Cancer
Neoadjuvant Chemotherapy
Surgery
Implant Residual tumor orthotopically
Testing for Receptor targeted theranostic nanoparticles

B.

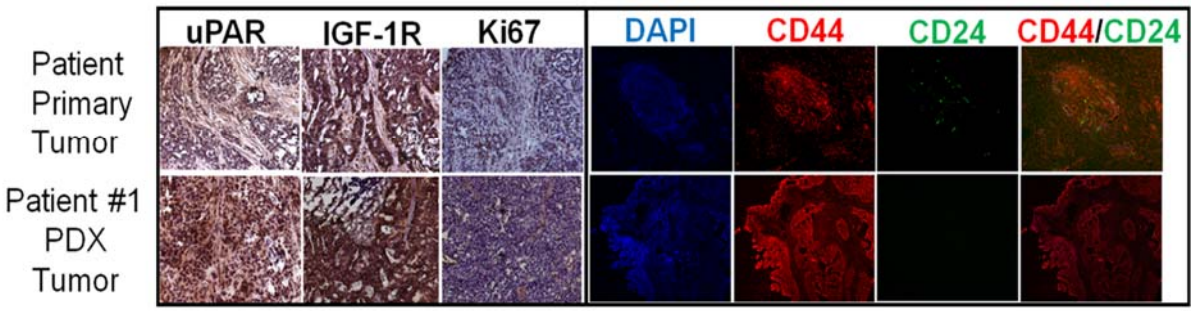
uPAR
IGF-1R
Ki67
DAPI
CD44
CD24
CD44/CD24
Patient Primary Tumor
Patient #1 PDX Tumor

C.

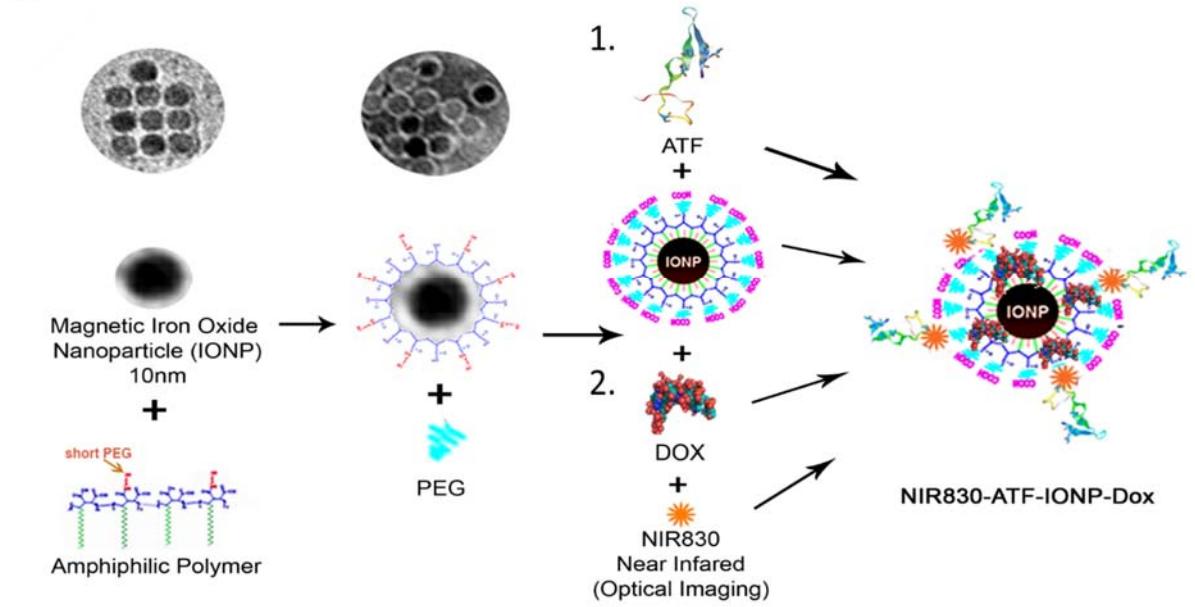
Magnetic Iron Oxide Nanoparticle (IONP) 10nm
short PEG
Amphiphilic Polymer
PEG
1.
ATF
IONP
2.
DOX
NIR830
Near Infared (Optical Imaging)
IONP
NIR830-ATF-IONP-Dox

Figure 2.2. Establishment and characterization of an orthotopic human TNBC PDX tumor model and uPAR targeted IONPs

A. Schematic illustration of the protocol for the establishment of an orthotopic PDX tumor model. **B.** Comparison of histological characteristics of surgically resected primary human TNBC tumor (patient #1) and the PDX-tumor derived from patient # 1 passage 4 in nude mice by immunohistochemistry for levels of uPAR, IGF-1R and Ki67 and immunofluorescence labelling of CD44 using Alexa Fluor 555 conjugated secondary antibody (red) and CD24 using Alexa Fluor 488 conjugated secondary antibody (green) in tissue sections with double immunofluorescence labelling resulting in orange-yellow where cells co-express CD44/CD24. **C.** Schematic illustration for first the conjugation of uPAR targeted ATF135 to amphiphilic polymer-polyethylene glycol (PEG)- coated 10 nm IONP and second the encapsulation of Dox to ATF-PEG-IONPs. NIR830 optical imaging can also be conjugated to the nanoparticle. An electron micrograph shows uniform 10 nm core size of IONP before and after amphiphilic polymer and PEG coating.

2.3.2 ATF-IONP-Dox inhibits tumor growth in PDX of Drug-Resistant TNBC

First, we treated nude mice bearing tumors from PDX of patient #1 passage 4 with free Dox or ATF-PEG-IONP-Dox at 10 mg/kg Dox equivalent via tail vein. Mice were treated once per week for 5 weeks. Tumors were removed for analysis one week following final treatment (**Figure 2.3A**).

In addition, tumor volume was measured one week after final treatment to determine effectiveness of treatment. Compared to no treatment control ATF-IONP-Dox and Dox significantly decreased tumor volume with p-values of 0.0007 and 0.0115, respectively as shown in **Figure 2.3B**.

Lastly, once mice were sacrificed their tumors were harvested for histological analysis, as shown in **Figure 2.3C**. There was a notable decrease in uPAR, CD44, and Ki67 in the ATF-IONP-Dox treated group compared to the no treatment control and Dox treated groups. While results indicate that the ATF-IONP-Dox treatment has an anti-tumor effect, further analysis is needed for the phenotypic effect of ATF-IONP-Dox on the tumor cell population.

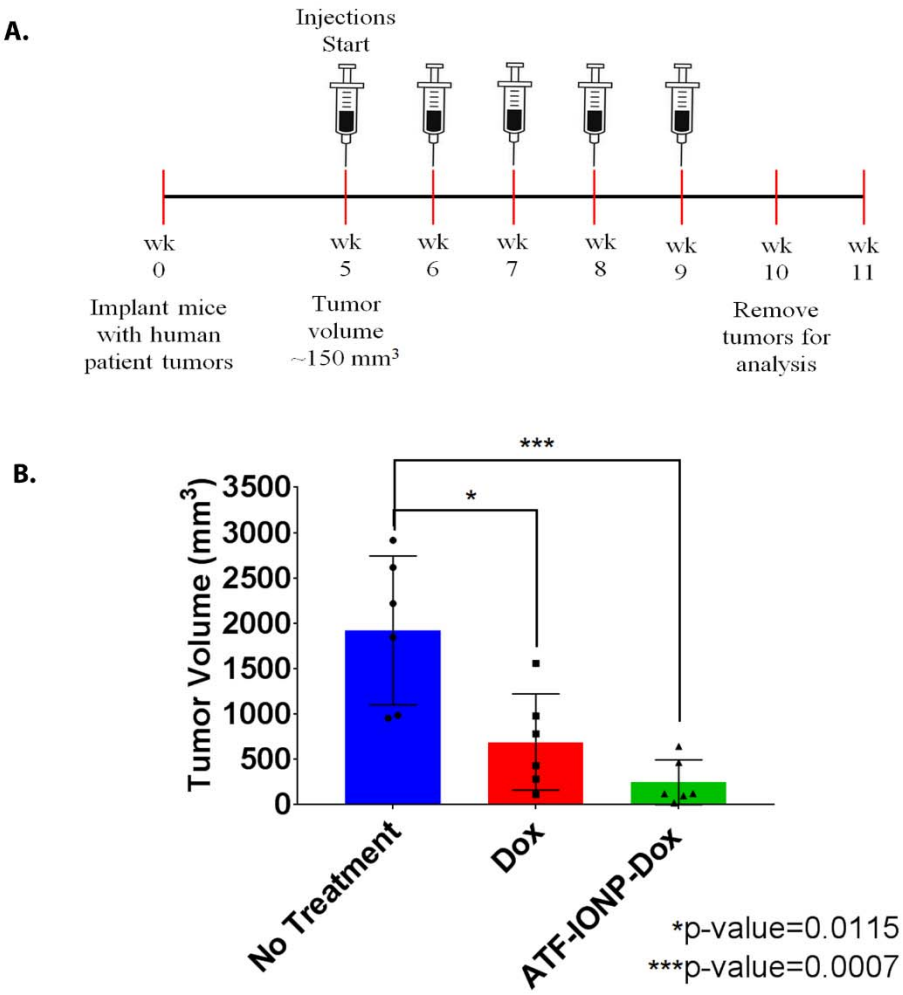
A.
Injections Start
wk 0
wk 5
wk 6
wk 7
wk 8
wk 9
wk 10
wk 11
Implant mice with human patient tumors
Tumor volume ~150 mm3
Remove tumors for analysis
B.
***
*
Tumor Volume (mm3)
3500
3000
2500
2000
1500
1000
500
0
No Treatment
Dox
ATF-IONP-Dox
*p-value=0.0115
***p-value=0.0007
C.
uPAR
CD44
Ki67
No Treatment
Doxorubicin
ATF-IONP-Dox

Figure 2.3. Effects of ATF-IONP-Dox in PDX of drug-resistant TNBC

A. Schematic of treatment schedule for drug-resistant TNBC PDX model **B.** Tumor growth inhibition. The mean tumor volume (bars) and individual tumor volume distribution (squares) after the treatment are shown *$p \leq 0.0115$ ***$p \leq 0.0007$. **C.** Histological characterization of no treatment control, free Doxorubicin and ATF-IONP-Dox treated tumors at the end-point of the study by immunohistochemistry looking for levels of uPAR, CD44, and Ki67. Brown represents expression of protein and blue stains cells.

2.3.3 Cytotoxicity in PDX of Drug-Resistant TNBC

To examine the effect of ATF-IONP-Dox on tumors directly after treatment, histological analysis was performed on the surgically resected tumors one week after final treatment. ATF-IONP-Dox and Dox treatment significantly decreased the expression of uPAR compared to no treatment control as shown in **Figure 2.4A**. ATF-IONP-Dox also significantly decreased the expression of CSC marker CD44 and Wnt10b, a ligand of the CSC associated Wnt/β-catenin pathway, compared to Dox treated groups. Quantification of expression of uPAR, CD44 and Wnt10b is shown in Figure 4B. Interestingly, treatment with free Dox increased the expression of the CSC associated markers CD44 and Wnt10b which indicates that while the tumor volume was decreasing, as shown in **Figure 2.4B**, the phenotype of the Dox treated tumors are becoming more aggressive.

Next, we wanted to determine the effect of ATF-IONP-Dox treatment on tumor cell proliferation. We observed the ATF-IONP-Dox treated tumors had a decrease in proliferating cells measured by Ki67 expression with 47% of cells expressing Ki67 compared to 55% in the no treatment control and 61% in the Dox treated groups (**Figure 2.4C**). Cytotoxic effects of ATF-IONP-Dox treatment were investigated by detecting apoptotic cells using the TUNEL assay. There was a significant increase in apoptotic cells in ATF-IONP-Dox treated group compared to the no treatment control and Dox treated groups as shown and quantified in **Figure 2.4D**.

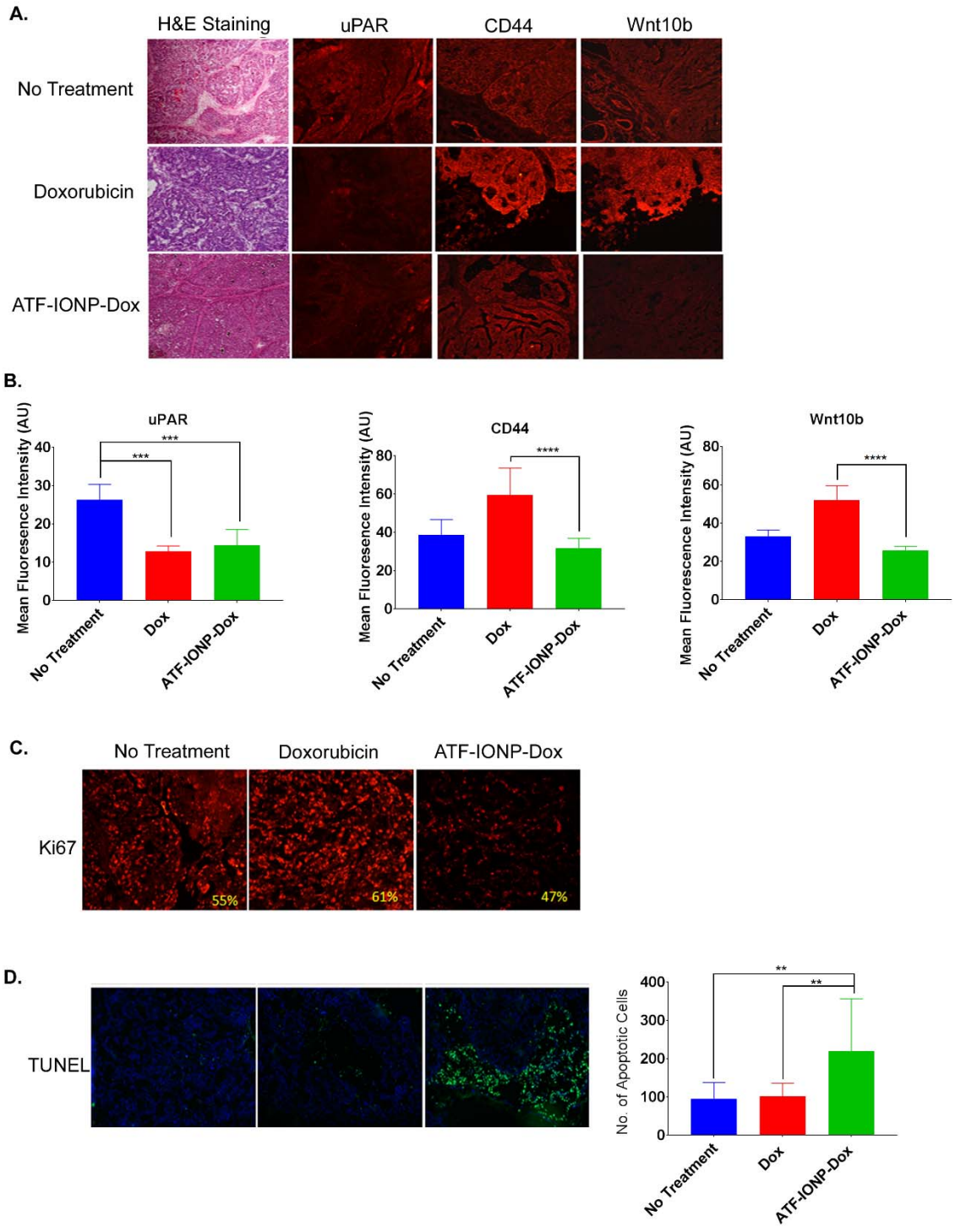
A.
H&E Staining
uPAR
CD44
Wnt10b
No Treatment
Doxorubicin
ATF-IONP-Dox
B.
uPAR
CD44
Wnt10b
Mean Fluoresence Intensity (AU)
Mean Fluorescence Intensity (AU)
***
****
No Treatment
Dox
ATF-IONP-Dox
C.
No Treatment
Doxorubicin
ATF-IONP-Dox
Ki67
55%
61%
47%
D.
TUNEL
No. of Apoptotic Cells
**

Figure 2.4. Histological characterization and effects of ATF-IONP-Dox on cell proliferation and induction of apoptotic cell death in TNBC PDX tumors.

Histological analysis of surgically resected tumors one week after final treatment. **A.** H&E staining of frozen tumor sections and immunofluorescence for uPAR, CD44, and Wnt10b using Alexa Fluor 555 conjugated secondary antibody (red). **B.** Quantification of the mean fluorescence intensity was performed by Image J software **p≤0.006 ***p≤0.0002 ****≤0.0001 **C.** Ki67-positive cells in tumor tissue sections were determined by immunofluorescence labeling using an anti-Ki67 antibody (red). Blue: Hoechst 33342 background staining. **D.** TUNEL labeling and quantitative analysis of apoptotic cells from six randomly selected microscopic fields of tumor section by ImageJ **p≤0.006

2.3.4 Heterogenous Response in Drug-Resistant TNBC after treatment with Dox or ATF-IONP-Dox

This study was conducted in a PDX model established from tumor fragments implanted from patient #1 into nude mice. We observed that while these mice had tumor fragments from the same patient there was a heterogeneity of response within the Dox and ATF-IONP-Dox treated groups. When monitoring tumor growth over the course of treatment we observed that in both Dox and ATF-IONP-Dox treatment groups there were some mice that had tumor growth regression, which we refer to as treatment sensitive, and some mice that had tumor growth progression which we deemed treatment insensitive (**Figure 2.5A**). Interestingly, mice in the no treatment control group also had heterogeneity in tumor growth rate between different mice, though all had tumor growth progression.

To determine whether treatment insensitive tumors had a more aggressive phenotype compared to tumors sensitive to treatment, we probed for protein expression of Wnt/β-catenin CSC pathway receptor LRP5/6 and ligand Wnt1. We also probed for CSC marker CD44 and uPAR. In the no treatment control group, we found expression of all of the CSC markers and uPAR regardless of tumor growth rate (**Figure 2.5B).** We found that in both Dox and ATF-IONP-Dox treated groups there was an increase in expression of LRP5/6, Wnt1, and CD44 in the treatment insensitive tumors compared to tumors sensitive to treatment as shown and quantified in **Figure 2.5B-D**. uPAR expression was increased in ATF-IONP-Dox insensitive tumors compared to those sensitive to treatment while uPAR expression remained high in tumors sensitive and insensitive to Dox treatment. In the ATF-IONP-Dox sensitive mouse we had a recurrent tumor (255R) that we also measured for the

CSC markers and uPAR. We saw that in recurrent tumors there is also an increase in LRP5/6, Wnt1, CD44 and uPAR (**Figure 2.5D**). These results further support these markers as indicative of a more aggressive, resistant phenotype.

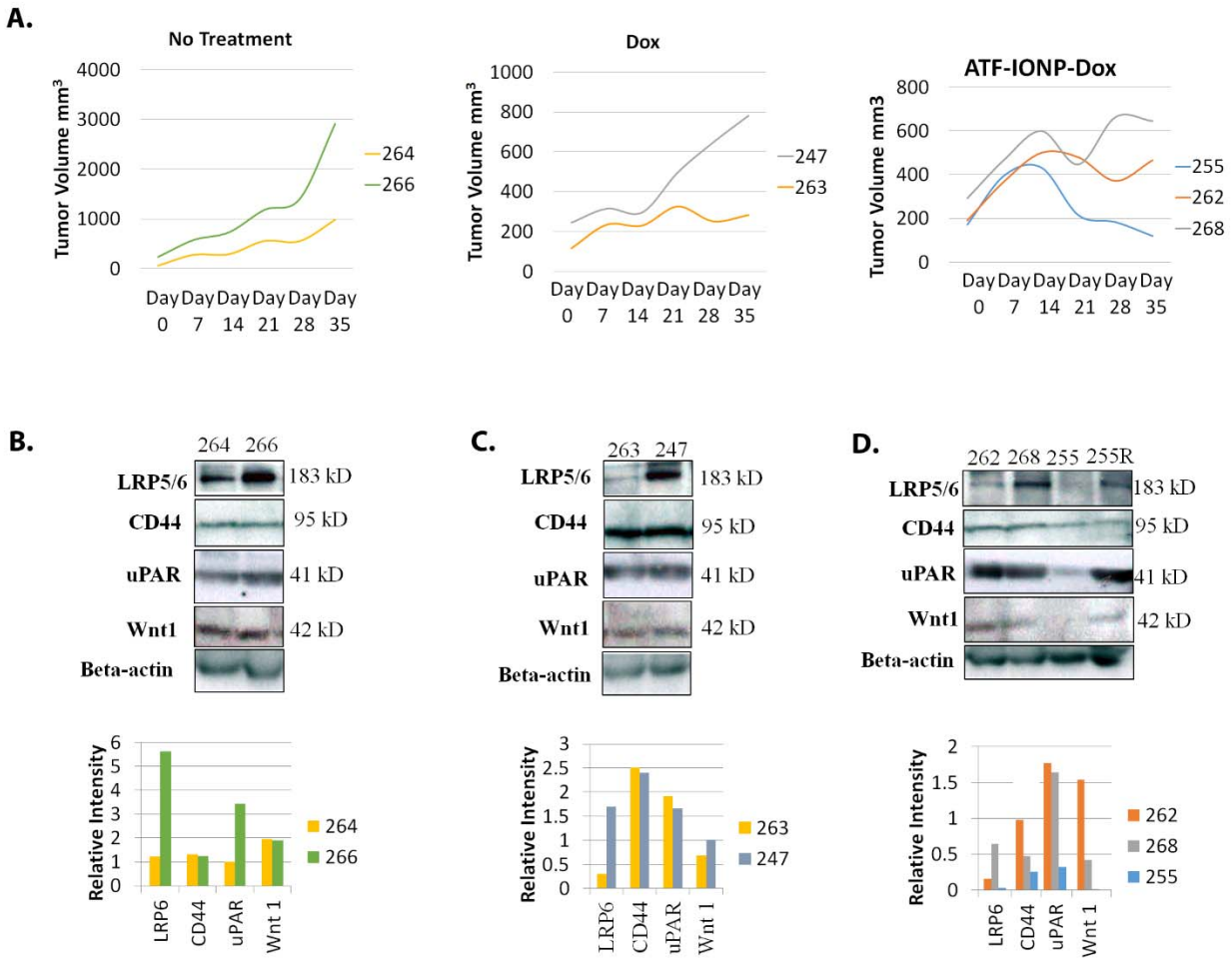

Figure 2.5. Heterogeneity of response to treatment with Dox or ATF-IONP-Dox in drug-resistant TNBC.

Nude mice bearing orthotopic TNBC PDX tumors derived from TNBC patient #1 received 10 mg/kg equivalent dose of free Dox or ATF-PEG-IONP-Dpx via tail vein injection once per week for 5 weeks. Tumors analysed from each group are labeled by the mouse study number. **A** Representative tumor growth curves of selected tumors in no treatment control mice and mice that are sensitive or insensitive to Dox or ATF-IONP-Dox treatment. Tumor tissue lysates were immunoblotted with anti-LRP5/6, anti-CD44, anti-Wnt-1 and anti-uPAR antibodies and band intensity was quantified relative to loading control for **B.** No

treatment control **C.** Dox treated, and **D.** ATF-IONP-Dox treated mice. 255R is the recurrent tumor of mouse #255. β-actin was used as a loading control.

2.3.5 Characterization of Heterogenous Phenotype in Drug-Resistant TNBC after treatment with Dox or ATF-IONP-Dox

Histological analysis confirmed that Dox and ATF-IONP-Dox insensitive tumors have an increase of CD44 and Wnt ligand compared to their respective treatment sensitive tumors as seen in **Figure 2.6A**. While there is marked decrease in proliferation marker Ki67 in treatment sensitive tumors compared to no treatment control, Dox, and ATF-IONP-Dox treatment insensitive tumors, only in the ATF-IONP-Dox sensitive treated group is there an observable increase in apoptotic cells (**Figure 2.6B**).These results suggest that while there are Dox and ATF-IONP-Dox sensitive tumors, the ATF-IONP-Dox sensitive tumors not only have a reduction in CSC markers and Ki67 but also an increase in cytotoxicity indicating a more potent anti-tumor effect than Dox alone.

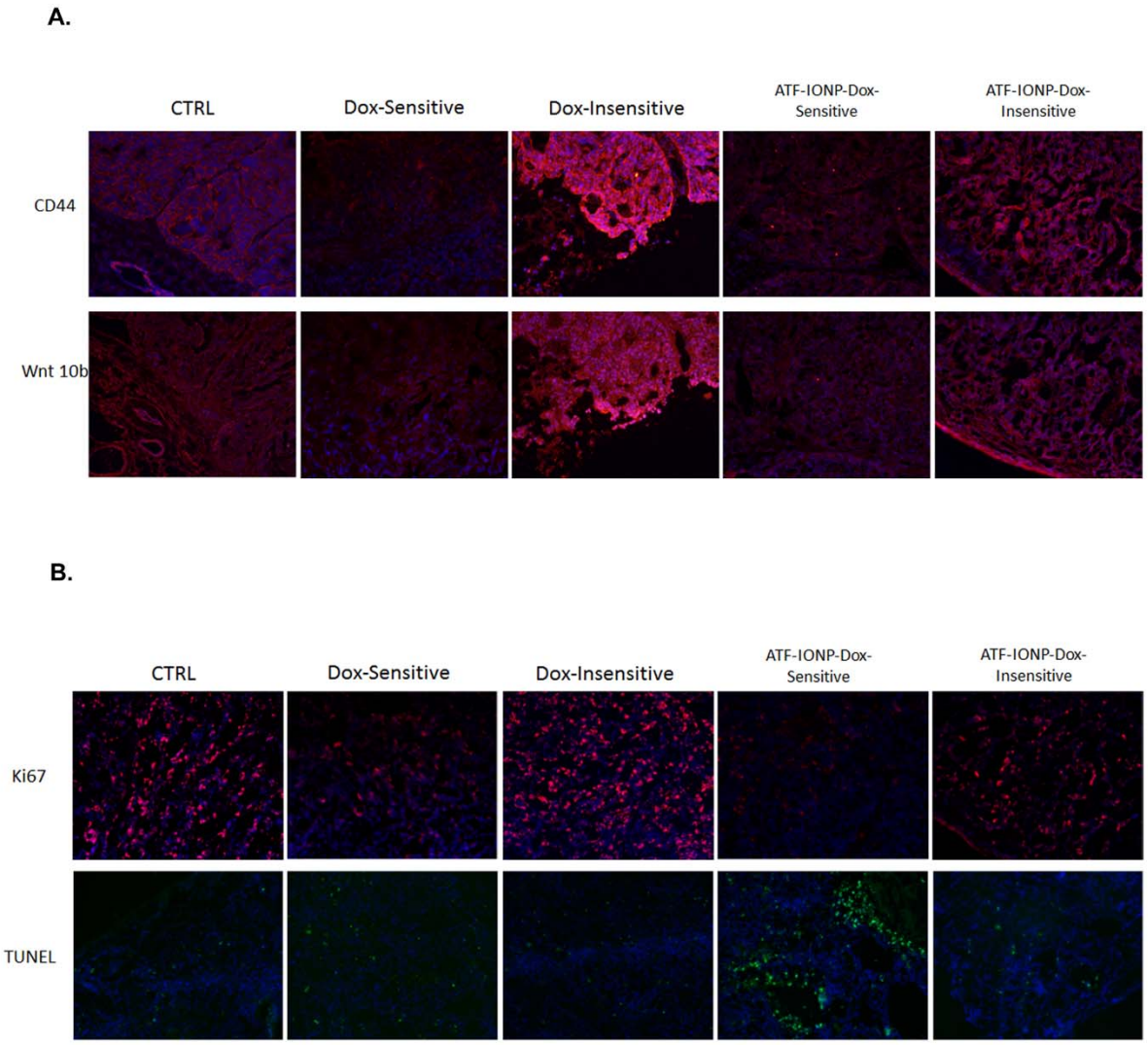

Figure 2.6. Heterogeneity of CSC phenotype, cell proliferation, and cell death in Dox and ATF-IONP-Dox treated tumors in drug-resistant TNBC.

A-B. Immunofluorescence labeling. Frozen tissue sections of the PDX tumors from Patient #1 passage 1 were labeled with anti-Wnt10b, anti-CD44, and anti-Ki67 primary antibodies and Alexafluor-555 conjugated secondary antibody (red). Blue: Hoechst 33342 nuclear background staining. TUNEL labeling of apoptotic cells (green).

2.3.6 Heterogeneity of targeted delivery of ATF-IONP-Dox in TNBC PDX Tumors

To determine whether there was a difference in the delivery of ATF-IONP-Dox in tumors that were sensitive to ATF-IONP-Dox treatment and tumors that were insensitive to treatment, NIR830 dye was conjugated on the ATF-IONP-Dox nanoparticles and optical imaging was conducted on the treated mice. Accumulation of NIR830-ATF-IONP-Dox was observed in both treatment sensitive and insensitive tumors as shown in **Figure 2.7A**. This indicates that ATF-IONP-Dox is delivered to the tumor site.

To further elucidate whether there is a difference in delivery of ATF-IONP-Dox in sensitive and insensitive tumors we examined the accumulation of the nanoparticle within the tumor. In treatment-sensitive tumors we observed an accumulation of ATF-IONP-Dox within the tumor cells as well as the tumor stroma as shown in **Figure 2.7B**. While ATF-IONP-Dox accumulated in the stroma of treatment insensitive tumors, there was minimal observation of ATF-IONP-Dox within the tumor cells. These results indicate that there is heterogeneity in ATF-IONP-Dox delivery within the TNBC PDX model. While ATF-IONP-Dox can be delivered to all tumors, the ability of the ATF-IONP-Dox to penetrate to the tumor cells is lacking in treatment insensitive tumors.

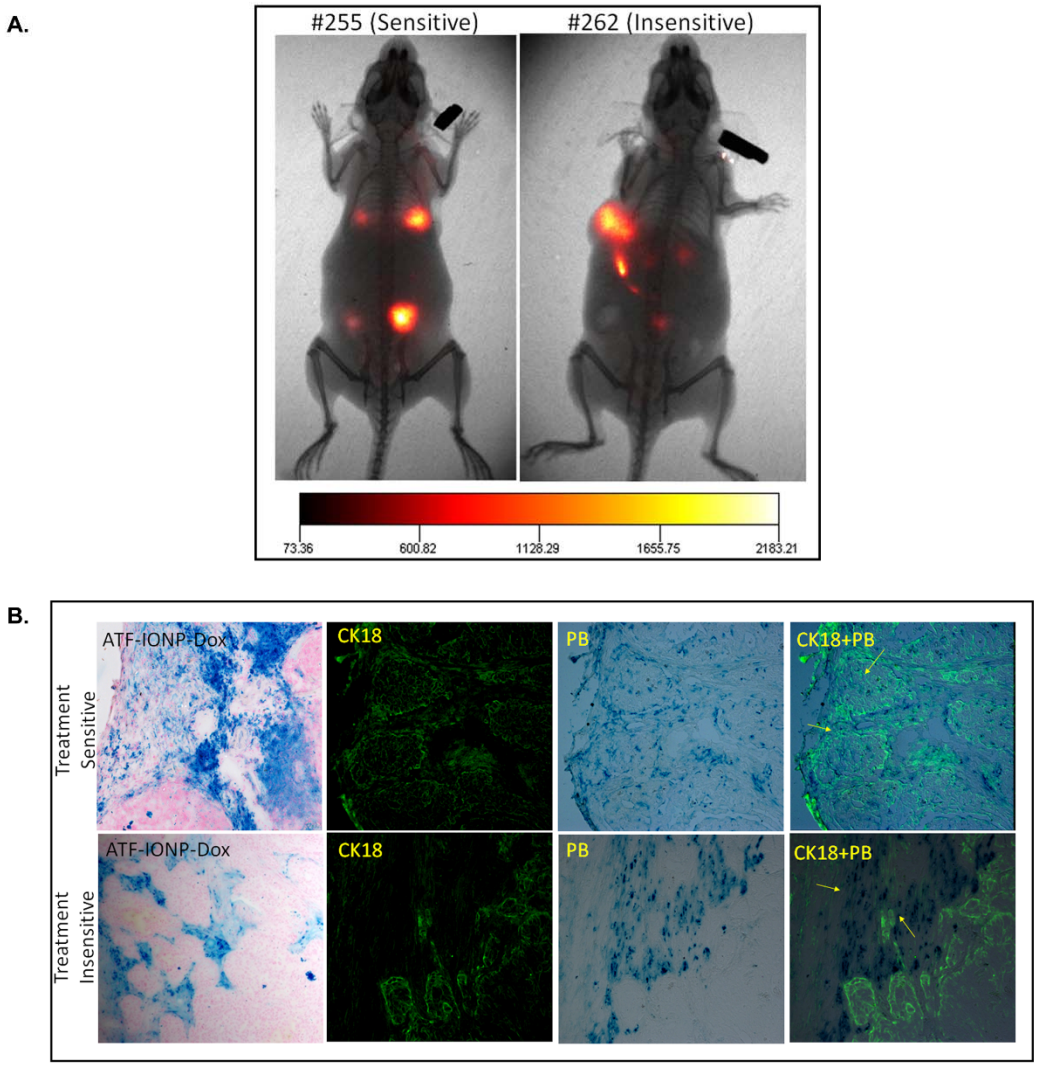

Figure 2.7. Heterogeneity of targeted delivery of ATF-IONP-Dox into orthotopic TNBC PDX tumors in nude mice by optical imaging.

A. The whole body NIR imaging of mice sensitive and insensitive to ATF-IONP-Dox treatment 48 hours after IONP administration. Optical images were overlaid with bright-field images of the mice. **B**. Prussian Blue staining and CK18 labeled frozen tissue sections from ATF-IONP-Dox treated tumors showing the colocalization of IONP and tumor cells indicated by yellow arrows.

2.3.7 Intra- and Inter- Phenotypic Characteristics of Drug-Resistant TNBC after treatment with Dox or ATF-IONP-Dox

The heterogeneity observed in our drug-resistant TNBC PDX model was observed within the same patient at different passages and in different patients. Each treatment group had tumors that were sensitive to treatment, determined by tumor regression, or insensitive to treatment with notable tumor progression. Tumors that were sensitive to treatment were characterized by having tumor volumes of less than 500 mm^3 by the end of treatment, while tumors insensitive to treatment ranging from 500 mm^3 to 2000 mm^3 (**Figure 2.8A**). Dox and ATF-IONP-Dox insensitive tumors in PDX of patient #1 passage 4, patient #1 passage 7 and patient #6 passage #1 had an increase in expression of Wnt/β-catenin pathway receptor LRP5/6 and ligand Wnt1 (**Figure 2.8B**). uPAR expression remained high in both the treatment sensitive and treatment insensitive tumors.

Taken together, these results indicate that using ATF-IONP-Dox can effectively target uPAR in a drug-resistant TNBC PDX model leading to an anti-tumor effect resulting in an increase in overall survival, an increase in recurrence-free survival, and a decrease in tumor aggression. Tumors that were resistant to treatment with free Dox or ATF-IONP-Dox had increased expression of the Wnt/β-catenin pathway components including Wnt receptor LRP5/6. Further investigation is required to determine the effectiveness of LRP5/6 as a target to overcome drug resistance in TNBCs.

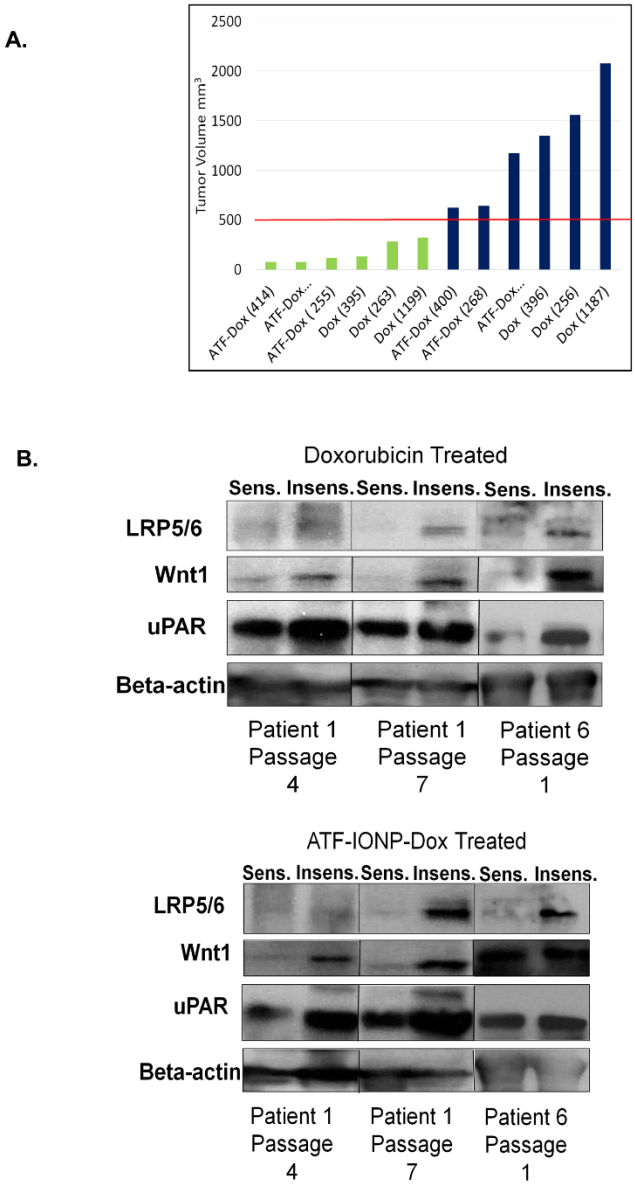

Figure 2.8. Evaluation of Intra- and Inter- Phenotypic Characteristics of Drug-Resistant TNBC after treatment with Dox or ATF-IONP-Dox

Nude mice bearing orthotopic TNBC PDX tumors derived from TNBC patient #1 and #6 received 5 mg/kg Dox i.v. once per week for 5 weeks. **A**. Representative final tumor volume of selected tumors in mice for three treatment studies using PDX tumors from Patient #1 at Passage 4 and Passage 7, and in Patient #6 at Passage 1. Within the PDX tumors from the same patient, there were tumors sensitive to Dox treatment and those that were insensitive to the treatment. Red line indicating tumor volume of 500 mm^3 **B**. Tumor tissue lysates from Dox or ATF-IONP-Dox sensitive (Sens.) and Dox or ATF-IONP-Dox insensitive (Insens.) were immunoblotted with anti-LRP5/6, anti-Wnt-1 and anti-uPAR antibodies. β-actin was used as a loading control.

2.4 Discussion

Patient derived xenograft models are increasingly becoming the standard for determining treatment efficacy of novel therapies. The ability of a PDX to recapitulate human tumors more closely than a cell-line derived model allows for more robust studies of drug response and drug-resistance. Due to popularity and demand, there are currently over 500 commercially available stable and transplantable PDX models of breast cancer [166]. Our results show that PDX models are also able to generate phenotypically heterogeneous tumors within a model of the same patient. This is not surprising since PDX models are generated by implanting tumor fragments into immunocompromised mice and even within the same tumor gene expression signatures can vary with different regions having signatures of good and poor prognosis [167].

Within the TNBC subtype is a genomic diversity that results in highly heterogeneous phenotypes and varying responses to treatment. It is important then for there to be heterogeneity within models of drug-resistant TNBC. These models can be used for the identification of drivers of drug-resistance which are important in order to develop treatments with long-lasting effect. Using our drug-resistant TNBC PDX models we were able to identify the Wnt/β-catenin pathway receptor, LRP5/6, as being overexpressed in tumors that were insensitive to Dox and ATF-IONP-Dox treatment. Targeting the Wnt/β-catenin pathway is attractive in drug-resistant TNBC because components of the Wnt/β-catenin pathway have been shown to be overexpressed in TNBC [85].

While our results support further investigation into the development of a uPAR-targeted nanoparticle for the treatment of drug-resistant TNBC, our findings also support the

development of a Wnt-targeted nanoparticle to further enhance the therapeutic response in drug-resistant TNBC. Additional studies will need to be conducted to determine the effectiveness of Wnt receptor-targeted drug delivery systems for drug-resistant TNBC.

Chapter 3: Dual-targeting Wnt and uPA Receptors inhibits Cancer Stem-Cell Phenotype in Chemo-Resistant Breast Cancer

Jasmine Miller-Kleinhenz[1], Xiangxue Guo[1], Weiping Qian[1], Hongyu Zhou[1], Erica N. Bozeman[1], Lei Zhu[1], Xin Ji[2], Y. Andrew Wang[2], Toncred Styblo[1], Ruth O'Regan[3], Hui Mao[4], and Lily Yang[1*]

[1]Winship Cancer Institute, Department of Surgery, Emory University School of Medicine, Atlanta, GA, [2]Ocean Nanotech, San Diego, CA, [3]University of Wisconsin Carbone Cancer Center, Madison, WI, [4]Department of Radiology and Imaging Sciences, Emory University School of Medicine, Atlanta, GA.

This chapter is adapted from a manuscript submitted by J Miller-Kleinhenz, X Guo, W Qian, H Zhou, EN Bozeman, L Zhu, YA Wang, T Styblo, R O'Regan, H Mao and L Yang. *Dual-targeting Wnt and uPA Receptors Using Peptide Conjugated Ultra-small Nanoparticle Drug Carriers Inhibited Cancer Stem-Cell Phenotype in Chemo-Resistant Breast Cancer.* Revised and under review at *Biomaterials*, 2017.

3.1 Abstract

Heterogeneous tumor cells, high incidence of tumor recurrence, and decrease in overall survival are major challenges for the treatment of chemo-resistant breast cancer. Results of our study showed differential chemotherapeutic responses among breast cancer patient derived xenograft (PDX) tumors established from the same patients. All doxorubicin(Dox)-resistant tumors expressed higher level of cancer stem-like cell biomarkers, including CD44, Wnt and its receptor LRP5/6, relative to Dox-sensitive tumors. To effectively treat resistant tumors, we developed an ultra-small magnetic iron oxide nanoparticle (IONP) drug carrier conjugated with peptides that dually targeted to Wnt/LRP5/6 and urokinase plasminogen activator receptor (uPAR). Our results showed that simultaneous binding to LRP5/6 and uPAR by the dual receptor targeted IONPs was required to inhibit breast cancer cell invasion. Molecular analysis revealed that the dual receptor targeted IONPs significantly inhibited Wnt/β-catenin signaling and cancer stem-like phenotype of tumor cells, with marked reduction of Wnt ligand, CD44 and uPAR. Systemic administration of the dual targeted IONPs led to nanoparticle-drug delivery into PDX tumors, resulting in stronger tumor growth inhibition compared to non-targeted or single-targeted IONP-Dox in a human breast cancer PDX model. Therefore, co-targeting Wnt/LRP and uPAR using IONP drug carriers is a promising therapeutic approach for effective drug delivery to chemo-resistant breast cancer.

3.2 Introduction

Breast cancer is the most commonly diagnosed form of cancer in women worldwide [168]. Chemotherapy remains the main therapeutic option for the treatment of breast cancer patients with metastatic diseases or that have the triple negative breast cancer (TNBC) subtype which lacks expression of estrogen receptor, progesterone receptor, and HER2. Unfortunately, a high percentage of those cancer patients are resistant to chemotherapy. The presence of residual chemo-resistant tumors following neoadjuvant therapy is one of the most important prognostic factors for tumor recurrence and short survival regardless of hormone receptor status, adjuvant hormone therapy, or pathologic stage of residual disease [169]. Therefore, the development of effective therapies for overcoming chemo-resistance is a critical unmet need.

Breast cancer tissues have been found to contain a sub-population of cancer stem-like cells (CSCs) or progenitor cells, which are identified as $CD44^{high}/CD24^{low}$ and are an important cell population to investigate when developing therapies for chemo-resistant breast cancers [89,90]. Breast cancers that are enriched with the CSC population appear to be more drug resistant and are associated with a poorer prognosis [91,92,170]. Because of their self-renewal capacity, failure to eliminate CSCs may mediate a patient's relapse. These recurrent tumors not only are resistant to the initial treatment but also exhibit a more aggressive phenotype than that of the original tumor. Therefore, more potent therapeutic agents are needed to treat drug-resistant breast cancer.

The Wnt/β-catenin pathway is involved in the regulation of proliferation and migration of tumor cells, the epithelial-mesenchymal transition, and the maintenance of stemness in cancer stem cells [79–82]. When the Wnt/β-catenin pathway is inactive, cytosolic β-catenin is modified by a complex consisting of adenomatous polyposis coli (APC) and Axin, which promotes phosphorylation of β-catenin by casein kinase-1 (CK1) and glycogen synthase kinase 3 (GSK3). Phosphorylated β-catenin is then ubiquitinated and degraded [83]. Upon Wnt ligand binding to co-receptors LRP5/6 and Frizzled, the Wnt/ β-catenin pathway is activated and β-catenin is freed from the APC/Axin destruction complex and accumulates in the nucleus where it binds to transcription factors to activate gene transcription. However, it has been shown that Axin is a multifunctional signal molecule that interacts with the Wnt-induced Frizzled-LRP6-DisheveIled complex to mediate GSK3 phosphorylation of LRP6, initiating activation of the Wnt signaling [171].

Phase 1 clinical trials to develop targeted therapies for the Frizzled receptor, such as Vantictumab, have been completed in solid tumors [172,173]. There are currently no LRP5/6 targeted therapies, though LRP6 has been shown to have an important role in Wnt pathway activation in breast cancer [174]. Upregulation of LRP6 has been found in a variety of solid tumors and, when overexpressed, LRP6 has been shown to promote tumorigenicity, cell invasion, and metastasis [175,176]. Studies in breast cancers have also shown that inhibition of Wnt/β-catenin signaling by blocking LRP6 resulted in the reduction in the ability of cancer cells to self-renew and for tumor cells to undergo epithelial to mesenchymal transition, resulting in suppression of tumor growth [174,177–179].

The urokinase plasminogen activator system, consisting of urokinase plasminogen activator (uPA) and its receptor uPAR, is also a target of interest in breast cancer. Binding of uPA to uPAR leads to the activation of plasminogen to plasmin, and then proteases, such as matrix metalloproteinases, which promote tumor cell invasion and metastases. Expression of uPA and uPAR have been identified as biomarkers associated with the development of recurrent and/or metastatic breast cancers [160]. Inhibition of uPAR decreased cell viability, migration, and cell invasion of breast cancer cells [156]. Overexpression of uPAR induced cancer stem-like properties in breast cancer and led to the activation the Wnt/ β-catenin pathway [180,181]. It has been shown that uPAR can bind to β-catenin in the cytoplasm and enter the nucleus to facilitate β-catenin-mediated gene transcription while inhibition of uPAR reduced the level of expression of Wnt/ β-catenin signal activated genes [181]. On the other hand, activation of Wnt/β-catenin signal pathway also increased the level of uPAR expression [182].

To develop a new therapy targeting chemo-resistant and stem-like breast cancer cells that have high levels of Wnt receptors and activated Wnt signaling, we designed a Wnt receptor LRP5/6 binding peptide (iWnt) based on the LRP5/6 binding region of Dickkopf-related protein-1 (DKK1). Previous studies showed that the binding of DKK1 to LRP5/6 inhibited the activation of Wnt/β-catenin pathway [183]. A DKK1 derived peptide should be a good mediator for both inhibition of Wnt signaling and delivery of nanoparticle drug carriers into tumor cells since the formation of the complex of DKK1, LRP6 and Kremen-2 induced endocytosis [184]. Therefore, the iWnt peptide conjugated nanoparticle was expected to block WNT/β-catenin signaling and allow targeted drug delivery into cancer stem-like cells.

To improve tumor cell targeting, facilitate internalization for drug delivery, and enhance the effect on inhibition of Wnt signaling in cancer stem-like cells, we developed a dual Wnt/LRP5/6 and uPAR targeted nanoparticle by conjugating both iWnt and uPAR targeting ATF_{24} peptides with three histidine residues (His tag) to nitrilotriacetic acid-copper (NTA-Cu) modified and amphiphilic polymer coated iron oxide nanoparticles (IONPs). We then evaluated the effect of conventional chemotherapy drugs and targeted nanoparticle drug carriers in human chemo-resistant breast cancer tissue derived tumor xenograft (PDX) models in nude mice. Here we report that chemo-resistant breast cancer PDX tumors exhibit heterogeneity in response to the chemotherapeutic drug, doxorubicin (Dox). We found that Dox-resistant breast cancers have increased levels of Wnt receptor LRP5/6 and uPAR expression compared to drug-sensitive tumors. Treatment of human breast cancer cells *in vitro* with the dual Wnt/LRP and uPAR-targeted nanoparticles reduced $CD44^{high}/CD24^{low}$ cancer stem cell population, and inhibited the epithelial to mesenchymal transition, resulting in decreased cell invasion. We further found that systemic delivery of the dual-targeted nanoparticles carrying Dox led to targeted delivery and inhibited the Wnt/β-catenin pathway, cancer stem cell phenotype, and tumor growth in the chemo-resistant breast cancer PDX models. Our results demonstrated that the NTA-Cu modified ultra-small IONP provides a drug delivery platform for the development of targeted nanoparticles using peptide-based targeting ligand and/or therapeutic peptides. The dual receptor targeted nanoparticle drug carrier developed in this study has the potential to provide new molecular targeted nanoparticle drug delivery systems for the treatment of chemo-resistant breast cancer.

3.3 Materials and Methods

Production of Wnt/LRP and/or uPAR targeted IONPs.

The designs of LRP targeting peptide derived from DKK1, iWnt, and uPAR targeting peptide derived from human uPA, ATF_{24}, are shown in **Figure 3.2**. His-tagged iWnt and ATF_{24} peptides were chemically synthesized by Pepmic Co (Suzhou, Jiangsu, China). To retain a high affinity binding of the short peptides when conjugating to nanoparticles, we used NTA-Cu--conjugated and amphiphilic polymer-coated IONPs with a core size of 5 nm (Ocean NanoTech, LLC, San Diego, CA, USA). To prepare NTA-Cu-IONP conjugates, the carboxylic groups available on the surface of IONPs were first activated via 1-ethyl-3(3-dimethylaminopropyl)-carbodiimide (EDC)/ *N*-hydroxysulfosuccinimide (Sulfo-NHS) coupling, followed by reaction with NTA-Cu complex (**Figure 3.2**). The mixture was further incubated at room temperature for 4 hours. The conjugates were then separated from unbound NTA-Cu and byproducts using a PD-10 size-exclusion column. His tagged peptides were conjugated to NTA-Cu on the IONP surface to retain a high binding affinity. ATF_{24}, iWnt, or a combination of ATF_{24} and iWnt were incubated with NTA-Cu-IONPs at a molar ratio of peptide to IONP of 20:1 for single-targeted and a 10:10:1 peptides to IONP for dual-targeted in 10 mM Borate buffer (pH 8.5) to produce iWnt-IONPs, ATF_{24}-IONPs, or iWnt-ATF_{24}-IONPs. The reaction was carried out for 1.5 hours at 4^0C. The final peptide-IONPs were purified using a Nanosep 100 K column for 5 min at 3000 RPM. Some targeted IONPs were labeled with NIR-830 dye for optical imaging. NIR-830–maleimide dye [185] as incubated with iWnt or ATF_{24} peptide with C-

terminal cystine. NIR-830 labeled peptides were then mixed with NTA-Cu-IONP as described as the above.

Encapsulation of Doxorubicin to IONPs.

Dox dissolved in DMSO (10 mg/ml stock solution) was added into the peptide-IONP conjugates at a ratio of 1 mg of Dox: 3 mg of iron equivalent IONP in 10 mM borate buffer (pH 8.5). The loading of Dox was carried out for 3 hours at 4^0C. The final peptide-IONPs loaded with Dox were purified using a Nanosep 100 K column.

His-tag bead Pulldown Assay

Using Pierce His Protein Interaction Pull Down Kit by ThermoFisher Scientific (Waltham, MA), 30 μg of iWnt or ATF_{24} 3x-his-tagged peptides was added to 100 μl of Cobalt resin beads and rotated for 3 hours at room temperature. 250 μg of protein from MDA-MB-231 cell lysate was then added to the bead : peptide mixture and incubated at 4 ^{0}C for 1 hour. The bead : peptide : protein mixture was then washed 5 times. Protein was then eluted using an imidazole elution buffer. Western blot analysis was conducted on eluted proteins to determine interacting proteins.

Specific binding and uptake of iWnt-ATF_{24}-IONP by breast cancer cells.

The MDA-MB-231 human breast cancer cell line was cultured in an 8-well chamber slide with a density of 50,000 cells/well for 24 hours, 4 μg/mL of iron equivalent IONP solution of iWnt-IONPs, ATF_{24}-IONPs, iWnt-ATF_{24}-IONPs or nontargeted IONPs was then added. Cells were incubated with the IONPs for 6 hours and then washed three times with cold PBS to remove unbound nanoparticles. Cells were then fixed with 4% paraformaldehyde

in PBS, and Prussian blue staining was used to determine the presence of IONPs in the cells.

Prussian blue staining.

Fixed cells were incubated with a mixture of 10% potassium ferrocyanide(II) trihydrate and 10% HCl solution for 3 hours at 37^{0}C. After being washed three times with distilled water, cells were counterstained with nuclear fast red solution for 5 min. Following consecutive dehydrations with 70% and 100% EtOH and two rinses in xylene, the slides were mounted. Result of Prussian blue staining was examined under a light microscopy.

Competition assay to determine specific binding of iWnt-IONP and iWnt-ATF$_{24}$-IONP to LRP5/6 in breast cancer cells.

MDA-MB-231 cells were cultured in a 24-well plate at a density of 100,000 cells/well. After 24 hours of plating, cells where treated with 50 μM or 100 μM of NCI8642 (Gallocyanine) purchased from Santa Cruz Biotechnology (Santa Cruz, CA) for 1 hour at room temperature. Cells were then washed twice with PBS. 20 pmol of NIR-830-labeled iWnt-IONP and iWnt-ATF$_{24}$-IONP were added for 2 hours at 4 ^{0}C. Cells were then washed twice with PBS and stored at 4 ^{0}C. Images were taken and analyzed using fluorescence microscopy (Keyence, USA).

Cell proliferation assay.

MDA-MB-231 cells were cultured in a 96-well plate at a density of 6,000 cells/well. After 24 hours of plating, different targeted IONP or IONP conjugates were diluted in the culture medium and added to cell culture. For examination of the effect of IONP carrying Dox,

0.1 μg/mL of Dox equivalent concentration of IONP-Dox or targeted IONPs was added into cell cultures. Unconjugated Dox was used as a treatment control. After incubating for 6 hours when IONP bound to and entered into tumor cells, cells were washed three times with cold PBS to remove unbound IONPs. A 100 μL of fresh medium was then added to the plate. Cells were incubated for an additional 72 hours, and viability of the cells was determined by the Alamar Blue assay (Life Technologies, NY, USA). Cells treated with culture medium alone were used as the no-treatment control. Results shown are the mean value of three repeat studies.

Immunofluorescence labeling.

Frozen tissue sections of tumor and normal tissues were used for immunofluorescence labeling. The following antibodies were purchased from Santa Cruz: goat anti-Wnt1 (G-19; no. sc6280, 1:200), rabbit anti-Axin (H-19; no. sc14029, 1:500), rabbit anti-uPAR (FL-290; no. sc10815, 1:200), and goat anti-HCAM (CD44) (N-18; no.sc7051, 1:200). The following antibodies were purchased from eBioscience (Cambridge, MA): mouse/rat anti-Ki67 (no. 14-5698-82, 1:200). Mouse anti-E-cadherin (no. 610181, 1:200) was purchased from BD Biosciences. Alexa Fluor 555 dye (red fluorescence, dilution 1:500) labeled secondary antibodies (Invitrogen) were used to detect biomarker-positive cells. Images were taken using fluorescence microscopy (Keyence, USA).

Invasion chamber assay.

Cells were pre-treated with 4 μg/mL of iron equivalent IONP solution of iWnt-IONPs, ATF_{24}-IONPs, iWnt-ATF_{24}-IONPs or nontargeted IONPs for 6 hours. Treatment was then

removed by replacment with culture medium with 2% serum for 24 hours. Cells were then plated in serum-free media in BD BioCoat Matrigel Invasion Chambers (BD Biosciences) (5×10^4 cells/ml) with 0.75 ml of chemoattractant (culture media containing 10% FBS) in the wells for 24 hours. Non-invading cells were removed from the interior surface of the membrane by scrubbing gently with a dry cotton-tipped swab. Each insert was then transferred into 100% methanol for 10 minutes followed by Crystal Violet staining for 20 minutes. Membranes were washed in water and allowed to air dry completely before being separated from the chamber. Membranes were mounted on slides with Permount permanent mounting medium (Fisher Scientific, Waltham, MA). Multiple photographs of each sample were taken at ×20 magnification, with triplicates performed per treatment group. The number of cells was counted in each field; the sum of the fields was calculated for each sample. Experiments were performed three times with reproducible results.

Western blot analyses.

MDA-MB-231 cells were incubated with 20 pmol of single-targeted iWnt-IONP, ATF_{24}-IONP or iWnt-ATF_{24}-IONPs for 6 hours and then cells were placed in fresh complete media at 37 ^{0}C for 48 hours. Cells were lysed in radioimmunoprecipitation assay buffer (Cell Signaling Technology, Danvers, MA) supplemented with protease and phosphatase inhibitors (Sigma-Aldrich). Total protein extracts were run on SDS-PAGE gel and blotted onto polyvinylidene difluoride (PVDF) membrane. Blots were probed overnight. The following antibodies were purchased from Santa Cruz: rabbit anti-Wnt10b (H-70; no. sc25524, 1:500), rabbit anti-phospho-LRP6 (H-300; no. sc15399, 1:500), rabbit anti-Axin (H-98; no. sc14029, 1:500), rabbit anti-β-catenin (H-102; no. sc7199 1:500), rabbit anti-

uPAR (FL-290; no. sc10815, 1:500), goat anti-HCAM (CD44) (N-18; no.sc7051, 1:500), and rabbit anti-CD24 (FL-80; no. sc11406, 1:500). The following antibodies were purchased from eBioscience (Cambridge, MA): mouse/rat anti-Ki67 (no. 14-5698-82, 1:500). Rabbit anti-non-phosphorylated (active) β-catenin (S33/S37/T41; no. D13A1, 1:500) and Rabbit anti-phospho-GSK3 β (S9; no 9336, 1:500) was purchased from Cell Signaling Technologies. Mouse anti-E-cadherin (no. 610181, 1:500) was purchased from BD Biosciences. Mouse anti-*β*-actin was purchased from Sigma-Aldrich (AC-15, 1:10,000). All primary antibodies were diluted in Tris-buffered saline and Tween 20. Goat anti-mouse secondary IgG-HRP antibody (no. sc-2005, 1:3,000), goat anti-rabbit secondary IgG-HRP antibody (no. sc-2004, 1:3,000), and donkey anti-goat secondary IgG-HRP antibody (no. sc-2020, 1:3,000) were purchased from Santa Cruz Biotechnology (Santa Cruz, CA). Protein bands were detected using ECL.

Cell cycle analysis.

MDA-MB-231 cells were cultured in a 6-well plate at a density of 300,000 cells/well using serum-free DMEM media from Corning (Manassas, VA) for 48 hours. Cells were then treated with 4 μg/mL of iron equivalent IONP solution of iWnt-IONPs, ATF_{24}-IONPs, iWnt-ATF_{24}-IONPs or nontargeted IONPs for 6 hours. After removing IONP agents, cells were placed in fresh complete media at 37˚C for 48 hours. Cells were then trypsinized and washed with PBS. Cells were then fixed in ice-cold 70% ethanol and placed in -20 ^{0}C overnight. Cells were then washed in PBS and re-suspended in PI/RNase buffer from BD/Bioscience (San Diego, CA) for 30 minutes at room temperature. Incorporation of PI was then measured using flow cytometry.

Dox Cell Uptake

MDA-MB-231 cells were cultured in an 8-well chamber slide overnight to reach 70% confluency. Cells were treated with 0.1 μg/mL of Dox equivalent concentration of IONP-Dox or targeted IONPs for 4 hours at 37 ^{0}C, then washed three times with cold PBS to remove unbound nanoparticles. Cells were then fixed with 4% paraformaldehyde in PBS. To determine the presence of Dox in the cells, cells were excited at 488 nm. Images were taken and analyzed (Keyence, USA).

Establishment of orthotopic human chemo-resistant breast cancer PDX tumor models in nude mice.

Fresh tumor tissues were collected from surgically resected tumors from breast cancer patients who completed neoadjuvant therapy and had large residual tumors using an Emory Institutional Review Board approved protocol (IRB#00071700). Breast cancer patient #1 had neoadjuvant therapy using Sorafenib in combination with Cisplatin followed by dose dense Paclitaxel. Breast cancer patient #6 had neoadjuvant therapy using Dox followed paclitaxel. Breast cancer patient #7 received the combination of Paclitaxel and Cyclophosphamide.

Within 2 hours of surgical resection, tumor tissues were cut into 1-2 mm fragments and implanted into the mammary fat pad of immune deficient SCID mice (8 to 10 weeks old, female) using a surgical procedure approved by Emory Institutional Animal Care and Use Committee (IACUC). Excess tissues were frozen in liquid nitrogen and stored for further

pathological analysis. After surgery, the tumor growth in the mice was monitored by a caliper weekly. Orthotopic tumors grew to 5 to 10 mm diameter in about 8 to 10 weeks. These PDX tumors then were harvested, and tumor fragments at 1 to 2 mm sizes were then implanted into the mammary fat pad of 6- to 8-week-old female nude mice for large-scale studies.

In vivo targeting and imaging.

Tumor bearing mice were subjected to NIR optical imaging 48 and 72 hours after the tail vein injection of 800 pmol of NIR-830-labeled iWnt-IONPs, ATF_{24}-IONPs, or iWnt-ATF_{24}-IONPs into the tumor-bearing mice. NIR optical imaging was conducted using the IVIS Spectrum *in vivo* imaging system (Perkin Elmer, Waltham, MA, USA). Mice were sacrificed and tumors and normal organs were collected for *ex vivo* optical imaging. All optical images were captured using an 800 nm excitation and 850 nm emission filter set with 3 min exposure time and a gamma value of 0.2. Optical images were analyzed using the software provided by the IVIS imaging system.

In Vivo effect of nanoparticle-Dox treatment.

IONP-Dox, iWnt-IONP-Dox, ATF_{24}-IONP-Dox, or iWnt-ATF_{24}-IONP-Dox was injected at 5mg/kg Dox equivalent dose via the tail vein into the nude mice bearing the first passage of breast cancer patient #7 PDX tumors every 3-4 days for a total of 3 treatments. Three days after final treatment, tumors were harvested and weighed. Western blot and immunofluorescence analysis were performed on tumor tissue lysates and frozen tissue sections.

3.4 Results:

3.4.1 Chemo-resistant breast cancer cells have upregulated levels of biomarkers associated with cancer stem cells.

To identify cell surface molecular targets for the development of novel targeted therapies for chemo-resistant breast cancer, we established orthotopic human breast cancer PDX models derived from surgically resected residual chemo-resistant breast cancer tissues in patients following neoadjuvant therapy. The PDX tumors were passaged in nude mice and *in vivo* studies were conducted using the passage number as indicated in **Figure 3.1**. Dox treatment was started once PDX tumors reached to tumor volumes around 50-100 mm^3. Following treatment with 5 mg/kg of Dox weekly for 5 treatments, we observed differential responses of the PDX tumors derived from the same breast cancer patients. Within the group of 6 mice that were treated with the same dose and schedule of Dox, PDX tumors showed significant differences in growth inhibition with drug sensitive tumors being 70 to 90% smaller than the resistant tumors. We selected representative tumor tissues that had significant tumor growth inhibition or stable tumor volume following the treatment to be Dox-sensitive, while those that had progressive tumor growth were determined to be Dox-resistant (**Figure 3.1A**). This heterogeneous response was observed both within the same patient's xenograft tumors at different passages and among different patient xenograft tumors. **Figure 3.1** shows examples of results in the PDX tumor bearing mice that were selected from Western blot analysis. We found that Dox-resistant tumors had an increase in expression of Wnt/β-catenin pathway receptor LRP5/6 and ligand Wnt1 as well as a high

level of uPAR expression compared to Dox-sensitive tumors (**Figure 3.1B**). In addition, a significant increase in Wnt10b ligand, which has been shown to induce Wnt/β-catenin activity and is significantly correlated with larger tumor size and poor survival in TNBC [186], was found in the Dox-resistant tumor tissues. High levels of cancer stem-like marker, CD44, were also detected in Dox-resistant tumors compared to no treatment control or Dox-sensitive tumors (**Figure 3.1C-E**).

Discovery of the expression of Wnt/β-catenin pathway receptor LRP5/6 and uPAR in Dox resistant breast PDX tumors provided the opportunity to develop Wnt/LRP and uPAR-targeted nanoparticle drug delivery systems that can assist in overcoming drug-resistance in breast cancer.

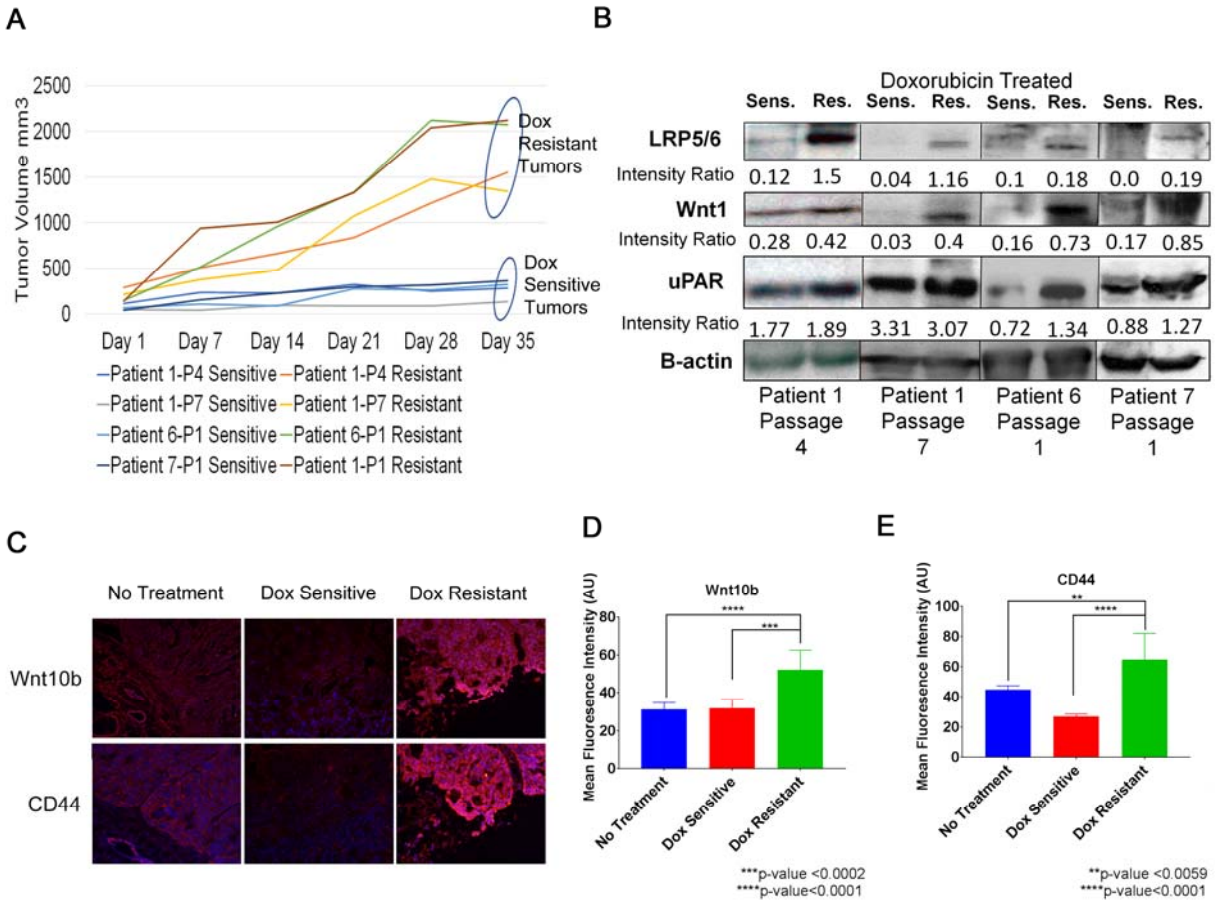

Figure 3.1: Differential tumor response to Dox treatment of human breast PDX tumors and phenotypic characterization of residual tumors following treatment

Nude mice bearing orthotopic PDX tumors derived from breast cancer patient #1, #6 and #7 received 5 mg/kg Dox via the tail vein injection once per week for 5 weeks. **A**. Representative tumor growth curves of selected tumors in mice from four treatment studies using PDX tumors from Patient #1 at Passage 4 and Passage 7, Patient #6 at Passage 1 and Patient #7 at passage 1. Within the PDX tumors from the same patient, there were tumors sensitive to Dox treatment and those that were resistant to the treatment. **B**. Tumor tissue lysates from Dox sensitive (Sens.) and Dox resistant (Res.) were immunoblotted with anti-LRP5/6, anti-Wnt-1 and anti-uPAR antibodies. β-actin was used as a loading control. Numbers of the intensity ratio shown in the Western blot were the ratio of the biomarker band relative to β-actin for each protein sample loading. **C**. Immunofluorescence labeling. Frozen tissue sections of the PDX tumors from Patient #1 passage 4 were labeled with anti-Wnt10b and anti-CD44 primary antibodies and Alexafluor-555 conjugated secondary

antibody (red). Blue: Hoechst 33342 nuclear background staining. **D-E**. Quantification of the mean fluorescence intensity of images in C was performed by Image J software. Bar graph shows the mean fluorescent intensity of six tissue sections.

3.4.2 Development and characterization of Wnt/LRP and uPAR single targeted and dual targeted IONPs

To develop a Wnt receptor targeted IONP for drug delivery and potential inhibition of the Wnt/β-catenin pathway, we designed a LRP antagonist peptide mimetic that contains the 38 to 44 amino acid sequence of the LRP binding region of Dickkopf-related protein-1 (DKK1). As described previously [187], DKK1 binds to E1 domain β-propeller of LRP5/6 through a conserved NXI sequence (**Figure 3.2A**). The inhibitor of Wnt (iWnt) DKK1 peptide mimetic has 7 amino acids from the human DKK1 sequence, including the NXI sequence, a 2-amino acid linker, and 3 histidine residuals that serve as a His-tag for conjugating the peptide to the NTA-Cu modified nanoparticle.

Results of our previous studies demonstrated that the full length amino terminal fragment (ATF, 135 aa) of uPA conjugated nanoparticles exhibited a high degree of target specificity into orthotopic tumors following systemic delivery in breast cancer mouse models for targeted tumor imaging and drug delivery [47]. The binding of ATF peptide conjugated nanoparticles to uPAR further mediates internalization of the nanoparticles [47]. In this study, we used a short peptide of the amino-terminal fragment of uPA from aa 3 to 26 (ATF_{24}) that contains the critical uPAR binding region fused with a 3-Histidine tag for nanoparticle conjugation and a unique cysteine at the amino-terminus for near-infrared (NIR) dye NIR-830-maleimide labeling (**Figure 3.2B**). The I-TASSER server [188,189] was used to generate and predict the peptide structure based on the amino acid sequence

(**Figure 3.2B**). The use of the short peptides as uPAR targeting ligands should make it possible to produce targeting peptides in a large scale by chemical synthesis and to increase the density of targeting ligands conjugated to the nanoparticle.

iWnt and ATF_{24} His-tagged peptides were conjugated to amphiphilic polymer coated IONPs (5 nm core size) modified with NTA-Cu using protocols described in the Materials and Methods. The molar ratios of IONP to peptide used for preparing the ligand conjugated IONPs were 1:20 for single targeted iWnt or ATF_{24} and 1:10:10 for the dual-targeted (iWnt and ATF_{24}) configurations as shown in **Figure 3.2C**. Targeted IONPs encapsulated with Dox were produced using our established protocol [190] (**Figure 3.2C**). Examination of the hydrodynamic size of iWnt and ATF_{24} peptide conjugated IONPs by dynamic light scattering (DLS) revealed that a polymer-coated IONP was 11.27 nm and conjugation of iWnt and ATF_{24} increased its size to 23.74 nm (**Figure 3.2D**). Loading the iWNT-ATF_{24}-IONPs with Dox lead to a slight increase in size to 25.8 nm (**Figure 3.2D**). Peptide conjugated nanoparticles have zeta potential of -30 mV (no Dox) or -34 mV (with Dox).

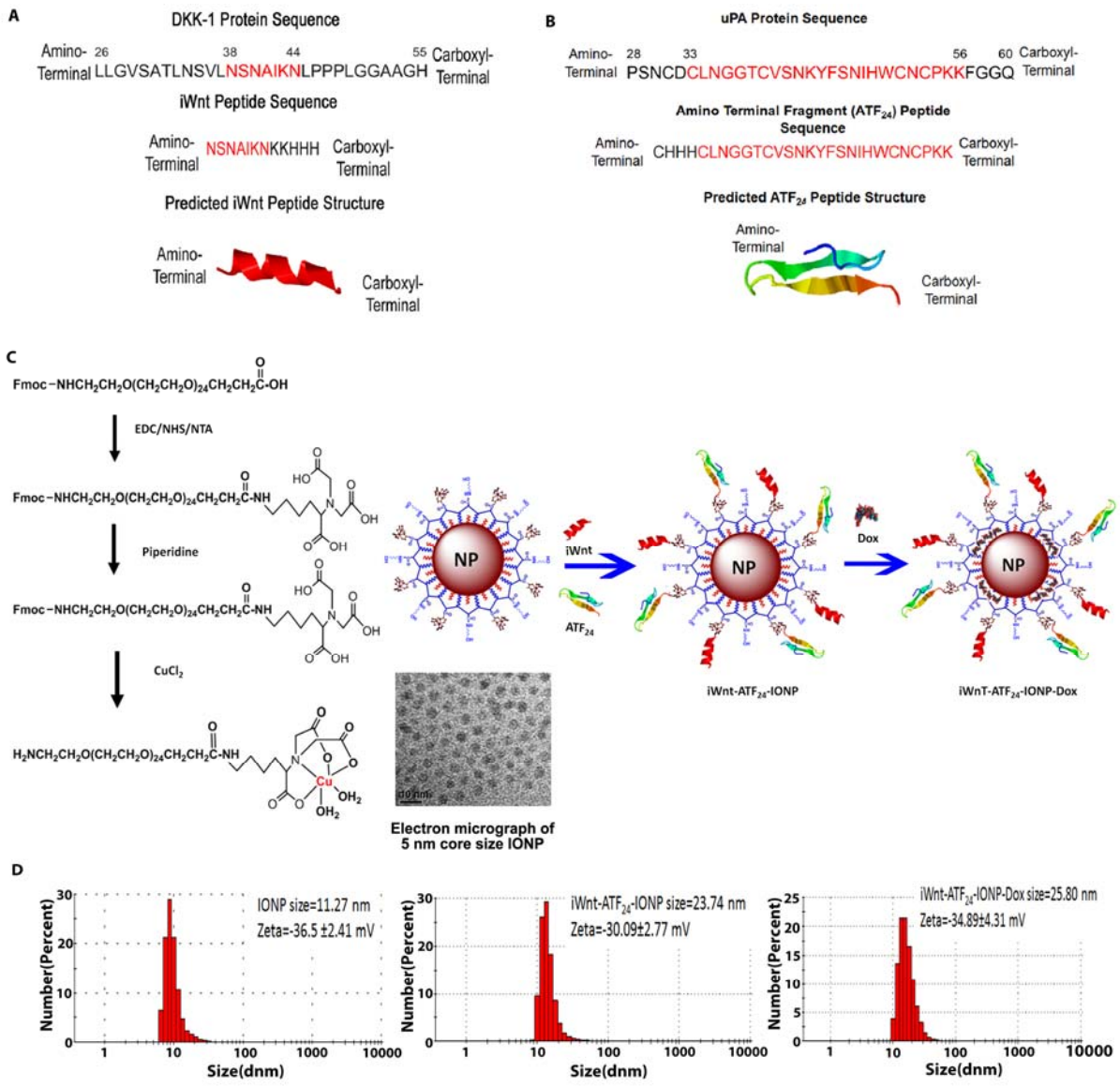

Figure 3.2: Design and preparation of Wnt/LRP and uPAR single targeted and dual targeted IONPs.

A. Sequence of the Wnt receptor targeted peptide (iWnt) derived from amino acid 38 to 44 of DKK1, a LRP5/6 receptor inhibitor. Two lysine linkers and three histidine tags were added at the carboxyl terminal. **B.** Sequence of uPAR targeted peptide (ATF_{24}) derived from the amino terminal 33 to 56 amino acid sequence of human uPA, the uPAR ligand. The predicted peptide structures of iWnt and ATF_{24} were generated using I-Tasser server (zhanglab.ccmb.med.umich.edu/I-TASSER/) [188,189]. **C**. Protocols used for the

preparation of single or dual-targeted IONPs by conjugation of iWnt and/or ATF_{24} peptides via NTA-Cu, and encapsulation of Dox into the hydrophobic layer of amphiphilic polymer coating of IONP. An electron micrograph shows uniform 5 nm core size of ultra-small IONPs. **D.** Hydrodynamic sizes and zeta potentials of IONPs, iWnt-ATF_{24}-IONPs, and iWnt-ATF_{24}-IONP-Dox were determined by the dynamic light scattering (DLS) method.

3.4.3 Characterization of iWnt and iWnt-ATF_{24} IONPs *in vitro*

First, we used a pull-down assay using NTA-Ni conjugated agarose beads to determine binding specificity of iWnt and/or ATF_{24} peptide conjugated IONPs in tumor cell lysates. Results indicated that iWnt and ATF_{24} peptides bound to their respective receptors (iWnt to LRP5/6, or ATF_{24} to uPAR) when compared to control shown in **Figure 3.3A**. Interestingly, iWnt peptide conjugated beads appeared to pull-down uPAR as well, which would indicate the possibility of the interaction between LRP5/6 and uPAR. Our result that ATF_{24} conjugated beads only pulled-down uPAR but iWnt-beads pulled-down both uPAR and Wnt/LRP suggested that a high portion of Wnt/LRP interacted with uPAR. Since the level of uPAR was much higher than that Wnt/LRP receptor in tumor cells as shown in the input sample in **Figure 3.3A**, considerable uPAR might not be associated with Wnt/LRP.

Specific binding and internalization of the iWnt and ATF_{24} conjugated IONPs to human breast cancer cells was determined using human breast cancer MDA-MB-231 cells *in vitro*. Following incubation of the non-targeted-IONPs, single or dual-targeted IONPs for 6 hours, Prussian blue staining for iron, shown in **Figure 3.3B**, revealed higher levels of

IONP in the cells incubated with targeted IONPs compared to that of non-targeted IONPs. However, there was no apparent difference between Wnt/LRP or uPAR single or dual targeted IONP treated cells.

The iWnt peptide was designed as a mimetic of the LRP5/6 inhibitor, DKK1. To demonstrate that iWnt-conjugated nanoparticle mimics DKK1 and binds to the DKK1 interaction site of the LRP, a competition assay was performed using a small molecule inhibitor of DKK1, NCI8642. NCI8642 has been shown to specifically bind to LRP5/6 at the DKK1 binding site [191]. In this assay, iWnt-IONPs or dual targeted iWnt-ATF_{24}-IONPs were labeled with a NIR 830 dye and incubated with MDA-MB-231 cells for 6 hours. By detection of NIR fluorescence signal in the cells, we found NIR fluorescence signals decreased with increasing NCI8642 concentrations, suggesting NCI8642 competing with iWnt-IONPs in binding tumor cells (**Figure 3.3C**). Quantification of fluorescence shows a significant decrease in binding of the iWnt-IONPs and dual targeted iWnt-ATF_{24}-IONPs at 50 μM and 100 μM of NCI8642 compared to no treatment control shown in **Figure 3.3C**. NCI8642 also reduced the binding of dual targeted iWnt-ATF_{24}-IONPs to cells. These results indicate that the interaction of iWnt with LRP5/6 was important for high affinity binding of dual targeted IONPs to tumor cells and addition of the ATF_{24} did not hinder iWnt binding to LRP5/6.

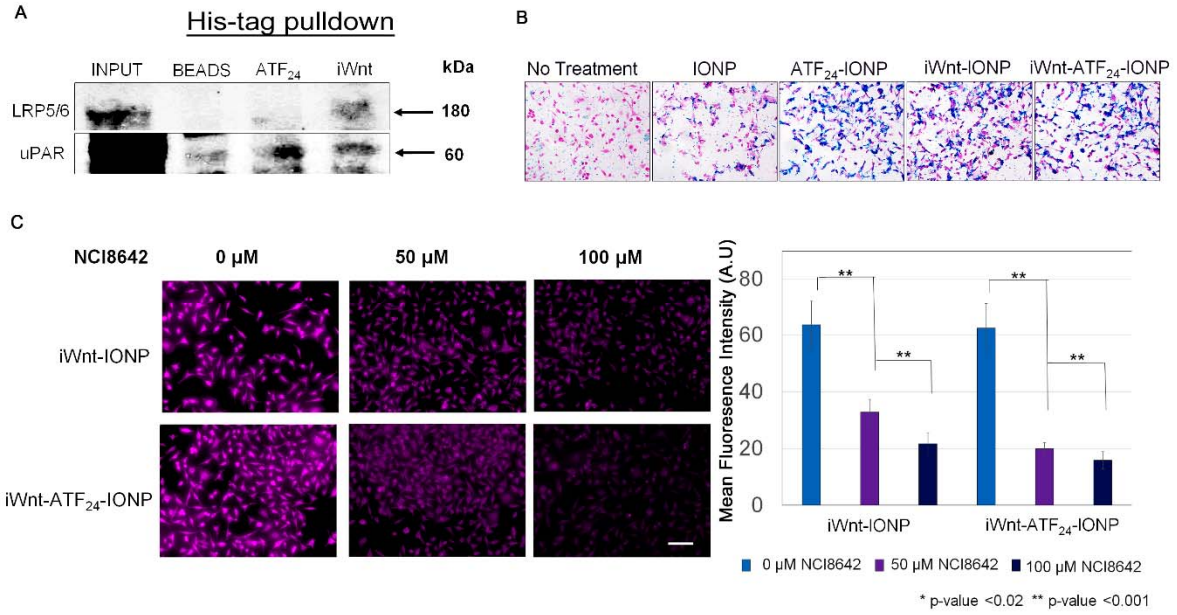

Figure 3.3: Determination of binding specificity of ATF_{24}-IONP, iWnt-IONP and iWnt-ATF_{24} IONPs in human breast cancer cells *in vitro.*

A. Agarose beads were used to conjugate the His-tagged iWnt and ATF_{24} peptides and then pull-down LRP5/6 or uPAR from MDA-MB-231 cell lysates. Western blot showed the levels of pulled-down receptors in each group using anti-uPAR and LRP5/6 antibodies. Input: the amount of uPAR and LRP5/6 in the cell lysate. **B.** Prussian blue staining of MDA-MB-231 cells following incubated with non-targeted IONP, ATF_{24}-IONP, iWnt-IONP, or iWnt-ATF_{24}-IONP at 4 μg/mL of iron equivalent dose for 6 hours. Cells were counterstained with nuclear fast red. **C**. Specific binding of iWnt-IONP to LRP5/6 was confirmed using a binding competition assay. Cells were treated for 1 hour with increasing concentration of NCI8642, a LRP5/6 inhibitor, and then NIR-830-labeled iWnt-IONP and iWnt-ATF_{24}-IONP was added. Images were taken and quantified using fluorescence microscopy with a NIR filter. Scale bar is 100 μm.

3.4.4 iWnt-ATF_{24} IONPs decreased the activation of Wnt/ β-catenin pathway and cell invasion in human breast cancer cells *in vitro*.

To determine the effects of the binding of iWnt-IONPs, ATF_{24}-IONP, or dual targeted iWnt-ATF_{24}-IONPs to Wnt receptor and/or uPAR on the canonical Wnt/β-catenin pathway and uPAR expression, MDA-MB-231 cells were incubated with iWnt-IONPs, ATF_{24}-IONP, and iWnt-ATF_{24}-IONPs. Western blot analysis of cell lysates showed that treatment of cells with the un-conjugated IONPs decreased the level of active β-catenin (3.1-fold decrease compared to no treatment control), while not affecting total β-catenin expression. However, cells treated with iWnt-IONPs or dual targeted iWnt-ATF_{24}-IONPs, had markedly lower levels of active β-catenin compared to no-treatment control, or non-targeted IONPs (6.5 and 10.6-fold decrease respectively compared to no-treatment control or 2.0 and 3.4-fold decrease compared to unconjugated IONP) (**Figure 3.4A**). ATF_{24}-IONP treatment did not further inhibit the level of active β-catenin compared with non-targeted IONP. Although IONP treatment alone affected the Wnt signals, the binding of Wnt/LRP or dual receptor targeted IONPs to LRP5/6 further enhanced the specific inhibitory effect on Wnt signaling. Supporting this, only iWnt/LRP or dual receptor targeted IONP treated cells showed increased levels of E-cadherin, a downstream signal molecule for reduced Wnt signaling (**Figure 3.4A**). Several molecular targets in the Wnt/LRP pathway were also examined. The level of Axin, a dual function molecule in the Wnt signaling pathway, was markedly inhibited in the cells treated with the dual receptor targeted IONPs (20-fold decreases compared to no treatment control) but was not affected by the treatment of either ATF_{24}-IONP or iWnt-IONPs (**Figure 3.4A**). Treatment with non-targeted IONP led to decreases in the levels of total GSK 3β (2.9-fold decrease) and

p-GSK 3β (15-fold decrease) in tumor cells. Single receptor targeted IONP had 1.5 to 2.8-fold decreases of the total GSK3β. In contrast, dual targeted IONP treated cells had very low levels of GSK 3β and p-GSK3β (14 to 120-fold decreases respectively compared to on treatment control). It is intriguing that the levels of two key molecules, Axin and GSK3β, in the β-catenin destruction complex, were markedly decreased in dual receptor targeted IONP treated cells, but the level of active β-catenin was still very low. The mechanism of this paradox observation regarding how β-catenin is degraded or inhibited in the absence of Axin and GSK3β has yet to be elucidated. Supporting the effect of inhibition of Wnt/β-catenin signaling, dual receptor targeted-IONP treated cells showed a decreased level of another Wnt/LRP regulated transcription factor, Snail, and upregulation of E-cadherin (**Figure 3.4A**).

The MDA-MB-231 cell line has a mesenchymal phenotype with limited expression of epithelial marker E-cadherin [192]. To determine whether the changes in the Wnt/β-catenin pathway following the IONP treatment affect tumor cell invasion, cells were incubated with 20 picomolar (pmol) of non-targeted-IONP, iWnt-IONP, ATF_{24}-IONP or iWnt-ATF_{24}-IONPs for 48 hours. The treated cells were then collected and seeded in Boyden chamber wells for an invasion assay. We found that only cells treated with dual-targeted iWnt-ATF_{24}-IONPs had a significant reduction (43.1 %) in cell invasion compared to no treatment control (**Figure 3.4B**). Although changes in the levels of β-catenin and E-cadherin were found in cells treated with iWnt-IONPs, the invasive phenotype of those cells was not altered. Treatment of cells with ATF_{24}-IONP and non-targeted IONPs also did not inhibit cell invasion. Together these results suggest that dual receptor targeting is

necessary for inhibition of Wnt/LRP signaling and, consequently, inhibition of cell invasion.

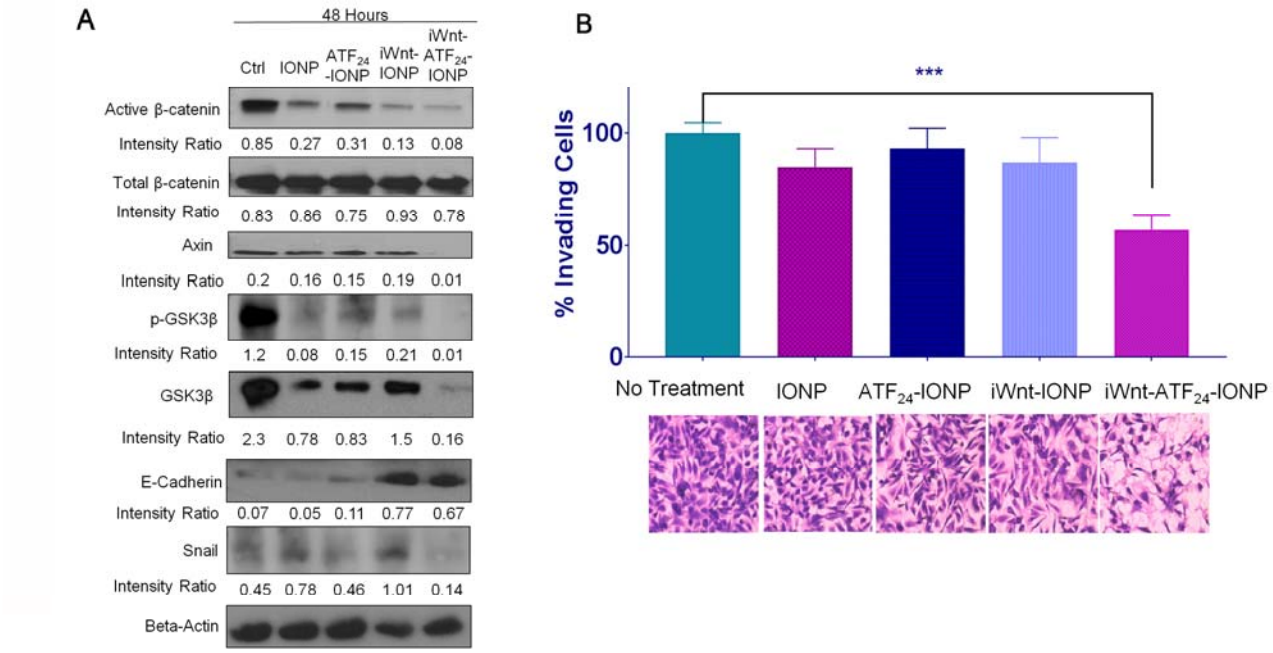

Figure 3.4: Effects of iWnt-ATF$_{24}$ IONPs on Wnt/ β-catenin pathway and cell invasion.

A. MDA-MB-231 cells were incubated with non-targeted IONP, ATF$_{24}$-IONP, iWnt-IONP, or iWnt-ATF$_{24}$-IONP for 6 hours. After removing the IONPs and cultured for 48 hours, cell lysates were immunoblotted with the following antibodies: anti-active β-catenin, anti-total β-catenin, anti-Axin, anti-phospho-GSK3β, anti-total GSK3β, anti-E-cadherin, and anti-Snail. β-actin was used as a loading control. Quantification of bands was the intensity ratio relative to β-actin of the same loading sample. **B**. Following incubation with IONP, ATF$_{24}$-IONP, iWnt-IONP, or iWnt-ATF$_{24}$-IONP, invasive potential of the MDA-MB-231 cells was determined using an invasion trans-well chamber assay. The percentage of invading cells was significantly reduced only in the iWnt-ATF$_{24}$-IONP treated cells compared to no treatment control cells (***$p \leq 0.0007$). Study was performed in triplicate and bar graph shows the mean and SD of studies.

3.4.5 Targeted IONP treatment reduced the levels of cancer stem cell associated biomarkers without affecting cell proliferation and cell cycle status.

Activation of the Wnt/β-catenin pathway is important for the maintenance of stemness properties of cells in normal tissue and in many types of human tumors. The Wnt/β-catenin pathway has been shown to be upregulated in cancer stem cells, such as $CD44^{high}/CD24^{low}$ cell population [193]. Activation of the Wnt/LRP pathway also increases uPAR expression, which is often used as an indicator of whether the Wnt pathway has been stimulated [86]. A high level of uPAR expression is found in the cancer stem-like cell population [194]. uPAR signaling has also been observed to induce stem cell-like characteristics in breast cancer cells, including $CD44^{high}/CD24^{low}$ phenotype [180]. To determine whether the binding of Wnt receptor targeted IONPs to LRP5/6 and modulation of Wnt signaling affect the cancer stem cell population and uPAR expression, we examined the levels of protein expression of CD44, CD24, and uPAR in MDA-MB-231 cells following incubation with single-targeted iWnt-IONP, ATF_{24}-IONP or dual targeted iWnt-ATF_{24}-IONPs by Western blot analysis as shown **Figure 3.5**. Within 24 hours following treatment, there was a notable decrease in uPAR in all treatment groups and by 48 hours there was a complete abrogation of uPAR expression in groups treated with the single-targeted iWnt-IONP and ATF_{24}-IONP as well as the dual targeted iWnt-ATF_{24}-IONP compared to those control groups received no treatment and non-targeted IONP (**Figure 3.5A**). Forty-eight hours following the treatment, there was a distinct decrease in CD44 in the Wnt/LRP or uPAR targeted-IONP treated cells. There was no detectable level of CD44 in the dual receptor targeted cells. Before and within 24 hours following treatment, CD24 was not detectable in tumor cells (**Figure 3.5A**). However, 48 hours following treatment, a marked increase

in the level of CD24 expression was observed in all treatment groups. While non-targeted IONP induced an upregulation of CD24, those cells also retained a high level of CD44. Cells treated with single Wnt/LRP or uPAR targeted IONP had intermediate levels of CD24 and a low level of CD44. In contrast, cells treated with dual receptor targeted IONPs had only expressed a high level of CD24 but lacked CD44 expression, suggesting that dual targeted IONPs has a stronger effect on the inhibition of cancer stem-like cells.

Next, we investigated the effect of the single-targeted iWnt-IONP and ATF_{24}-IONP as well as the dual targeted iWnt-ATF_{24}-IONP on cell proliferation. After 48 hours of treatment with non-targeted-IONP, iWnt-IONP, ATF_{24}-IONP or iWnt-ATF_{24}-IONPs, there was no significant difference in the total cell numbers of MDA-MB-231 cells compared to untreated control cells (**Figure 3.5B**). We further conducted flow cytometry analysis to determine if changes in the CD44 positive cell population affected the cell cycle status of the total cell population. We found that 48 hours following treatment, there was no observable difference in the percentage of cells in different phases of the cell cycle amongst different treatment groups (**Figure 3.5C**).

Results of this study indicated that the binding of the dual Wnt/LRP and uPAR targeted IONP to tumor cells strongly inhibited the proliferation of $CD44^{high}/CD24^{low}$ cancer stem-like cell population, but had a minimal effect on the cell population that has a $CD44^{low}/CD24^{high}$ phenotype. Therefore, selective proliferation of $CD44^{low}/CD24^{high}$ cells *in vitro* caused no significant change in the cell number or in cell cycling among the cells treated with single and dual receptor targeted IONPs. This result also suggested that uPAR and Wnt/LRP targeted IONPs acted upon the same cell population in the tumor cells.

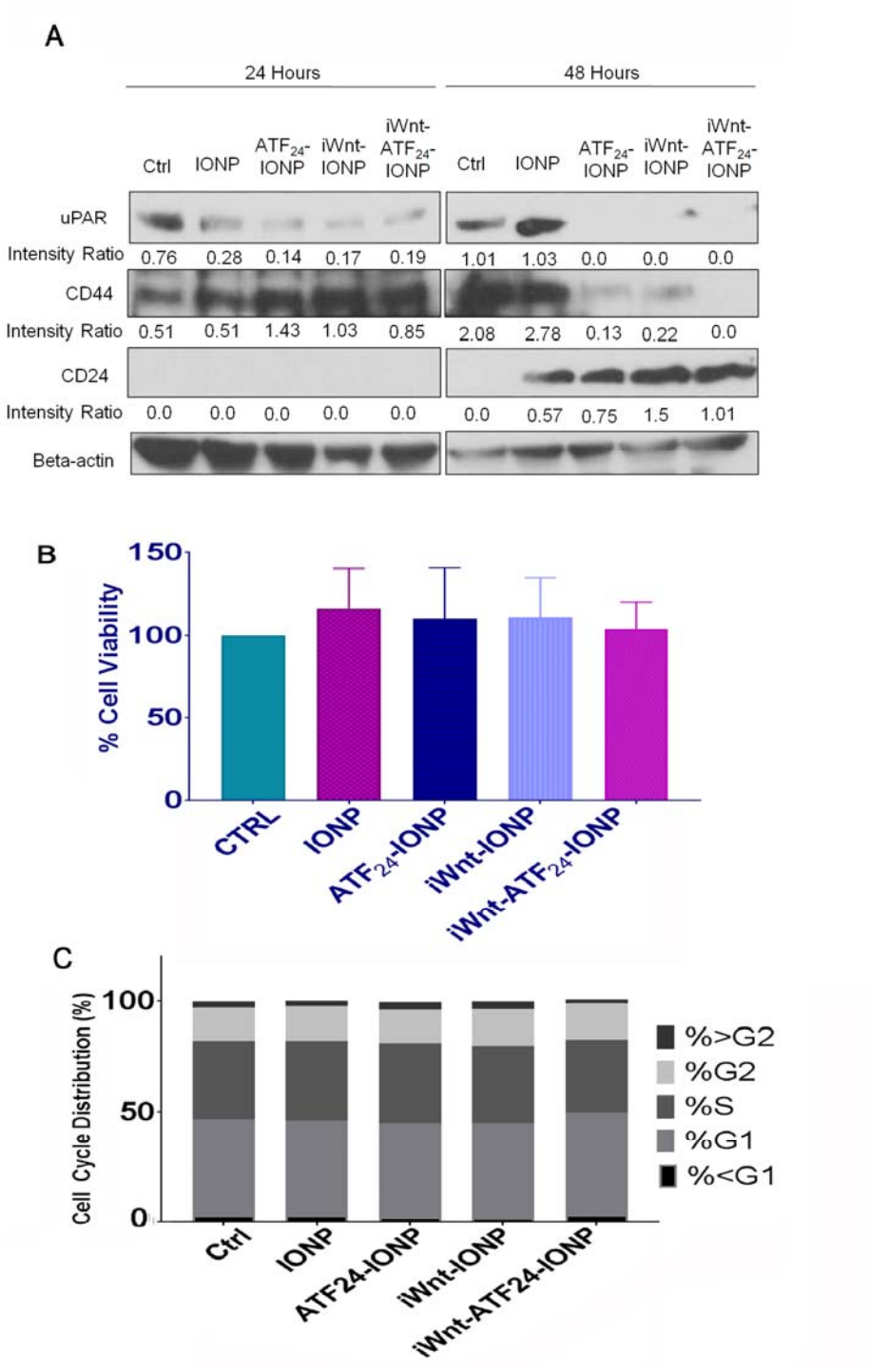
A
24 Hours
48 Hours
Ctrl
IONP
ATF24-IONP
iWnt-IONP
iWnt-ATF24-IONP
uPAR
Intensity Ratio 0.76 0.28 0.14 0.17 0.19 1.01 1.03 0.0 0.0 0.0
CD44
Intensity Ratio 0.51 0.51 1.43 1.03 0.85 2.08 2.78 0.13 0.22 0.0
CD24
Intensity Ratio 0.0 0.0 0.0 0.0 0.0 0.0 0.57 0.75 1.5 1.01
Beta-actin
B
% Cell Viability
150
100
50
0
CTRL
IONP
ATF24-IONP
iWnt-IONP
iWnt-ATF24-IONP
C
Cell Cycle Distribution (%)
100
50
0
Ctrl
IONP
ATF24-IONP
iWnt-IONP
iWnt-ATF24-IONP
%>G2
%G2
%S
%G1
%<G1

Figure 3.5: Effects of single or dual receptor targeted IONPs on tumor cell populations expressing cancer stem cell biomarkers, cell cycle and proliferation.

A. MDA-MB-231 cells were incubated with IONP, ATF_{24}-IONP, iWnt-IONP, or iWnt-ATF_{24}-IONP for 6 hours. 24 and 48 hours. Cells were then lysed and immunoblotted with anti-uPAR, anti-CD44, and anti-CD24 antibodies. β-actin was used as a loading control. **B.** Cell Proliferation Assay. 48 hours after cells were incubated with targeted and non-targeted IONPs, Alamar blue cell proliferation assay was performed in triplicate and bar figure showed the mean and SD of measurements. **C**. Cell cycle analysis using flow cytometry. Cell cycle analysis was performed on cells 48 hours after incubation with targeted and non-targeted IONPs.

3.4.6 Inhibition of Wnt/LRP signaling and uPAR using single or dual receptor targeted IONP carrying Dox had a similar effect on tumor cell viability as the conventional Dox *in vitro.*

Next, we tested the effect of Wnt/LRP and uPAR targeted IONPs carrying Dox on MDA-MB-231 cells *in vitro*. Amphiphilic polymer coated IONPs have a hydrophobic space between the core and coating polymer, which allows for encapsulation of hydrophobic chemotherapeutic agents, such as Dox, and have pH-dependent drug release after being internalized into cells [190]. First, we characterized the IONPs carrying Dox to determine the encapsulation efficiency and drug-loading of the different IONP formulations. We found that the encapsulation efficiency ranged from 96.8% to 97.3% and Dox loading ranged from 42.8% to 48.5%. These results are summarized in Supplementary Table 1.

To determine uptake of Dox alone or Dox encapsulated within non-targeted-IONPs, iWnt-IONP, ATF_{24}-IONP, or dual-targeted iWnt-ATF_{24}-IONP, we treated MDA-MB-231 cells for 4 hours and then determined Dox uptake by observing the fluorescent signal of Dox. No observable difference between free Dox or encapsulated Dox within the different IONP was detected (**Figure 3.6A**). Next, we treated MDA-MB-231 cells for 72 hours with Dox equivalent concentration of 170 nM either as Dox alone or Dox encapsulated within non-targeted-IONPs, iWnt-IONP, ATF_{24}-IONP, or dual-targeted iWnt-ATF_{24}-IONP. The treatment led to a 41.3%, 42.8%, 47.1%, 45.1%, and 45.6% of reduction in cell viability, respectively, compared to no treatment control (**Figure 3.6B**). There was no difference in tumor cell killing among different treatment groups. Together, these results showed that encapsulated Dox within receptor-targeted IONPs can be delivered into tumor cells to

generate a similar cytotoxic effect as free Dox. It is likely that prolonged culture of Dox and non-targeted IONP-Dox also led to drug internalization into tumor cells to induce cytotoxic effect. The effect of targeted delivery and therapeutic response for receptor targeted nanoparticle drug carriers was generally more prominent in *in vivo* studies compared with *in vitro* examination in cultured cells.

Next, we tested the effect of the receptor targeted IONPs carrying Dox on the Wnt/β-catenin pathway, cancer stem-like cells ($CD44^{high}/CD24^{low}$) and the level of uPAR expression. Cells were treated for 6 hours and then cultured for an additional 42 hours. Results showed that iWnt-IONP-Dox, ATF_{24}-IONP-Dox, and iWnt-ATF_{24}-IONP-Dox could inhibit the Wnt/β-catenin pathway through a decrease in active β-catenin, total β-catenin, and decreased uPAR expression compared to no treatment control (**Figure 3.6C**). In addition, iWnt-IONP-Dox, ATF_{24}-IONP-Dox, and iWnt-ATF_{24}-IONP-Dox treatment induced expression of the epithelial marker E-cadherin (**Figure 3.6C**). Interestingly, $CD44^{low}/CD24^{high}$ cells were only observed in the dual targeted iWnt-ATF_{24}-IONP-Dox treated cells. There was no apparent change in the Wnt pathway co-receptor, LRP5/6, following treatment. Those changes in Wnt/LRP, CD44 and uPAR were similar to the receptor targeted IONPs that did not show tumor cell growth inhibition. It is likely that the alteration of Wnt, CD44, or uPAR by binding of Wnt/LRP and uPAR targeted IONP-Dox to breast cancer cells *in vitro* only had an impact on a small percentage of cancer stem-like cells but did not affect cell proliferation and viability of most cells as their growth is not dependent on the Wnt/LRP and uPAR signals *in vitro* and they do not have cancer stem-

like properties. Although Wnt and uPAR pathways are known to be involved in cell invasion and migration, these effects may not be detectable in cell culture.

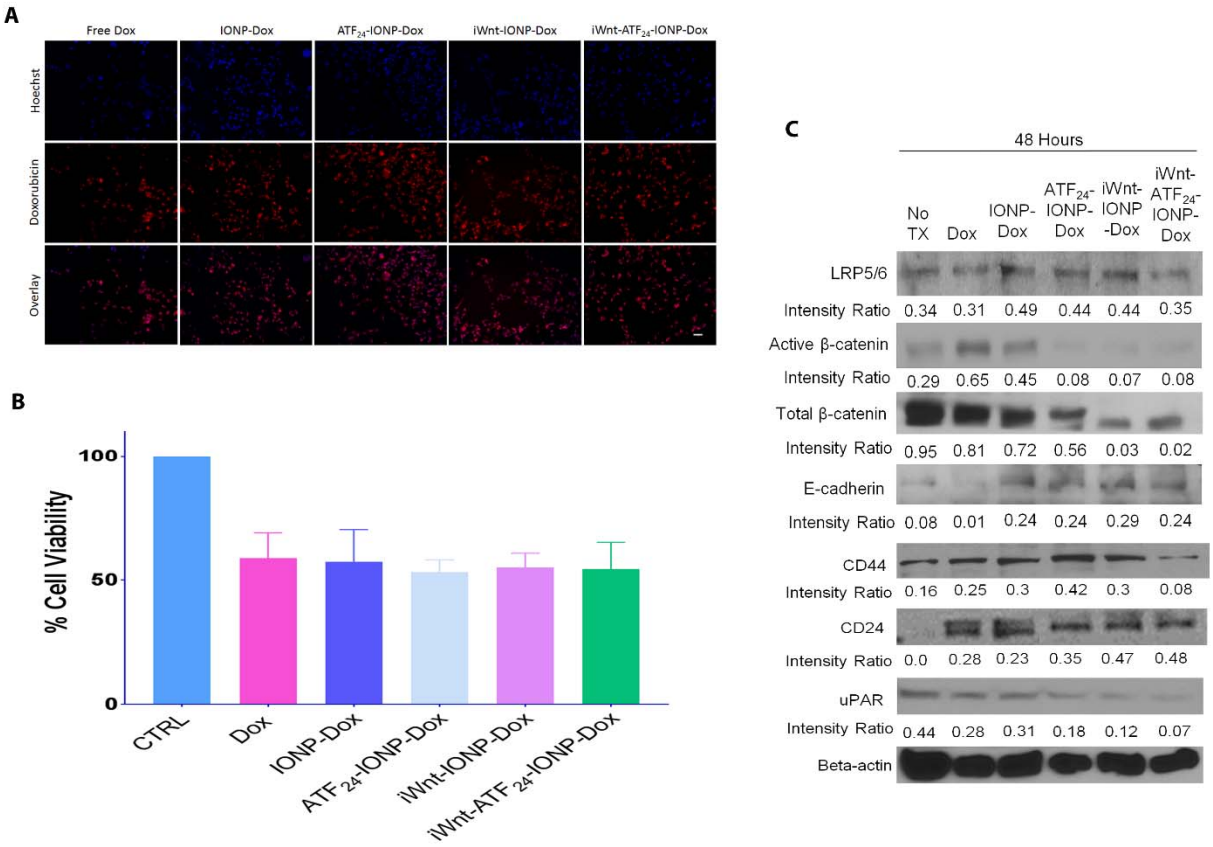

Figure 3.6: Effects of iWnt-ATF$_{24}$ IONPs carrying Doxorubicin on cell viability and signal molecules in the Wnt/ β-catenin pathway.

A. Cell uptake of Doxorubicin. MDA-MB-231 cells were incubated with free Dox, IONP-Dox, ATF$_{24}$-IONP-Dox, iWnt-IONP-Dox, or iWnt-ATF$_{24}$-IONP-Dox (170 nM) for 4 hours. Uptake of Dox was measured using fluorescence microscopy (red fluorescence). **B.** Cell Proliferation assay. MDA-MB-231 cells were incubated with free Dox, IONP-Dox,

ATF_{24}-IONP-Dox, iWnt-IONP-Dox, or iWnt-ATF_{24}-IONP-Dox (170 nM) for 6 hours. *In vitro* cell viability assay was conducted 72 hours after treatment. Study was performed in triplicate and bar figure showed the mean and standard deviation of values of each treatment. **C**. Western blot analysis of the cell lysates of MDA-MB-231 cells following the above treatment using anti-LRP5/6, anti-active β-catenin, anti-total β-catenin, anti-E-cadherin, anti-CD44, anti-CD24, and anti-uPAR antibodies. β-actin was used as a loading control. Numbers show quantification of bands relative to loading control (β-actin).

3.4.7 Targeted delivery of iWnt-IONPs, ATF_{24}-IONPs and iWnt-ATF_{24}-IONPs into orthotopic breast PDX tumors in nude mice following systemic administration.

To determine target specificity and nanoparticle accumulation *in vivo*, we used near infrared (NIR) optical imaging to track the single or dual receptor targeted-IONPs labeled with NIR-830-maleimide dye by directly conjugating to the iWnt or ATF_{24} peptides. Following the tail vein delivery of 800 pmol of iron-equivalent amount of single-targeted iWnt-IONP, or ATF_{24}-IONP, or dual-targeted iWnt-ATF_{24}-IONP into nude mice bearing breast PDX tumors, strong NIR fluorescence signals were detected in the tumors of the mice that received single or dual receptor targeted IONPs (**Figure 3.7A**).

To precisely locate optical signals that would indicate IONP accumulation, tumor and normal organs were collected from nanoparticle treated mice for *ex vivo* imaging following sacrifice. We found the highest accumulation of the single and dual-targeted IONPs in the PDX tumors compared to the normal organs. Low levels of signals were detected in the liver, spleen, lung, heart, and kidney (**Figure 3.7B**). This data suggests that iWnt-IONP, ATF_{24}-IONP, and dual-targeted iWnt-ATF_{24}-IONP can be used as targeted drug delivery carriers for systemic administration of therapeutic agents into the breast PDX tumors in nude mice.

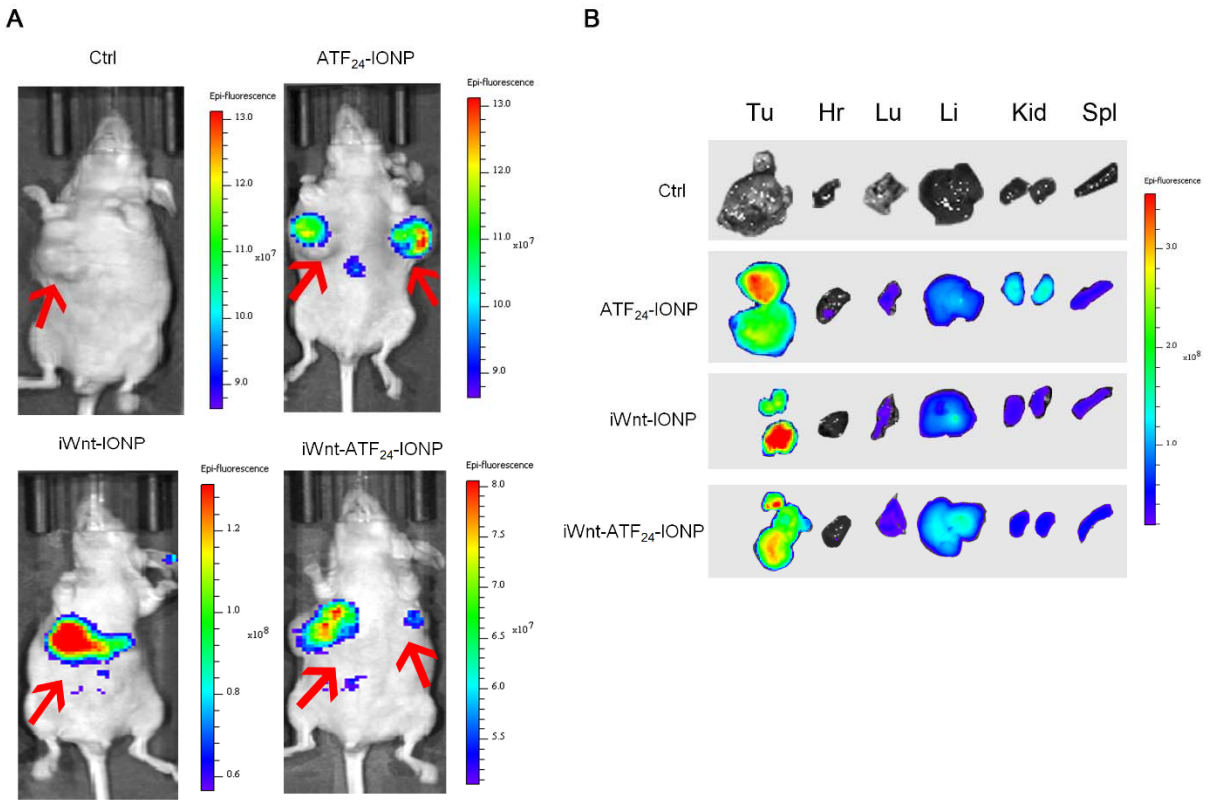

Figure 3.7: Detection of targeted delivery of ATF_{24}-IONP, iWnt-IONP, or iWnt-ATF_{24}-IONP into orthotopic breast PDX tumors in nude mice by optical imaging.

A. The whole body NIR imaging of mice 48 hours after IONP administration. Optical images were overlaid with bright-field images of the mice. Red arrows indicate location of tumors. **B**. *Ex vivo* optical imaging of the tumors and organs. Optical images were overlaid with bright-field images to show location and size of tumor and organs. Tumor (Tu), Heart (Hr), Lungs (Lu), Liver (Li), Kidneys (Kid), Spleen (Spl). Fluorescence Intensity scale bars show the intensity of optical signals.

3.4.8 Targeted delivery of iWnt-ATF$_{24}$-IONP-Dox downregulated CD44, uPAR, and Wnt signaling, leading to decreased cell proliferation and tumor growth inhibition in an orthotopic chemo-resistant breast cancer PDX model

We examined the effect of the Wnt/LRP and uPAR receptor targeted IONPs carrying Dox *in vivo* on tumor cell proliferation, Wnt/β-catenin pathway signaling, cancer stem-like cells ($CD44^{high}/CD24^{low}$), levels of uPAR and E-cadherin expression. Using nude mice bearing the first passage of orthotopic human chemo-resistant breast cancer PDX tumors derived from a surgically resected residual tumor that was resistant to paclitaxel and cyclophosphamide, we found that systemic delivery of 5 mg/kg Dox equivalent dose of single or dual receptor targeted IONP-Dox inhibited tumor growth. Furthermore, the strongest effect on tumor growth inhibition was seen in the mice treated with the dual receptor targeted iWnt-ATF$_{24}$-IONP-Dox (student's t-test, *$p \leq 0.03$) (**Figure 3.8A**). Histological analysis of residual tumors in different treatment groups following the targeted IONP-Dox treatment showed significant inhibition of cell proliferation, presented as a low level of Ki67 positive cells, in the tumors treated with dual targeted iWnt-ATF$_{24}$-IONP-Dox, compared with no treatment, non-targeted IONP-Dox and single receptor targeted ATF$_{24}$-IONP-Dox or iWnt-IONP-Dox (student's t-test: ***$p \leq 0.008$, ****$p \leq 0.0001$) (**Figure 3.8B**). H&E stained PDX tumor tissue sections also showed reduced tumor cell intensity in the tumors collected from the mice treated with dual receptor targeted IONP-Dox but not in the no treatment control and single receptor targeted IONP-Dox treated tumors (**Figure 3.8C**). Immunofluorescence staining of tumor tissue sections revealed significant downregulation of the levels of Wnt1 ligand, Axin, uPAR and CD44, and marked upregulation of E-cadherin only in the tumor tissues treated with the dual receptor

targeted IONP-Dox (**Figure 3.8C**). Tumor tissues from the mice treated with iWnt-IONP-Dox and ATF_{24}-IONP-Dox had an increase in the levels of Wnt pathway proteins including Wnt1 and Axin (**Figure 3.8C**). Western blot analysis of tumor tissue lysates showed that in the residual tumor tissues, iWnt-ATF_{24}-IONP-Dox treated tumors had no detectable levels of CD44, uPAR, p-GSK3β and Axin (**Figure 3.8D**). However, the levels of active β-catenin and GSK3β were not decreased in the treatment resistant tumors (**Figure 3.8D**). Furthermore, a high level of CD24 was found in the tumors treated with dual targeted IONP-Dox, suggesting that the remaining tumor cells were $CD44^{low}/CD24^{high}$, non-cancer stem cell population. In the tumors treated with single targeted IONP-Dox, the levels of CD44 and uPAR were reduced compared to no treatment control. However, there was no decrease in the level of Axin in single receptor targeted IONP-Dox treated tumors. Results from the PDX tumors treated with the dual targeted iWnt-ATF_{24}-IONP-Dox *in vivo* are consistent with results obtained from cell line studies *in vitro,* except for the levels of active β-catenin and total GSK3β. In residual breast cancer tumor tissues, there was no significant change in the level of active β-catenin in iWnt-IONP-Dox, ATF_{24}-IONP-Dox or iWnt-ATF_{24}-IONP-Dox treated tumors. There was a slight decrease in the level of total GSK3β compared to the no treatment control. However, the level of p-GSK3β was consistently absent in the dual targeted IONP treated tumor, which was similar to what was observed *in vitro* study on the tumor cell line. It is likely that highly heterogeneous tumor cells in the breast PDX tumors including the presence of chemo-resistant tumor cells in residual tumors were the causes for the differences in expression levels of β-catenin and total GSK3β between the breast PDX tumors *in vivo* and MDA-MB-231 cells *in vitro*.

Together these results indicate that the dual Wnt/LRP and uPAR targeted delivery of Dox can enhance therapeutic response in multi-drug resistant breast cancer through efficient delivery of Dox into tumor cells and inhibition of the Wnt/β-catenin and uPAR pathways and cancer stem cell population.

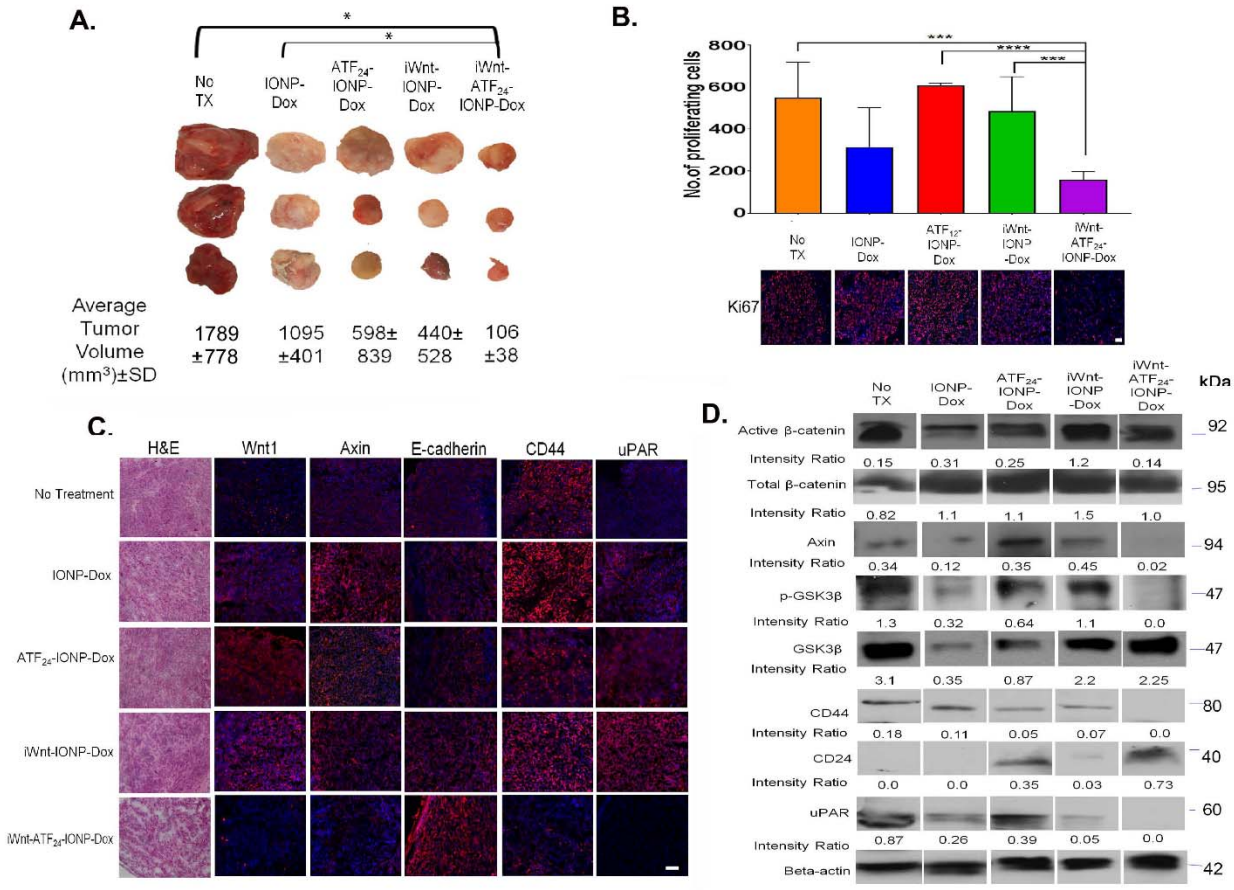

Figure 3.8: Evaluation of *in vivo* effects of targeted delivery of single and dual receptor targeted IONP-carrying Dox on tumor growth, signaling molecules, and cancer stem cell biomarkers in an orthotopic, drug-resistant breast PDX tumor model.

Nude mice bearing orthotopic breast PDX tumors (Patient #7) received 5 mg/kg Dox equivalent concentration of different IONP-Dox theranostic nanoparticles via the tail vein injections 3 times over the course of 2 weeks (n=3). **A.** Bright field images of representing

PDX tumors collected from different groups following the treatment. Mean and standard deviation of tumor volume (mm^3) are shown. **B**. Effect of IONP-Dox, ATF_{24}-IONP-Dox, iWnt-IONP-Dox, or iWnt-ATF_{24}-IONP-Dox treatment on cell proliferation *in vivo*. Ki67-positive cells in tumor tissue sections were determined by immunofluorescence labeling using an anti-Ki67 antibody (red). Blue: Hoechst 33342 background staining. ***$p \leq 0.008$, ****$p < 0.0001$, Student's t-test. **C.** Histological characterization of the residual tumors by H&E staining and immunofluorescence using anti-Wnt1, anti-Axin, anti-E-cadherin, anti-CD44 and anti-uPAR primary antibodies and Alexafluor 555 conjugated secondary antibody (red). **D.** Tumor lysates were immunoblotted with anti-active β-catenin, anti-total β-catenin, anti-Axin, anti-phospho-GSK3β, anti-total GSK3β, anti-CD44, anti-CD24, and anti-uPAR antibodies. β-actin was used as a loading control. Quantification of bands relative to loading control. Bands are from the same gel and organized based on treatment groups. Scale bar is 50 μm. No Tx: no treatment control group.

3.5 Discussion

Increasing evidence supports the significant role of cancer stem-like cells in resistance to chemotherapeutics [195,196]. It is well recognized that therapeutic strategies acting upon tumor cells as well as cancer stem-like cell populations have the potential to overcome drug resistance and improve therapeutic responses in highly heterogeneous human cancer. Results of this study suggest a new targeted drug delivery approach aimed at inhibition of Wnt/LRP signaling and cancer stem cell properties while delivering a potent chemotherapeutic drug, Dox, into tumor cells.

Various chemotherapeutic drugs have been used to treat breast cancer patients as neoadjuvant therapy to reduce tumor recurrence or as the main therapeutic option for metastatic breast cancer. Unfortunately, chemo-resistance has been the major obstacle for effective treatment of breast cancer. For those patients with large residual tumors after chemotherapy, they have a high incidence of development of local and distant recurrent tumors and an extremely poor prognosis. Therefore, new therapeutic approaches targeting aggressive and drug resistant breast tumor cells offer the opportunity to improve the prognosis of the breast cancer patients with drug resistant tumors. Our research demonstrates the ability to target chemo-resistant breast cancer with a novel nanoparticle co-directed against Wnt/LRP and uPAR, both of which we found to be over-expressed in these cancers. Such a targeted therapy has potential to overcome the chemo-resistance found in a number of breast cancers and could provide therapeutic approaches for pre-operative neoadjuvant therapy as well as for the treatment of metastatic breast cancer.

Current developments in the field of nanotechnology offer promising platforms for effective treatment of chemo-resistant breast cancer. Theranostic nanoparticles are able to deliver therapeutic agents into the cancer cells, assist in monitoring the tumor's response to treatment, and conduct image-guided identification of residual tumor lesions for surgical removal. This work developed theranostic magnetic iron oxide nanoparticles (IONPs) targeting Wnt receptor LRP5/6 and uPAR that carry a clinically relevant chemotherapeutic agent (Dox) [190]. Although we examined targeted nanoparticle drug delivery using non-invasive optical imaging, IONP-based drug carriers are also MRI contrast agents that can be utilized for detection of IONP-drug delivery by MRI, which has been demonstrated in our previous studies [47,190].

Studies have shown that there is an interplay between the Wnt/β-catenin pathway and uPAR [181]. The interaction between these two pathways has been observed but not extensively studied. uPAR and Wnt/LRP signaling are upstream of GSK-3β and Snail, a transcription factor that promotes epithelial mesenchymal transition [197,198]. When uPAR and Wnt signaling is activated, GSK-3β is inhibited and β-catenin can promote transcription of Wnt target genes such as CD44, Axin, and uPAR. In addition, when GSK-3β is inhibited, the expression of Snail leads to the inhibition of epithelial marker E-cadherin and promotes more mesenchymal phenotype [199,200]. In this study, we showed that uPAR, Wnt/LRP, and dual Wnt/LRP targeted IONPs allowed targeted delivery of chemotherapeutics into breast cancer cells *in vitro* and human chemo-resistant breast PDX tumors *in vivo*. Although single-receptor targeted iWnt-IONP and ATF_{24}-IONPs can lead to intermediate levels of reduction in Wnt/β-catenin signaling and in the $CD44^{high}/CD24^{low}$ cancer stem cells in breast cancer cells *in vitro*, dual Wnt/LRP and uPAR receptor targeted

IONP treated tumor cells showed a marked increase in inhibition of the Wnt/β-catenin signal pathway, including the lowest level of β-catenin and lack of detectable levels of uPAR, CD44, Axin, p–GSK3β/GSK3β, and Snail. Despite these noted changes in the Wnt/β-catenin pathway, the binding of single or dual receptor targeted IONPs in the absence of the chemotherapeutic Dox did not affect cell cycle status nor cell proliferation in cultured human breast cancer MDA-MB-231 cells. Interestingly, only the dual receptor targeted IONPs inhibited cell invasion of the tumor cells. It has been shown that tumor cells with activated Wnt signaling can maintain cancer stemness and undergo the epithelial to mesenchymal (EMT) transition without a reduction in cell proliferation [177]. Thus, blocking Wnt and/or uPAR signaling using the peptide conjugated nanoparticles may only inhibit EMT and has no apparent effect on inhibition of cell proliferation. This should be a favorable property of a targeted drug delivery nanoparticle since the effect of many cancer therapeutic agents requires DNA replication and cell proliferation.

In comparison to the levels of signaling molecules in the Wnt pathway (LRP5/6, β-catenin, Axin and GSK3β) and downstream Wnt pathway regulated genes (CD44, uPAR, Snail), we found that a marked difference between single receptor targeted and dual receptor targeted IONP-treated tumor cells was lack of Axin in the dual receptor targeted IONP treated tumor cells. This observation was further confirmed in the PDX tumor tissues following treatment with dual Wnt/LRP and uPAR targeted theranostic IONP carrying Dox. Axin was discovered to act as a negative regulator of the Wnt pathway that formed the β-catenin degradation complex with GSK3β, APC and CK1 to induce GSK3β-dependent phosphorylation and degradation of β-catenin [83]. However, several studies also showed that Axin has multiple functions in cells [171]. For example, the binding of

Wnt ligand to Frizzled receptor-LRP6 complex leads to the recruitment of Disheveled and then Axin-GSK3β complex to promote LRP phosphorylation, initiating WNT/β-catenin signaling [171]. Recruiting Axin to the membrane by LRP5/6 further resulted in degradation of Axin, which prevents β-catenin degradation and activation of β-catenin regulated gene transcription. Simultaneous binding of iWnt-ATF_{24}-IONP to uPAR and LRP5/6 completely abolished the level of Axin while mediating Axin/GSK3β independent downregulation of β-catenin and its downstream signaling. These results suggest a potential new mechanism of regulation of Axin and β-catenin when the Wnt and uPAR are blocked simultaneously.

It is likely that the combined effect of inhibition of uPAR, CD44, and Snail leads to a reduction of invasiveness in breast cancer cells treated with dual Wnt/LRP and uPAR targeted IONPs. It is also clear that blocking Wnt/LRP and uPAR by iWnt-ATF_{24}-IONP alone is not sufficient for the development of cancer therapeutic agents. However, this dual receptor targeted IONP could be an appropriate drug carrier for targeted delivery of therapeutic agents into tumor cells with activated Wnt signaling and cancer stem-like cells. In this study, we developed iWnt-ATF_{24}-IONP carrying Dox that served as a multifunctional therapeutic agent and evaluated its effect on Wnt signaling and tumor growth in an orthotopic human chemo-resistant breast cancer PDX model in nude mice. Early passage chemo-resistant breast PDX tumors resemble primary breast cancer pathologically, being highly heterogeneous and enriched with tumor stroma. Systemic delivery of various IONP-Dox in the PDX tumor bearing nude mice supported stronger tumor growth inhibition in the dual receptor targeted IONP-Dox treated mice compared to non-targeted IONP-Dox, single Wnt/LRP or uPAR targeted IONP-Dox treated mice.

Unlike the effect of the receptor targeted IONPs on cell proliferation in cultured cells, the finding of significant inhibition of cell proliferation in the tumors treated with the dual receptor targeted IONP-Dox, but not with the single receptor targeted IONP-Dox, suggested that the combination of targeted Dox delivery and Wnt/LRP signaling inhibition enhanced therapeutic responses in tumor cells. Additionally, the effect of inhibition of cell invasion as a result of downregulation of Wnt/LRP signaling may also contribute to the tumor growth inhibition. In the residual PDX tumors obtained after nanoparticle treatment, the effects of inhibition of Wnt/LRP signaling on downregulation of CD44, uPAR, and Axin and upregulation of E-cadherin and CD24 were consistent with those observed in the MDA-MB-231 breast cancer cells *in vitro*. However, the expression level of β-catenin in these chemo-resistant breast cancer cells was not reduced. Since breast PDX tumors contain highly heterogeneous tumor cells, it is possible that the growth of the tumor cell population with downregulated β-catenin in response to the targeted IONP-Dox therapy was significantly inhibited in the PDX tumors. Tumor cells that retained β-catenin activity survived the treatment but had low cell proliferation.

Taken together, the results of this study suggest that dual Wnt/LRP and uPAR-targeted delivery of therapeutic agents offers a multifunctional drug carrier for effective cancer therapy that can overcome resistance to standard chemotherapeutics through the combinatorial effect of chemotherapy with inhibition of the Wnt/β-catenin signal pathway, cancer stem cell population, and cell invasive properties. The development of targeted nanoparticle drug carriers using multiplexed peptide-based targeting ligands could provide

a new approach for the targeting and delivery of therapeutic peptides and chemotherapy drugs into cancer stem-like cell population.

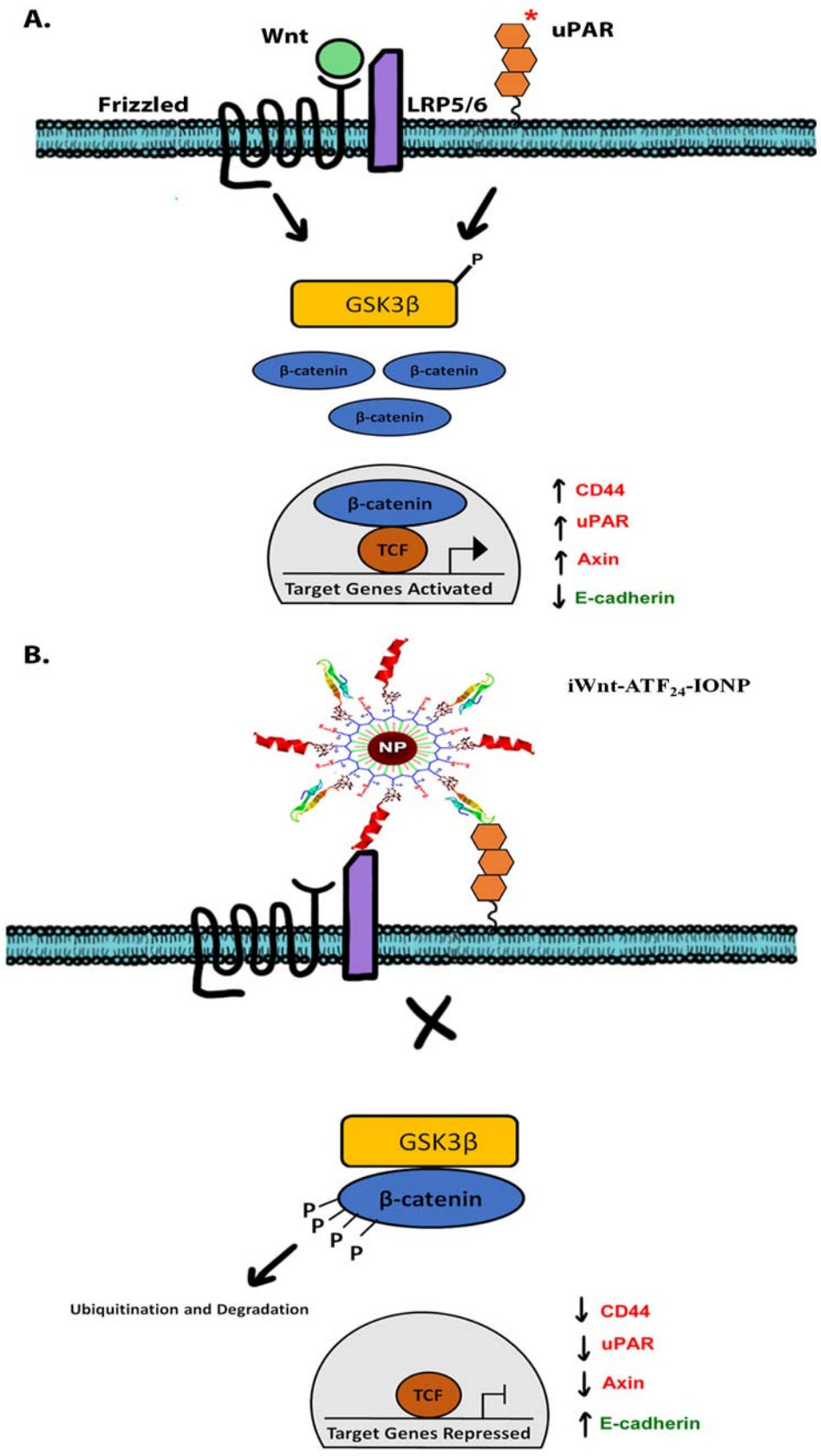
A.
Wnt
uPAR
Frizzled
LRP5/6
GSK3β
β-catenin
β-catenin
β-catenin
β-catenin
TCF
Target Genes Activated
CD44
uPAR
Axin
E-cadherin
B.
iWnt-ATF24-IONP
NP
GSK3β
β-catenin
Ubiquitination and Degradation
TCF
Target Genes Repressed
CD44
uPAR
Axin
E-cadherin

Figure 3.9: Proposed Mechanism of Action of Dual Targeted iWnt-ATF$_{24}$-IONP

Our study shows that dual targeting and blocking the Wnt/β catenin and uPAR signaling pathways are required for a robust repression of the cancer stem-cell phenotype, a decrease in the epithelial to mesenchymal transition and cell invasion, and an anti-tumorigenic response. **A.** Wnt/β catenin and uPAR signaling are both upstream of GSK3-β and when either pathway is activated, GSK3-β is phosphorylated and is unable to phosphorylate β-catenin. Un-phosphorylated β-catenin is able to translocate into the nucleus and bind with transcription factors leading to transcription of Wnt target genes resulting in an increase in CSC phenotype and EMT. **B.** Our dual-targeted iWnt-ATF$_{24}$-IONP is able bind to both Wnt receptor LRP5/6 and uPAR to simultaneously inhibit both signaling pathways allowing GSK3-β to phosphorylate β-catenin leading to its ubiquitination and degradation. Transcript of Wnt target genes are repressed resulting in a decrease in CSC phenotype and a decrease in EMT.

3.6 Supporting Information

A.

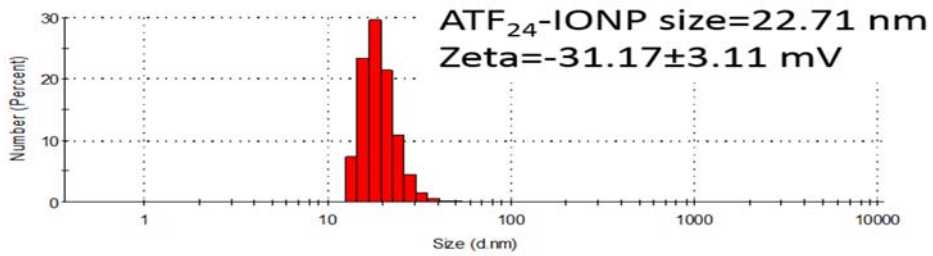

B.

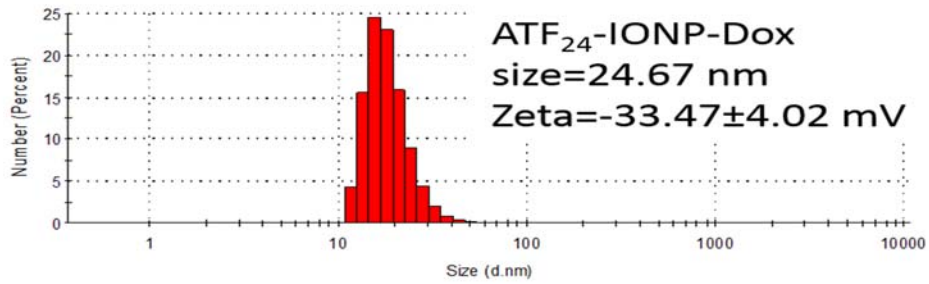

C.

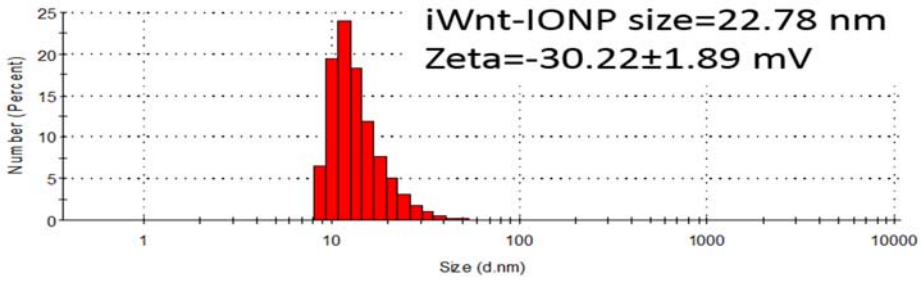

D.

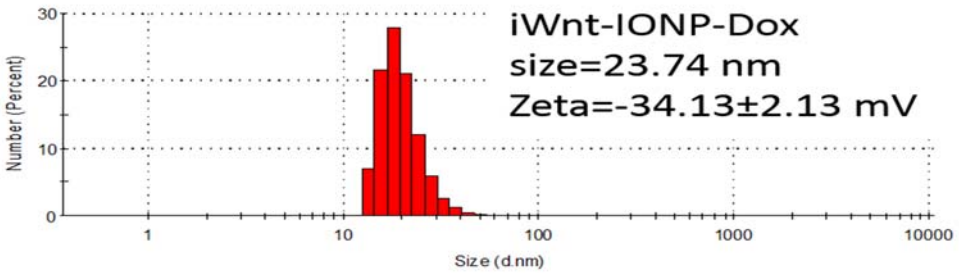

Figure 3.1S: Sizes and Zeta Potential of Single Targeted IONPs and Dox Loaded Single Targeted IONPs

Hydrodynamic sizes and Zeta Potential of ATF_{24}-IONPs (A), ATF_{24}-IONP-Dox (B), iWnt-IONPs (C), and iWnt-IONP-Dox (D) were determined by the dynamic light scattering (DLS) method.

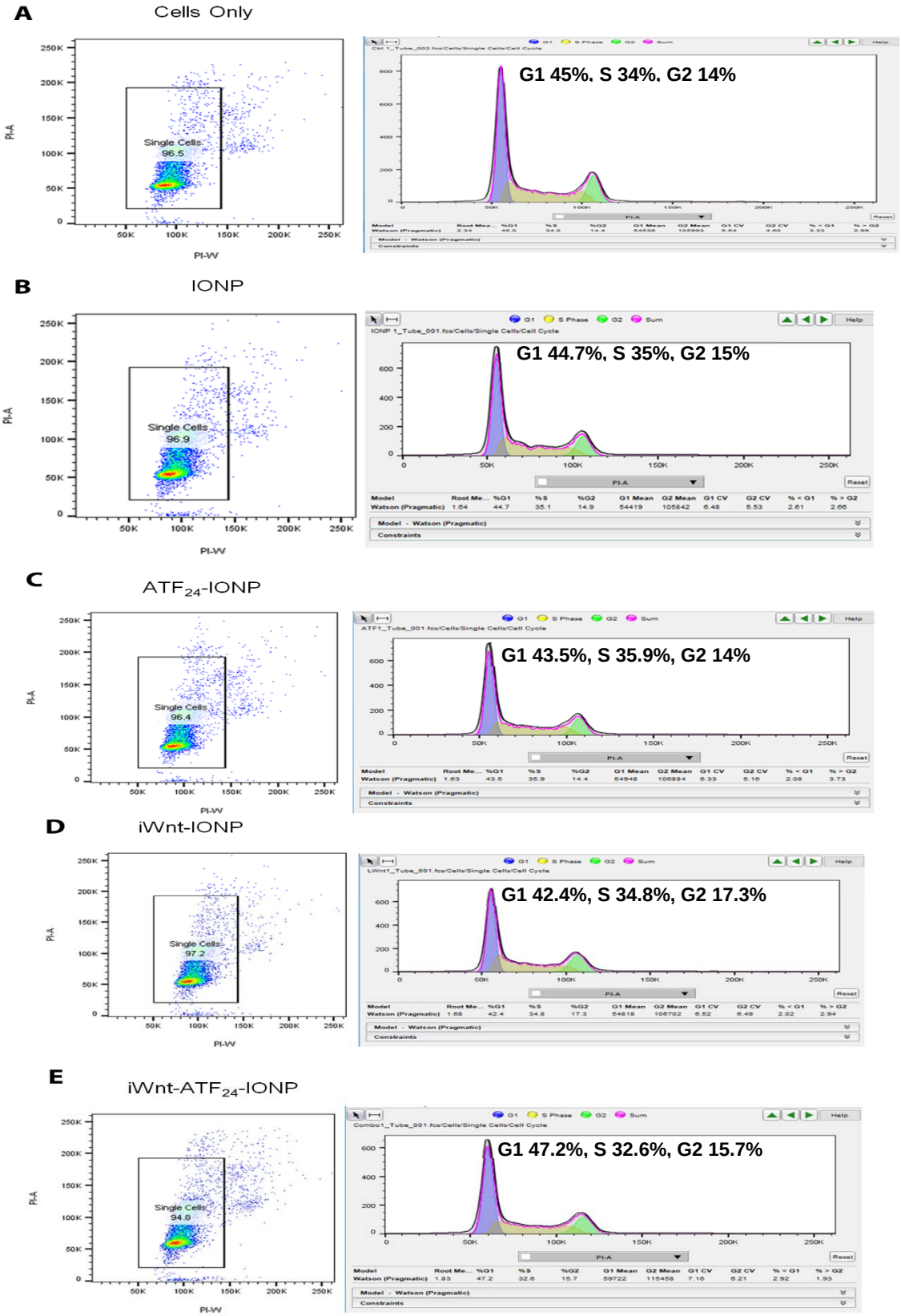
A
Cells Only
Single Cells
96.5
G1 45%. S 34%. G2 14%
B
IONP
Single Cells
96.9
G1 44.7%, S 35%, G2 15%
C
ATF24-IONP
Single Cells
96.4
G1 43.5%, S 35.9%, G2 14%
D
iWnt-IONP
Single Cells
97.2
G1 42.4%, S 34.8%, G2 17.3%
E
iWnt-ATF24-IONP
Single Cells
94.8
G1 47.2%, S 32.6%, G2 15.7%
PI-A
PI-W

Figure 3.2S: Cell cycle Analysis of breast cancer cells following treatment

Cell Gating and Plot: (A-E) Flow cytometry was performed on permeabilized cells treated with propidium iodide (PI). Gating was performed to select single cells for analysis, with 94.8% to 97.2% of the cells being in singlets across the different treatment groups. The amount of PI was measured in each cell and plotted to determine the cycle that each cell was in with G1(blue) is n=1, G2 (green) is n=2, and S (yellow) is $1<n<2$.

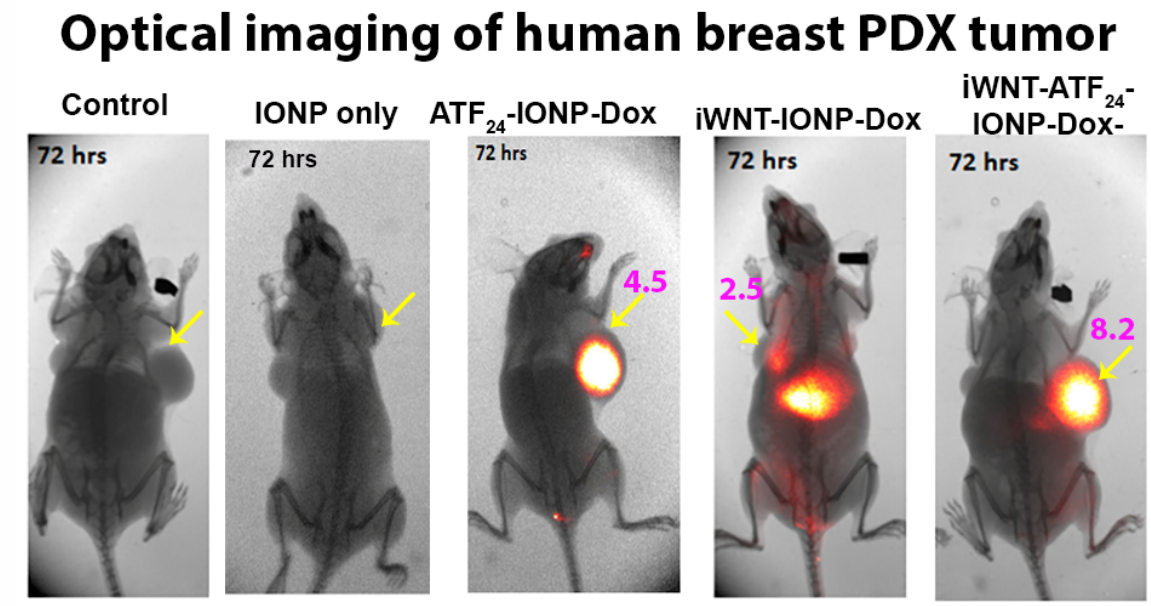

Figure 3.3S: Optical imaging detection of targeted delivery of single or dual receptor targeted IONPs carrying Dox 72 hours following systemic delivery

Nude mice bearing breast cancer PDX tumors received one injection of 800 pmol of iron equivalent concentration of different theranostic nanoparticles carrying Dox via the tail vein for 72 hours. NIR optical imaging was performed using the Kodak in vivo FX imaging system. Control mice that received non-targeted and NIR-830 dye labeled IONP or without treatment did not have detectable imaging signal in tumors.

Table 3.1S: Dox-loaded Nanoparticle Encapsulation Efficiency, and Drug Loading

Formulation	Encapsulation Efficiency (%)	Drug Loading Efficiency w/w (%)
IONP-DOX	97.0±5.2	14.6±3.0
ATF_{24}-IONP-Dox	96.8±5.5	14.8±5.0
iWnt-IONP-Dox	97.3±4.63	13.9±2.0
iWnt-ATF_{24}-IONP-Dox	97.0±5.14	14.3±2.6

Data shown are the mean and SD from three repeat studies.

Chapter 4: Discussion

4.1 Summary:

Triple negative breast cancer is a highly heterogeneous, aggressive form of breast cancer consisting of at least seven different subtypes [29]. The majority of patients diagnosed with TNBC are resistant to the initial chemotherapeutics that they will receive as standard of care. It is paramount that novel approaches are investigated that can overcome drug-resistance in TNBC leading to sustained response to treatment and improvement of prognosis. The data presented in this thesis elucidates a targeted theranostic nanoparticle approach to overcoming drug-resistance in TNBC using a PDX model which is able to recapitulate the heterogeneity found in TNBC.

Nanoparticles take advantage of the enhanced permeability and retention effect (EPR) to increase intratumoral drug delivery and decrease systemic toxicity. While there are clinically available non-targeted nanoparticles for use by TNBC, the development of receptor targeted nanoparticles has the potential to significantly increase the effectiveness of nanoparticle treatment. A variety of targets can be selected such that the nanoparticles can target tumor cells and/or cells within the tumor microenvironment. Receptor targeted nanoparticles can also promote intercellular drug delivery and bypass efflux of drug through the multi-drug resistance protein by utilizing targets that undergo receptor mediated endocytosis.

Our lab had developed a cohort of receptor targeted theranostic nanoparticles that were able to encapsulate or conjugate a variety of chemotherapeutic drugs and also conjugate NIR dyes for optical imaging of nanoparticle delivery and tumor response. In addition, our nanoparticles were formulated with an iron-oxide core for MRI imaging. Urokinase

plasminogen activator receptor (uPAR) was identified as a desirable target because it is overexpressed in several cancer types, including TNBC. Additionally, uPAR can actively target the tumor and the tumor microenvironment because it is expressed on tumor cells, macrophages, tumor endothelial cells, and stromal fibroblasts [43,44]. Previous studies in our lab had shown that our uPAR-targeted IONP accumulated within the tumors of 4T1 or MDA-MB-231 cell-line derived xenografts [47] and *in vitro* studies showed that uPAR-targeted IONP with Dox delivered high levels of Dox into 4T1 and MDA-MB-231 cells resulting in a strong inhibition of cell growth when compared to free Dox and non-targeted-IONP-Dox treated groups [140]. To further investigate the effectiveness of our uPAR-targeted IONPs with Dox for overcoming drug-resistance in TNBC we developed a patient derived xenograft (PDX) model of TNBC. Compared to the cell-line derived xenograft models used in our previous studies, our PDX model are more effective at recapitulating the biology, morphology, and heterogeneity of TNBC.

We discovered that following systemic delivery there was a strong anti-tumor effect in mice treated with our ATF-IONP-Dox compared to free Dox and no treatment control. Mice treated with ATF-IONP-Dox had a decrease in tumor volume, a decrease in recurrence and an increase in overall survival compared to other treatment groups. These findings indicate that using uPAR-targeted IONP-Dox enhanced drug response in our PDX model. To further elucidate the mechanism for the enhanced response with our targeted nanoparticle with Dox compared to free Dox, we probed for markers of tumor aggression including uPAR, cancer stem cell marker CD44, and Wnt/β-catenin pathway ligand Wnt10b. We found that ATF-IONP-Dox decreased the expression of these markers while free Dox increased the levels of their expression. These findings support the concept that

while our ATF-IONP-Dox can have an enhanced anti-tumor effect in TNBC, treatment with free Dox can result in an aggressive phenotype resulting in relapse and poor prognosis.

While our findings support further investigation of ATF-IONP-Dox for use of treatment in drug-resistant TNBC, further analysis of our *in vivo* data revealed that there was heterogeneity of response to treatment in both the free Dox and the ATF-IONP-Dox treated groups though the PDX was generated from tumor fragments of the same patient. Tumors that were resistant to treatment had progressive tumor growth over the course of treatment and had overexpression for markers found in aggressive TNBC tumors including uPAR and CD44 (**Figure 4.1**). In addition, an increase expression in the Wnt/β-catenin pathway was also found, including receptor LRP5/6. This pathway was of particular interest because it has been shown to be overexpressed in a number of TNBC subtypes and is involved in the promotion of a cancer stem cell phenotype. Studies have shown that the CSC phenotype is overexpressed in drug-resistant breast cancer tumors and has the potential to recapitulate tumors resulting in patient relapse.

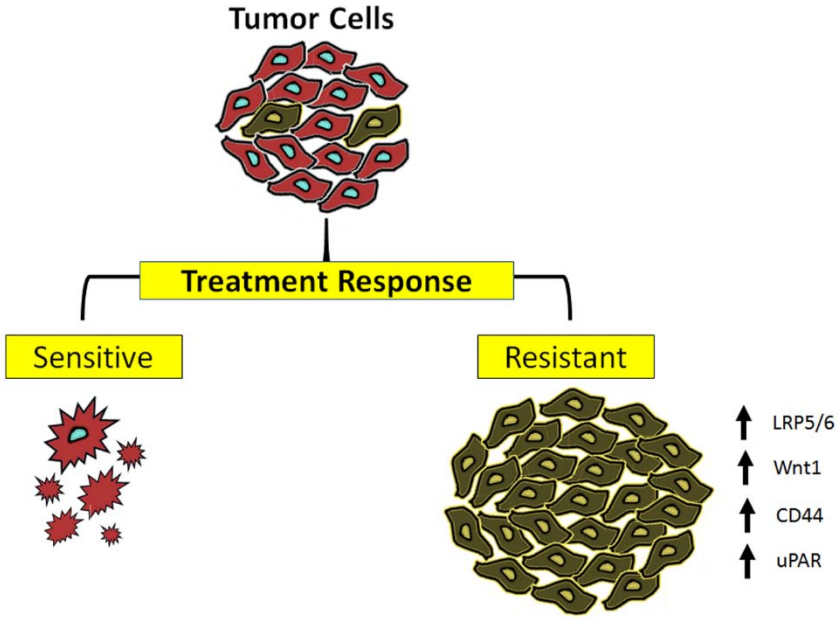

Figure 4.1: Phenotype of Drug-Resistant TNBC

In this dissertation research, we found heterogeneity of response to conventional chemotherapeutic Dox or ATF-IONP-Dox in our PDX model of TNBC. Some tumors were sensitive to treatment resulting in tumor growth regression, while others were resistant to treatment and had persistent tumor growth. Tumors that were resistant to either Dox or ATF-IONP-Dox had an increase in the Wnt/β-catenin pathway receptor LRP5/6 and ligand Wnt1. There was also an increase of expression in CSC marker CD44 and uPAR.

Our ultimate goal was to enhance therapeutic response in drug-resistant TNBC. Our observation that the Wnt/β-catenin pathway is overexpressed in Dox and ATF-IONP-Dox treatment resistant tumors provided us with a rationale to develop a nanoparticle to target the Wnt pathway. To develop a receptor-targeted nanoparticle we focused on co-receptor LRP5/6 to utilize its ability for receptor mediated endocytosis which could be used to enhance efficient delivery of Dox into LRP5/6 expressing tumor cells. As previously mentioned, uPAR is an attractive target because of its ability to not only target tumor cells but to also target cells within the tumor microenvironment. We investigated the effectiveness of developing a dual Wnt and uPAR targeted nanoparticle *in vitro* and *in vivo*. Our results indicate that dually targeting Wnt and uPAR, is more effective than singly targeting each receptor. The combination of targeting Wnt and uPAR can overcome drug-resistance through the inhibition of the Wnt/β-catenin signal pathway, cancer stem cell population, and cell invasive properties as summarized in **Figure 4.2**. The addition of chemotherapeutic Dox did not alter the effect of the Wnt and uPAR targeting but resulted in an additive cytotoxic effect.

Interestingly, our results are not limited to TNBC but also are applicable to ER-positive breast cancers. Our lab has established drug-resistant breast cancer PDX models that include breast cancers that are ER-positive. We found that regardless of hormone receptor status Dox resistant tumors overexpressed LRP5/6 and uPAR, as shown in **Figure 3.1**, in which Patient #7 is ER-positive. It is not surprising that the Wnt/β-catenin pathway would play a role in drug-resistance in ER-positive breast cancers. A study has reported that the Wnt/β-catenin pathway is active in 60% of human breast cancer specimens through expression of cytoplasmic and/or nuclear β-catenin and that the staining of β-catenin

correlates with a poor prognosis [201]. In addition, the Wnt/β-catenin pathway has been shown to be highly expressed in ER-positive breast cancer stem cells [202]. *In vitro* studies have also shown that treatment with Dox can induce resistance in ER-positive and TN breast cancer cells resulting in an increase in expression of the cancer stem-like phenotype and EMT [203]. Together these results, along with our observations, suggest that drug-resistant ER-positive breast cancers could also benefit from our dual targeted Wnt -uPAR-IONPs and further investigation of this therapeutic approach is warranted.

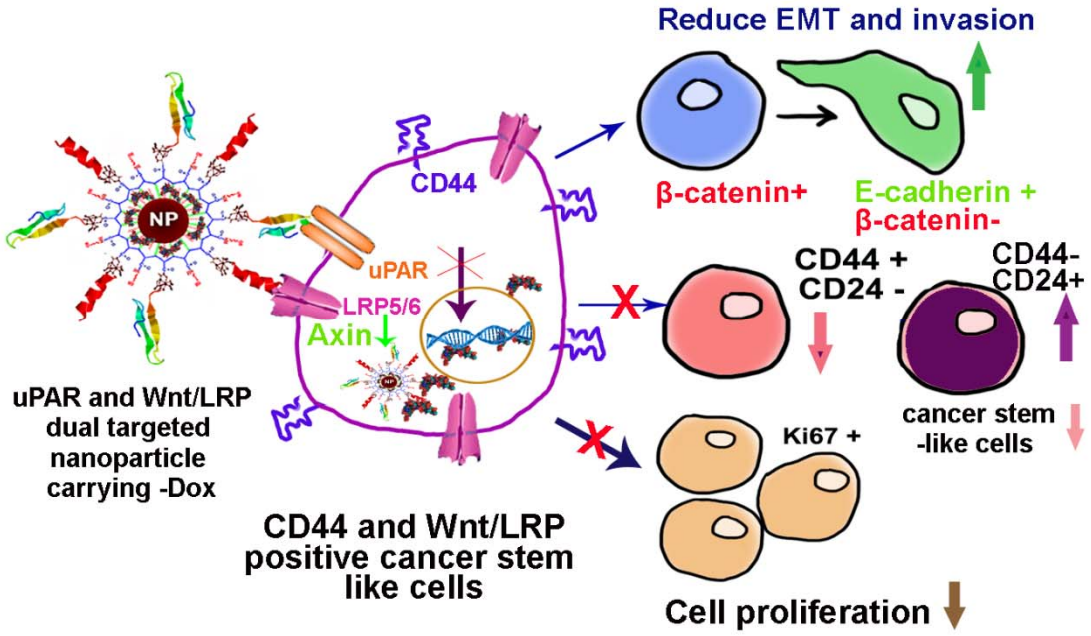

Figure 4.2. Novel Activity of Dual Wnt/LRP and uPAR targeted IONP carrying Dox.

In this dissertation research, we identified uPAR and LRP5/6 as receptors that overexpressed in drug-resistant TNBC. We developed dual Wnt and uPAR targeted nanoparticle carrying chemotherapeutic, Dox. We demonstrated that with our Wnt -uPAR-IONP-Dox we are able to decrease the $CD44^{hi}/CD24^{lo}$ phenotype, cell proliferation, and the epithelial mesenchymal transition in models of drug-resistant breast cancer. This work may provide novel targeted drug delivery system to overcome drug-resistance in TNBC.

4.2 Limitations of Study:

The *in vivo* work for this dissertation was entirely conducted in PDX models of drug-resistant breast cancer. There are many benefits to using a PDX model which make the results more clinically relevant, including their ability to recapitulate human tumors more closely than cell-line derived models and the heterogeneity of tumors that a PDX model can generate. The benefits provided by the PDX are also the primary limitation of the model. Because of the heterogeneity within each individual patient tumor that generates a PDX there is large variability to how individual implanted tumors will respond within each treatment group. Then we probed for markers that helped us to phenotypically characterize resistant tumors. Our study design did not allow for further elucidation into why these tumors were sensitive or resistant to treatment. A key question to answer would be whether the resistant tumors already overexpressed these biomarkers of drug-resistant, such as CD44, uPAR, or LRP5/6, prior to implantation. This question could be addressed if a study were designed that took a tissue sample of each tumor fragment prior to implantation and after treatment to compare their molecular profiles.

While the results of our dual targeted Wnt and uPAR nanoparticle study were promising for the development of a targeted approach to drug-resistant TNBC, there were some limitations in both the *in vitro* and *in vivo* studies. The *in vitro* studies were primarily conducted in one TNBC cell line, MDA-MB-231. Preliminary studies were also conducted in TNBC cell line MDA-MB-468 but due to their inherently low expression of LRP5/6 and uPAR the findings were not as robust as in MDA-MB-231 cells and further studies were discontinued. To determine the broader application of these findings it would be necessary

to replicate these studies in more drug-resistant TNBC cell-lines, including cell-lines derived from drug-resistant PDX that express LRP5/6 and uPAR.

Our *in vivo* data, conducted in a drug-resistant PDX model, largely confirmed what was observed *in vitro.* Our *in vivo* studies only had 3 mice per treatment group. Larger *in vivo* studies, with each group having at least 6 mice, would be needed to provide more robust and statistically significant data. The data from our study provides support for investing in conducting a larger study. It is also important to evaluate the effect in the PDX tumors from different breast cancer patients to determine whether these findings reproducible in other breast cancers.

4.3 Future Directions

An interesting finding of our dual Wnt and uPAR-targeted IONP study was that dually targeting these receptors resulted in a marked decrease in the level of Axin which is a key molecule of the APC destruction complex that targets the β-catenin for degradation in absence of Wnt signaling [83]. Axin is a scaffolding protein that forms in a complex with GSK3-β and has been shown to have dual roles in Wnt signaling, including inhibition of Wnt signaling through the phosphorylation of β-catenin or activation of Wnt signaling via the phosphorylation on LRP6 [171]. The question remains as to what happens to β-catenin if there are low levels of Axin in cells. Studies have shown that under normal physiological conditions Axin concentrations are several magnitudes lower than other components of the APC destruction complex [204,205]. The MDA-MB-231 cells that we used have constitutive activation of the Wnt pathway so the Axin that we measured in control cells is the expression of Axin in Wnt pathway activated cells. The relatively low expression of

Axin that we detected could be normal for cells that have the absence of Wnt signaling and be sufficient for β-catenin degradation. We could test this by blocking the Wnt pathway either through pharmacological inhibition of one to the Wnt receptors or we could use a knockdown model of the Wnt receptors to see how changes in Wnt signaling modulates expression of Axin. It is also possible that because the dually targeted cells have a more epithelial phenotype and have an increase of E-cadherin the cellular pools of β-catenin are being sequestered by E-cadherin. Studies would need to be designed to determine whether there is another mechanism for degrading in the absence of Axin or whether there is a redistribution of cytosolic β-catenin in cells that are targeted for Wnt and uPAR.

Further evaluation of how Wnt/β-catenin pathway receptor LRP5/6 interacts with uPAR in order to reduce Wnt/β-catenin signaling, cancer stem cell population, and cell invasive properties is needed. Our results indicate that targeting both receptors results in a more dramatic response compared to singly targeting the receptors. The necessity to target both receptors suggests that there might be some redundancy in their pathways. Both the Wnt/β-catenin pathway and uPAR signaling are upstream serine-threonine kinase GSK3-β. When active, GSK3-β downregulates many cellular processes involved in tumorigenesis including cell proliferation, survival, and invasion. uPAR activation can lead to inhibition of GSK3-β through activation of the AKT pathway. GSK3-β is also a member of the APC destruction complex, and is inhibited upon activation of Wnt signaling. Further studies need to be conducted to determine whether GSK3-β is the key protein that connects these two pathways or whether there is another mechanism causing this interaction. Another possibility is that the receptors are directly interacting. Data from **Figure 3.3**, show that our Wnt targeted peptide was able to pull-down both LRP5/6 and uPAR. These results

indicate that there might be some direct interactions of the two receptors. Further studies would need to be conducted to see whether LRP5/6 and uPAR directly interact, and if so what is the function of their interaction.

While the work of this dissertation focused on the utility of our Wnt and uPAR targeted IONPs for overcoming drug-resistance in TNBC, there are a number of cancers that might benefit from single or dual targeting these pathways. Wnt/ β-catenin signaling has been identified as a driver of carcinogenesis in cancers including gastrointestinal, leukemia, melanoma, prostate, ovarian, and pancreatic [206–209]. The uPAR system has also been implicated as playing an important role in tumorigenesis in these cancer types among others [210]. To determine the versatility of this dual receptor targeted nanoparticle drug carrier in other primary or drug-resistant cancer types, *in vitro* and *in vivo* studies would need to be conducted. Our lab has developed ovarian and pancreatic orthotopic and PDX models that can readily be used to investigate the impact of this dual targeted nanoparticle drug delivery targeted system.

While we identified LRP5/6 receptor of the Wnt/β-catenin pathway as an advantageous approach to develop a targeted nanoparticle to overcome drug-resistance in TNBC there are presumably other receptors that would be beneficial for targeting. Our studies identified, IFG-1R as a receptor that is expressed in drug-resistant TNBC, as seen in **Figure 2.1**, in the original patient tumor and in the PDX model. Other studies support that IGF-1R is highly expressed in TNBC [61,62]. Our lab has shown that IGF-1R targeted IONPs can effectively target drug-resistant pancreatic tumors cells resulting in a strong anti-tumor response [211]. We have also found that uPAR and IGF-1R are co-expressed in TNBC

PDX tumors (**Figure 4.1S**). Adding an IGF-1R targeted peptide to our multiplexed Wnt and uPAR targeted IONP or singly targeting IGF-1R in drug-resistant TNBC could provide intriguing results.

Overall, the work presented in this dissertation provides a foundation for the development of receptor targeted theranostic nanoparticles for overcoming drug-resistance in TNBC. Further investigation is needed to determine whether these findings can be translated such that they can meet the clinical need of TNBC patients for targeted treatments, ultimately expanding their therapeutic options and improving their overall prognosis.

4.4 Supporting Information

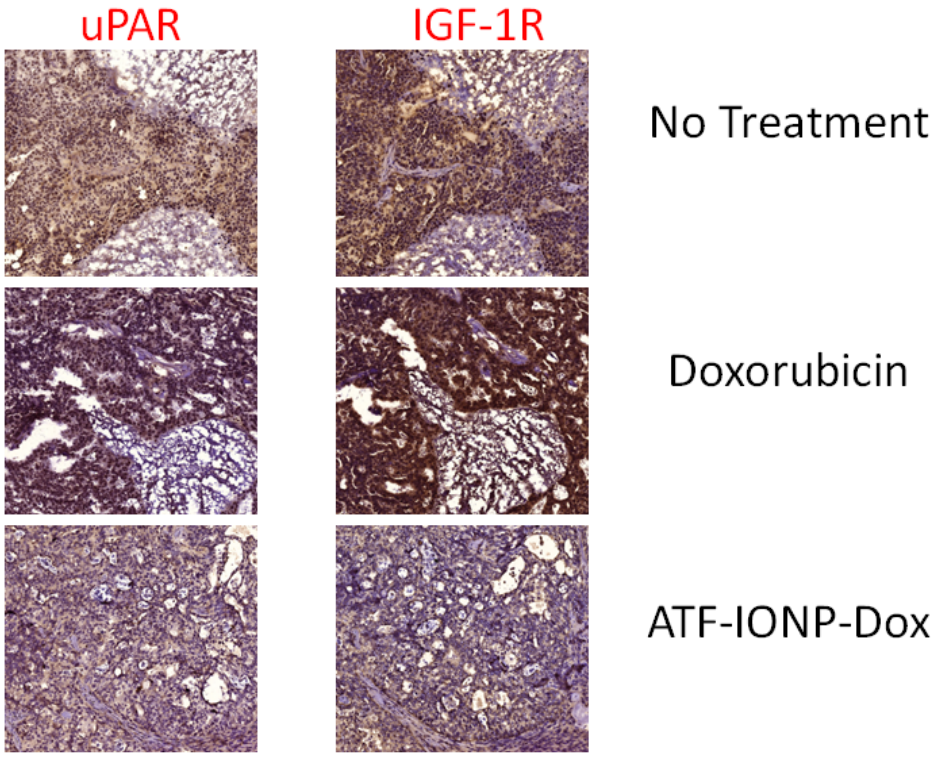

Figure 4.1S: Colocalization of uPAR and IGF-1R in Primary TNBC PDX Tumors

Histological characterization of serial sections of no treatment control, free Doxorubicin and ATF-IONP-Dox treated PDX tumors from TNBC Patient #1 at the end-point of the study by immunohistochemistry staining for uPAR and IGF-1R.

References

1. Siegel R, Ma J, Zou Z, Jemal A. Cancer statistics, 2014. CA Cancer J Clin. 2014; 64: 9–29. doi: 10.3322/caac.21208.

2. Ferlay J, Ervik M, Dikshit R, Eser S, Mathers C, Rebelo M, Parkin D, Forman D, Bray F. Cancer Incidence and Mortality Worldwide: IARC. CancerBase No112013 [Internet]. 2014; . Available from http://globocan.iarc.fr

3. Jemal A, Bray F, Center MM, Ferlay J, Ward E, Forman D. Global cancer statistics. CA Cancer J Clin. 2011; 61: 69–90. doi: 10.3322/caac.20107.

4. Sorlie T, Perou CM, Tibshirani R, Aas T, Geisler S, Johnsen H, Hastie T, Eisen MB, van de Rijn M, Jeffrey SS, Thorsen T, Quist H, Matese JC, et al. Gene expression patterns of breast carcinomas distinguish tumor subclasses with clinical implications. Proc Natl Acad Sci U S A [Internet]. 2001; 98: 10869–74. doi: 10.1073/pnas.191367098.

5. Nielsen TO, Hsu FD, Jensen K, Cheang M, Karaca G, Hu Z, Hernandez-Boussard T, Livasy C, Cowan D, Dressler L, Akslen LA, Ragaz J, Gown AM, et al. Immunohistochemical and Clinical Characterization of the Basal-Like Subtype of Invasive Breast Carcinoma. Clin Cancer Res. 2004; 10: 5367 LP-5374.

6. Prat A, Adamo B, Cheang MCU, Anders CK, Carey LA, Perou CM. Molecular Characterization of Basal-Like and Non-Basal-Like Triple-Negative Breast Cancer. Oncologist. Durham, NC, USA: AlphaMed Press; 2013; 18: 123–33. doi: 10.1634/theoncologist.2012-0397.

7. Baselga J, Cortés J, Kim S-B, Im S-A, Hegg R, Im Y-H, Roman L, Pedrini JL, Pienkowski T, Knott A, Clark E, Benyunes MC, Ross G, et al. Pertuzumab plus Trastuzumab plus Docetaxel for Metastatic Breast Cancer. N Engl J Med. Massachusetts Medical Society; 2011; 366: 109–19. doi: 10.1056/NEJMoa1113216.

8. Early Breast Cancer Trialists' Collaborative Group. Effects of chemotherapy and hormonal therapy for early breast cancer on recurrence and 15-year survival: an overview of the randomised trials. Lancet. 2005; 365: 1687–717. doi: 10.1016/S0140-6736(05)66544-0.

9. LA C, CM P, CA L, Al E. Race, breast cancer subtypes, and survival in the carolina breast cancer study. JAMA. 2006; 295: 2492–502.

10. Bauer KR, Brown M, Cress RD, Parise CA, Caggiano V. Descriptive analysis of estrogen receptor (ER)-negative, progesterone receptor (PR)-negative, and HER2-negative invasive breast cancer, the so-called triple-negative phenotype. Cancer. 2007; 109: 1721–8. doi: 10.1002/cncr.22618.

11. Foulkes WD, Stefansson IM, Chappuis PO, Bégin LR, Goffin JR, Wong N, Trudel

M, Akslen LA. Germline BRCA1 mutations and a basal epithelial phenotype in breast cancer. JNCI J Natl Cancer Inst. Oxford University Press; 2003; 95: 1482–5.

12. Dogan BE, Gonzalez-Angulo AM, Gilcrease M, Dryden MJ, Yang WT. Multimodality Imaging of Triple Receptor–Negative Tumors With Mammography, Ultrasound, and MRI. Am J Roentgenol [Internet]. American Roentgen Ray Society; 2010; 194: 1160–6. doi: 10.2214/AJR.09.2355.

13. Wahba HA, El-Hadaad HA. Current approaches in treatment of triple-negative breast cancer. Cancer Biol Med [Internet]. Chinese Anti-Cancer Association; 2015; 12: 106–16. doi: 10.7497/j.issn.2095-3941.2015.0030.

14. Oakman C, Viale G, Di Leo A. Management of triple negative breast cancer. The Breast. 2010; 19: 312–21. doi: 10.1016/j.breast.2010.03.026.

15. Dent R, Trudeau M, Pritchard KI, Hanna WM, Kahn HK, Sawka CA, Lickley LA, Rawlinson E, Sun P, Narod SA. Triple-Negative Breast Cancer: Clinical Features and Patterns of Recurrence. Clin Cancer Res. 2007; 13: 4429 LP-4434.

16. Liedtke C, Mazouni C, Hess KR, André F, Tordai A, Mejia JA, Symmans WF, Gonzalez-Angulo AM, Hennessy B, Green M, Cristofanilli M, Hortobagyi GN, Pusztai L. Response to Neoadjuvant Therapy and Long-Term Survival in Patients With Triple-Negative Breast Cancer. J Clin Oncol [Internet]. American Society of Clinical Oncology; 2008; 26: 1275–81. doi: 10.1200/JCO.2007.14.4147.

17. Dent R, Hanna WM, Trudeau M, Rawlinson E, Sun P, Narod SA. Pattern of metastatic spread in triple-negative breast cancer. Breast Cancer Res Treat [Internet]. 2009; 115: 423–8. doi: 10.1007/s10549-008-0086-2.

18. Haffty BG, Yang Q, Reiss M, Kearney T, Higgins SA, Weidhaas J, Harris L, Hait W, Toppmeyer D. Locoregional Relapse and Distant Metastasis in Conservatively Managed Triple Negative Early-Stage Breast Cancer. J Clin Oncol [Internet]. American Society of Clinical Oncology; 2006; 24: 5652–7. doi: 10.1200/JCO.2006.06.5664.

19. Liedtke C, Mazouni C, Hess KR, Andre F, Symmans WF, Gonzalez-angulo AM, Hennessy B, Green M, Cristofanilli M. Response to Neoadjuvant Therapy and Long-Term Survival in Patients With Triple-Negative Breast Cancer. 2017; 26: 1275–81. doi: 10.1200/JCO.2007.14.4147.

20. Sikov WM, Berry DA, Perou CM, Singh B, Cirrincione CT, Tolaney SM, Kuzma CS, Pluard TJ, Somlo G, Port ER, Golshan M, Bellon JR, Collyar D, et al. Impact of the Addition of Carboplatin and/or Bevacizumab to Neoadjuvant Once-per-Week Paclitaxel Followed by Dose-Dense Doxorubicin and Cyclophosphamide on Pathologic Complete Response Rates in Stage II to III Triple-Negative Breast Cancer: CALGB 40603 (A. J Clin Oncol [Internet]. American Society of Clinical Oncology; 2015; 33: 13–21. doi: 10.1200/JCO.2014.57.0572.

21. Isakoff SJ, Mayer EL, He L, Traina TA, Carey LA, Krag KJ, Rugo HS, Liu MC, Stearns V, Come SE, Timms KM, Hartman A-R, Borger DR, et al. TBCRC009: A Multicenter Phase II Clinical Trial of Platinum Monotherapy With Biomarker Assessment in Metastatic Triple-Negative Breast Cancer. J Clin Oncol [Internet]. American Society of Clinical Oncology; 2015; 33: 1902–9. doi: 10.1200/JCO.2014.57.6660.

22. Isakoff SJ. Triple Negative Breast Cancer: Role of Specific Chemotherapy Agents. Cancer J [Internet]. 2010; 16: 53–61. doi: 10.1097/PPO.0b013e3181d24ff7.

23. Adkins FC, Gonzalez-Angulo AM, Lei X, Hernandez-Aya LF, Mittendorf EA, Litton JK, Wagner J, Hunt KK, Woodward WA, Meric-Bernstam F. Triple-Negative Breast Cancer Is Not a Contraindication for Breast Conservation. Ann Surg Oncol [Internet]. 2011; 18: 3164–73. doi: 10.1245/s10434-011-1920-z.

24. Nanda R, Chow LQM, Dees EC, Berger R, Gupta S, Geva R, Pusztai L, Pathiraja K, Aktan G, Cheng JD, Karantza V, Buisseret L. Pembrolizumab in Patients With Advanced Triple-Negative Breast Cancer: Phase Ib KEYNOTE-012 Study. J Clin Oncol [Internet]. American Society of Clinical Oncology; 2016; 34: 2460–7. doi: 10.1200/JCO.2015.64.8931.

25. Traina TA, Miller K, Yardley DA, O'Shaughnessy J, Cortes J, Awada A, Kelly CM, Trudeau ME, Schmid P, Gianni L, García-Estevez L, Nanda R, Ademuyiwa FO, et al. Results from a phase 2 study of enzalutamide (ENZA), an androgen receptor (AR) inhibitor, in advanced AR+ triple-negative breast cancer (TNBC). J Clin Oncol [Internet]. American Society of Clinical Oncology; 2015; 33: 1003. doi: 10.1200/jco.2015.33.15_suppl.1003.

26. Li X, Lewis MT, Huang J, Gutierrez C, Osborne CK, Wu M-F, Hilsenbeck SG, Pavlick A, Zhang X, Chamness GC, Wong H, Rosen J, Chang JC. Intrinsic Resistance of Tumorigenic Breast Cancer Cells to Chemotherapy. JNCI J Natl Cancer Inst [Internet]. 2008; 100: 672–9. Available from http://dx.doi.org/10.1093/jnci/djn123

27. Guarneri V, Broglio K, Kau S-W, Cristofanilli M, Buzdar AU, Valero V, Buchholz T, Meric F, Middleton L, Hortobagyi GN, Gonzalez-Angulo AM. Prognostic Value of Pathologic Complete Response After Primary Chemotherapy in Relation to Hormone Receptor Status and Other Factors. J Clin Oncol [Internet]. American Society of Clinical Oncology; 2006; 24: 1037–44. doi: 10.1200/JCO.2005.02.6914.

28. Prat A, Perou CM. Deconstructing the molecular portraits of breast cancer. Mol Oncol [Internet]. 2011 [cited 2017 Jul 17]; 5: 5–23. doi: 10.1016/j.molonc.2010.11.003.

29. Lehmann BD, Bauer JA, Chen X, Sanders ME, Chakravarthy AB, Shyr Y, Pietenpol JA. Identification of human triple-negative breast cancer subtypes and preclinical models for selection of targeted therapies. J Clin Invest [Internet].

American Society for Clinical Investigation; 2011; 121: 2750–67. doi: 10.1172/JCI45014.

30. Masuda H, Baggerly KA, Wang Y, Zhang Y, Gonzalez-Angulo AM, Meric-Bernstam F, Valero V, Lehmann BD, Pietenpol JA, Hortobagyi GN, Symmans WF, Ueno NT. Differential response to neoadjuvant chemotherapy among 7 triple-negative breast cancer molecular subtypes. Clin Cancer Res [Internet]. 2013; 19: 10.1158/1078-0432.CCR-13-0799. doi: 10.1158/1078-0432.CCR-13-0799.

31. Prat A, Lluch A, Albanell J, Barry WT, Fan C, Chacón JI, Parker JS, Calvo L, Plazaola A, Arcusa A, Seguí-Palmer MA, Burgues O, Ribelles N, et al. Predicting response and survival in chemotherapy-treated triple-negative breast cancer. Br J Cancer. Nature Publishing Group; 2014; 111: 1532–41. doi: 10.1038/bjc.2014.444.

32. Chekhun VF, Zhylchuk VE, Lukyanova NY, Vorontsova AL, Kudryavets YI. Expression of drug resistance proteins in triple-receptor-negative tumors as the basis of individualized therapy of the breast cancer patients. Exp Oncol. 2009; 31: 123–4.

33. Emilienne Soma C, Dubernet C, Bentolila D, Benita S, Couvreur P. Reversion of multidrug resistance by co-encapsulation of doxorubicin and cyclosporin A in polyalkylcyanoacrylate nanoparticles. Biomaterials [Internet]. 2000 [cited 2017 Jul 17]; 21: 1–7. doi: 10.1016/S0142-9612(99)00125-8.

34. Kennedy RD, Quinn JE, Mullan PB, Johnston PG, Harkin DP. The Role of BRCA1 in the Cellular Response to Chemotherapy. JNCI J Natl Cancer Inst. 2004; 96: 1659–68.

35. Loi S, Pommey S, Haibe-Kains B, Beavis PA, Darcy PK, Smyth MJ, Stagg J. CD73 promotes anthracycline resistance and poor prognosis in triple negative breast cancer. Proc Natl Acad Sci U S A. National Academy of Sciences; 2013; 110: 11091–6. doi: 10.1073/pnas.1222251110.

36. Kobayashi H, Watanabe R, Choyke PL. Improving Conventional Enhanced Permeability and Retention (EPR) Effects; What Is the Appropriate Target? Theranostics [Internet]. Sydney: Ivyspring International Publisher; 2014; 4: 81–9. doi: 10.7150/thno.7193.

37. Maeda H, Wu J, Sawa T, Matsumura Y, Hori K. Tumor vascular permeability and the EPR effect in macromolecular therapeutics: a review. J Control Release. 2000; 65: 271–84. doi: 10.1016/S0168-3659(99)00248-5.

38. Yang W-T, Dryden M, Broglio K, Gilcrease M, Dawood S, Dempsey PJ, Valero V, Hortobagyi G, Atchley D, Arun B. Mammographic features of triple receptor-negative primary breast cancers in young premenopausal women. Breast Cancer Res Treat. 2008; 111: 405–10. doi: 10.1007/s10549-007-9810-6.

39. de Kruijf EM, van Nes JGH, van de Velde CJH, Putter H, Smit VTHBM, Liefers

GJ, Kuppen PJK, Tollenaar RAEM, Mesker WE. Tumor–stroma ratio in the primary tumor is a prognostic factor in early breast cancer patients, especially in triple-negative carcinoma patients. Breast Cancer Res Treat. 2011; 125: 687–96. doi: 10.1007/s10549-010-0855-6.

40. Jain RK, Stylianopoulos T. Delivering nanomedicine to solid tumors. Nat Rev Clin Oncol. 2010; 7: 653–64. doi: 10.1038/nrclinonc.2010.139.

41. Sykes EA, Chen J, Zheng G, Chan WCW. Investigating the Impact of Nanoparticle Size on Active and Passive Tumor Targeting Efficiency. ACS Nano. American Chemical Society; 2014; 8: 5696–706. doi: 10.1021/nn500299p.

42. Bertrand N, Wu J, Xu X, Kamaly N, Farokhzad OC. Cancer Nanotechnology: The impact of passive and active targeting in the era of modern cancer biology(). Adv Drug Deliv Rev. 2014; 66: 2–25. doi: 10.1016/j.addr.2013.11.009.

43. Mazar AP. Urokinase Plasminogen Activator Receptor Choreographs Multiple Ligand Interactions: Implications for Tumor Progression and Therapy. Clin Cancer Res. 2008; 14: 5649 LP-5655.

44. Nielsen BS, Rank F, Illemann M, Lund LR, Danø K. Stromal cells associated with early invasive foci in human mammary ductal carcinoma in situ coexpress urokinase and urokinase receptor. Int J Cancer. 2007; 120: 2086–95. doi: 10.1002/ijc.22340.

45. Pyke C, Græm N, Ralfkiær E, Rønne E, Høyer-Hansen G, Brünner N, Danø K. Receptor for Urokinase Is Present in Tumor-associated Macrophages in Ductal Breast Carcinoma. Cancer Res. 1993; 53: 1911 LP-1915.

46. Han, B., Nakamura, M., Mori, I., Nakamura, Y., & Kakudo K. Urokinase-type plasminogen activator system and breast cancer. Oncol Rep. 2005; 14: 105–12.

47. Yang L, Peng X, Wang YA, Wang X, Cao Z, Ni C, Karna P, Zhang X, Wood WC, Gao X, Nie S, Mao H. Receptor-Targeted Nanoparticles for In vivo Imaging of Breast Cancer. Clin Cancer Res. 2009; 15: 4722–33. doi: 10.1158/1078-0432.CCR-08-3289.

48. Yang L, Sajja HK, Cao Z, Qian W, Bender L, Marcus AI, Lipowska M, Wood WC, Wang YA. uPAR-targeted Optical Imaging Contrasts as Theranostic Agents for Tumor Margin Detection. Theranostics. Sydney: Ivyspring International Publisher; 2014; 4: 106–18. doi: 10.7150/thno.7409.

49. LeBeau AM, Duriseti S, Murphy ST, Pepin F, Hann B, Gray JW, VanBrocklin HF, Craik CS. Targeting uPAR with Antagonistic Recombinant Human Antibodies in Aggressive Breast Cancer. Cancer Res. 2013; 73: 2070–81. doi: 10.1158/0008-5472.CAN-12-3526.

50. Gelder MEM, Look MP, Peters HA, Schmitt M, Brünner N, Harbeck N, Klijn

JGM, Foekens JA. Urokinase-Type Plasminogen Activator System in Breast Cancer. Cancer Res. 2004; 64: 4563 LP-4568.

51. LeBeau AM, Sevillano N, King ML, Duriseti S, Murphy ST, Craik CS, Murphy LL, VanBrocklin HF. Imaging the Urokinase Plasminongen Activator Receptor in Preclinical Breast Cancer Models of Acquired Drug Resistance. Theranostics. Sydney: Ivyspring International Publisher; 2014; 4: 267–79. doi: 10.7150/thno.7323.

52. Tan DSP, Marchió C, Jones RL, Savage K, Smith IE, Dowsett M, Reis-Filho JS. Triple negative breast cancer: molecular profiling and prognostic impact in adjuvant anthracycline-treated patients. Breast Cancer Res Treat. 2008; 111: 27–44. doi: 10.1007/s10549-007-9756-8.

53. Viale G, Rotmensz N, Maisonneuve P, Bottiglieri L, Montagna E, Luini A, Veronesi P, Intra M, Torrisi R, Cardillo A, Campagnoli E, Goldhirsch A, Colleoni M. Invasive ductal carcinoma of the breast with the "triple-negative" phenotype: prognostic implications of EGFR immunoreactivity. Breast Cancer Res Treat. 2009; 116: 317–28. doi: 10.1007/s10549-008-0206-z.

54. Masuda H, Zhang D, Bartholomeusz C, Doihara H, Hortobagyi GN, Ueno NT. Role of epidermal growth factor receptor in breast cancer. Breast Cancer Res Treat. 2012; 136: 331–45. doi: 10.1007/s10549-012-2289-9.

55. Baselga J, Gómez P, Greil R, Braga S, Climent MA, Wardley AM, Kaufman B, Stemmer SM, Pêgo A, Chan A, Goeminne J-C, Graas M-P, Kennedy MJ, et al. Randomized Phase II Study of the Anti–Epidermal Growth Factor Receptor Monoclonal Antibody Cetuximab With Cisplatin Versus Cisplatin Alone in Patients With Metastatic Triple-Negative Breast Cancer. J Clin Oncol. American Society of Clinical Oncology; 2013; 31: 2586–92. doi: 10.1200/JCO.2012.46.2408.

56. Dickler MN, Cobleigh MA, Miller KD, Klein PM, Winer EP. Efficacy and safety of erlotinib in patients with locally advanced or metastatic breast cancer. Breast Cancer Res Treat. 2009; 115: 115–21. doi: 10.1007/s10549-008-0055-9.

57. Filmus J, Trent JM, Pollak MN, Buick RN. Epidermal growth factor receptor gene-amplified MDA-468 breast cancer cell line and its nonamplified variants. Mol Cell Biol. 1987; 7: 251–7.

58. Fitzpatrick SL, LaChance MP, Schultz GS. Characterization of Epidermal Growth Factor Receptor and Action on Human Breast Cancer Cells in Culture. Cancer Res. 1984; 44: 3442 LP-3447.

59. Pollak MN, Schernhammer ES, Hankinson SE. Insulin-like growth factors and neoplasia. Nat Rev Cancer. Nature Publishing Group; 2004; 4: 505–18.

60. Resnik JL, Reichart DB, Huey K, Webster NJG, Seely BL. Elevated Insulin-like

Growth Factor I Receptor Autophosphorylation and Kinase Activity in Human Breast Cancer. Cancer Res. 1998; 58: 1159 LP-1164.

61. Yerushalmi R, Gelmon KA, Leung S, Gao D, Cheang M, Pollak M, Turashvili G, Gilks BC, Kennecke H. Insulin-like growth factor receptor (IGF-1R) in breast cancer subtypes. Breast Cancer Res Treat. 2012; 132: 131–42. doi: 10.1007/s10549-011-1529-8.

62. Law JH, Habibi G, Hu K, Masoudi H, Wang MYC, Stratford AL, Park E, Gee JMW, Finlay P, Jones HE, Nicholson RI, Carboni J, Gottardis M, et al. Phosphorylated Insulin-Like Growth Factor-I/Insulin Receptor Is Present in All Breast Cancer Subtypes and Is Related to Poor Survival. Cancer Res. 2008; 68: 10238 LP-10246.

63. Litzenburger BC, Creighton CJ, Tsimelzon A, Chan BT, Hilsenbeck SG, Wang T, Carboni JM, Gottardis MM, Huang F, Chang JC, Lewis MT, Rimawi MF, Lee A V. High IGF-IR activity in triple-negative breast cancer cell lines and tumorgrafts correlates with sensitivity to anti-IGF-IR therapy. Clin Cancer Res. 2011; 17: 2314–27. doi: 10.1158/1078-0432.CCR-10-1903.

64. Balko JM, Giltnane JM, Wang K, Schwarz LJ, Young CD, Cook RS, Owens P, Sanders ME, Kuba MG, Sánchez V, Kurupi R, Moore PD, Pinto JA, et al. Molecular profiling of the residual disease of triple-negative breast cancers after neoadjuvant chemotherapy identifies actionable therapeutic targets. Cancer Discov. 2014; 4: 232–45. doi: 10.1158/2159-8290.CD-13-0286.

65. Siroy A, Abdul-Karim FW, Miedler J, Fong N, Pingfu F, Hannah G, Baar J. MUC1 is Expressed at High Frequency in Early-Stage Basal-Like Triple Negative Breast Cancer. Hum Pathol. 2013; 44: 2159–66. doi: 10.1016/j.humpath.2013.04.010.

66. Ren J, Agata N, Chen D, Li Y, Yu W, Huang L, Raina D, Chen W, Kharbanda S, Kufe D. Human MUC1 carcinoma-associated protein confers resistance to genotoxic anticancer agents. Cancer Cell. 2004; 5: 163–75.

67. Kufe DW. MUC1-C Oncoprotein as a Target in Breast Cancer; Activation of Signaling Pathways and Therapeutic Approaches. Oncogene. 2013; 32: 1073–81. doi: 10.1038/onc.2012.158.

68. Raina D, Ahmad R, Joshi MD, Yin L, Wu Z, Kawano T, Vasir B, Avigan D, Kharbanda S, Kufe D. Direct Targeting of the MUC1 Oncoprotein Blocks Survival and Tumorigenicity of Human Breast Carcinoma Cells. Cancer Res. 2009; 69: 5133–41. doi: 10.1158/0008-5472.CAN-09-0854.

69. Alam M, Rajabi H, Ahmad R, Jin C, Kufe D. Targeting the MUC1-C oncoprotein inhibits self-renewal capacity of breast cancer cells. Oncotarget. Impact Journals LLC; 2014; 5: 2622–34.

70. O'Shannessy DJ, Somers EB, Maltzman J, Smale R, Fu Y-S. Folate receptor alpha (FRA) expression in breast cancer: identification of a new molecular subtype and association with triple negative disease. Springerplus [Internet]. Heidelberg: Springer International Publishing AG; 2012; 1: 22. doi: 10.1186/2193-1801-1-22.

71. Leamon C. Folate-targeted chemotherapy. Adv Drug Deliv Rev. 2004; 56: 1127–41. doi: 10.1016/j.addr.2004.01.008.

72. Zhang Z, Wang J, Tacha DE, Li P, Bremer RE, Chen H, Wei B, Xiao X, Da J, Skinner K, Hicks DG, Bu H, Tang P. Folate Receptor α Associated With Triple-Negative Breast Cancer and Poor Prognosis. Arch Pathol Lab Med. College of American Pathologists; 2013; 138: 890–5. doi: 10.5858/arpa.2013-0309-OA.

73. Leamon CP, Low PS. Folate-mediated targeting: from diagnostics to drug and gene delivery. Drug Discov Today. 2001; 6: 44–51. doi: 10.1016/S1359-6446(00)01594-4.

74. Chu QD, Panu L, Holm NT, Li BDL, Johnson LW, Zhang S. High Chemokine Receptor CXCR4 Level in Triple Negative Breast Cancer Specimens Predicts Poor Clinical Outcome. J Surg Res. 2010; 159: 689–95. doi: 10.1016/j.jss.2008.09.020.

75. Chen H, Du C, Wei W, Khoo U, Zhang G. Cytoplasmic CXCR4 High-Expression Exhibits Distinct Poor Clinicopathological Characteristics and Predicts Poor Prognosis in Triple-Negative Breast Cancer. Curr Mol Med. 2013; 13: 410–6.

76. Orimo A, Gupta PB, Sgroi DC, Arenzana-Seisdedos F, Delaunay T, Naeem R, Carey VJ, Richardson AL, Weinberg RA. Stromal Fibroblasts Present in Invasive Human Breast Carcinomas Promote Tumor Growth and Angiogenesis through Elevated SDF-1/CXCL12 Secretion. Cell. 2005; 121: 335–48. doi: 10.1016/j.cell.2005.02.034.

77. Kojima Y, Acar A, Eaton EN, Mellody KT, Scheel C, Ben-Porath I, Onder TT, Wang ZC, Richardson AL, Weinberg RA, Orimo A. Autocrine TGF-β and stromal cell-derived factor-1 (SDF-1) signaling drives the evolution of tumor-promoting mammary stromal myofibroblasts. Proc Natl Acad Sci U S A. National Academy of Sciences; 2010; 107: 20009–14. doi: 10.1073/pnas.1013805107.

78. Liang Z, Zhan W, Zhu A, Yoon Y, Lin S, Sasaki M, Klapproth J-MA, Yang H, Grossniklaus HE, Xu J, Rojas M, Voll RJ, Goodman MM, et al. Development of a Unique Small Molecule Modulator of CXCR4. Yang P-C, editor. PLoS One. San Francisco, USA: Public Library of Science; 2012; 7: e34038. doi: 10.1371/journal.pone.0034038.

79. Lindvall C, Bu W, Williams BO, Li Y. Wnt Signaling , Stem Cells , and the Cellular Origin of Breast Cancer. Stem Cell Rev. 2007; 3: 157–68. doi: 10.1007/s12015-007-0025-3.

80. King TD, Suto MJ, Li Y. The Wnt/B-Catenin Signaling Pathway: A Potential

Therapeutic Target in the Treatment of Triple Negative Breast Cancer. J Cell Biochem. 2012; 18: 13–8. doi: 10.1002/jcb.23350.

81. Yin S, Xu L, Bon RD, Banerjee S, Sarkar FH, Sethi S, Reddy KB. Tumor-Initiating Cells and FZD8 Play a Major Role in Drug Resistance in Triple-Negative Breast Cancer. Mol Cancer Ther. 2013; 12: 491–8. doi: 10.1158/1535-7163.MCT-12-1090.

82. Xu W, Liu Z, Yang C, Qin W, Shao Z. Expression of Dickkopf-1 and Beta-Catenin Related to the Prognosis of Breast Cancer Patients with Triple Negative Phenotype. PLoS One. 2012; 7: 1–7. doi: 10.1371/journal.pone.0037624.

83. Pohl S, Brook N, Agostino M, Arfuso F, Kumar AP, Dharmarajan A. Wnt signaling in triple-negative breast cancer. Oncogenesis. 2017; 6: 1–12. doi: 10.1038/oncsis.2017.14.

84. Yang L, Wu X, Wang Y, Zhang K, Wu J, Yuan Y-C, Deng X, Chen L, Kim CCH, Lau S, Somlo G, Yen Y. FZD7 has a critical role in cell proliferation in triple negative breast cancer. Oncogene [Internet]. 2011; 30: 4437–46. doi: 10.1038/onc.2011.145.

85. Bilir B, Kucuk O, Moreno CS. Wnt signaling blockage inhibits cell proliferation and migration, and induces apoptosis in triple-negative breast cancer cells. J Transl Med [Internet]. 2013; 11: 280. doi: 10.1186/1479-5876-11-280.

86. Dey N, Barwick BG, Moreno CS, Ordanic-Kodani M, Chen Z, Oprea-Ilies G, Tang W, Catzavelos C, Kerstann KF, Sledge GW, Abramovitz M, Bouzyk M, De P, et al. Wnt signaling in triple negative breast cancer is associated with metastasis. BMC Cancer. 2013; 13: 537. doi: 10.1186/1471-2407-13-537.

87. Yang L, Perez AA, Fujie S, Warden C, Li J, Wang Y, Yung B, Chen Y-R, Liu X, Zhang H, Zheng S, Liu Z, Ann D, et al. Wnt modulates MCL1 to control cell survival in triple negative breast cancer. BMC Cancer. BioMed Central; 2014; 14: 124. doi: 10.1186/1471-2407-14-124.

88. Willnow TE, Nykjaer A, Herz J. Lipoprotein receptors: new roles for ancient proteins. Nat Cell Biol. Macmillan Magazines Ltd.; 1999; 1: E157–62.

89. Visvader JE, Lindeman GJ. Cancer stem cells in solid tumours : accumulating evidence and unresolved questions. Nat Rev Cancer. 2008; 8: 755–68. doi: 10.1038/nrc2499.

90. Kakarala M, Wicha MS. Implications of the Cancer Stem-Cell Hypothesis for Breast Cancer Prevention and Therapy. J Clin Oncol. 2008; 26: 2813–20. doi: 10.1200/JCO.2008.16.3931.

91. Li X, Lewis MT, Huang J, Gutierrez C, Osborne CK, Wu MF, Hilsenbeck SG, Pavlick A, Zhang X, Chamness GC, Wong H, Rosen J, Chang JC. Intrinsic

resistance of tumorigenic breast cancer cells to chemotherapy. J Natl Cancer Inst. 2008; 100: 672–9. doi: 10.1093/jnci/djn123.

92. Yu F, Yao H, Zhu P, Zhang X, Pan Q, Gong C, Huang Y, Hu X, Su F, Lieberman J, Song E. let-7 Regulates Self Renewal and Tumorigenicity of Breast Cancer Cells. Cell. 2007; 131: 1109–23. doi: 10.1016/j.cell.2007.10.054.

93. Idowu MO, Kmieciak M, Dumur C, Burton RS, Grimes MM, Powers CN, Manjili MH. CD44+/CD24−/low cancer stem/progenitor cells are more abundant in triple-negative invasive breast carcinoma phenotype and are associated with poor outcome. Hum Pathol. 2012; 43: 364–73. doi: 10.1016/j.humpath.2011.05.005.

94. Tammi RH, Kultti A, Kosma V-M, Pirinen R, Auvinen P, Tammi MI. Hyaluronan in human tumors: Pathobiological and prognostic messages from cell-associated and stromal hyaluronan. Semin Cancer Biol. 2008; 18: 288–95. doi: 10.1016/j.semcancer.2008.03.005.

95. Auvinen P, Rilla K, Tumelius R, Tammi M, Sironen R, Soini Y, Kosma V-M, Mannermaa A, Viikari J, Tammi R. Hyaluronan synthases (HAS1–3) in stromal and malignant cells correlate with breast cancer grade and predict patient survival. Breast Cancer Res Treat. 2014; 143: 277–86. doi: 10.1007/s10549-013-2804-7.

96. Sajja HK, East MP, Mao H, Wang AY, Nie S, Yang L. Development of Multifunctional Nanoparticles for Targeted Drug Delivery and Non-invasive Imaging of Therapeutic Effect. Curr Drug Discov Technol. 2009; 6: 43–51.

97. O'Brien MER, Wigler N, Inbar M, Rosso R, Grischke E, Santoro A, Catane R, Kieback DG, Tomczak P, Ackland SP, Orlandi F, Mellars L, Alland L, et al. Reduced cardiotoxicity and comparable efficacy in a phase III trial of pegylated liposomal doxorubicin HCl (CAELYX (TM)/Doxil (R)) versus conventional doxorubicin for first-line treatment of metastatic breast cancer. Ann Oncol. 2004; 15: 440–449 ST–Reduced cardiotoxicity and comparabl. doi: 10.1093/annone/mdh097.

98. Huober J, Fett W, Nusch A, Neise M, Schmidt M, Wischnik A, Gerhardt S, Goehler T, Lück H-J, Rost A. A multicentric observational trial of pegylated liposomal doxorubicin for metastatic breast cancer. BMC Cancer. BioMed Central; 2010; 10: 2. doi: 10.1186/1471-2407-10-2.

99. Gradishar WJ. Albumin-bound paclitaxel: a next-generation taxane. Expert Opin Pharmacother. Taylor & Francis; 2006; 7: 1041–53. doi: 10.1517/14656566.7.8.1041.

100. Yamamoto Y, Kawano I, Iwase H. Nab-paclitaxel for the treatment of breast cancer: efficacy, safety, and approval. Onco Targets Ther. Dove Medical Press; 2011; 4: 123–36. doi: 10.2147/OTT.S13836.

101. Miele E, Spinelli GP, Miele E, Tomao F, Tomao S. Albumin-bound formulation of

paclitaxel (Abraxane(®) ABI-007) in the treatment of breast cancer. Int J Nanomedicine. Dove Medical Press; 2009; 4: 99–105.

102. Allen TM, Cullis PR. Liposomal drug delivery systems: From concept to clinical applications. Adv Drug Deliv Rev. 2013; 65: 36–48. doi: 10.1016/j.addr.2012.09.037.

103. Ahn RW, Chen F, Chen H, Stern ST, Clogston JD, Patri AK, Raja MR, Swindell EP, Parimi V, Cryns VL, O'Halloran T V. A Novel Nanoparticulate Formulation of Arsenic Trioxide with Enhanced Therapeutic Efficacy in a Murine Model of Breast Cancer. Clin Cancer Res. 2010; 16: 3607–17. doi: 10.1158/1078-0432.CCR-10-0068.

104. Lee ES, Bae YH. Recent progress in tumor pH targeting nanotechnology. J Control Release. 2008; 132: 164–70. doi: 10.1016/j.jconrel.2008.05.003.

105. Awada A, Bondarenko IN, Bonneterre J, Nowara E, Ferrero JM, Bakshi A V, Wilke C, Piccart M. A randomized controlled phase II trial of a novel composition of paclitaxel embedded into neutral and cationic lipids targeting tumor endothelial cells in advanced triple-negative breast cancer (TNBC). Ann Oncol. 2014; 25: 824–31.

106. Mamot C, Ritschard R, Wicki A, Küng W, Schuller J, Herrmann R, Rochlitz C. Immunoliposomal delivery of doxorubicin can overcome multidrug resistance mechanisms in EGFR-overexpressing tumor cells. J Drug Target. Taylor & Francis; 2012; 20: 422–32. doi: 10.3109/1061186X.2012.680960.

107. Guo P, You J-O, Yang J, Jia D, Moses MA, Auguste DT. Inhibiting Metastatic Breast Cancer Cell Migration via the Synergy of Targeted, pH-triggered siRNA Delivery and Chemokine Axis Blockade. Mol Pharm. American Chemical Society; 2014; 11: 755–65. doi: 10.1021/mp4004699.

108. Gao Z-G, Tian L, Hu J, Park I-S, Bae YH. Prevention of Metastasis in a 4T1 Murine Breast Cancer Model by Doxorubicin Carried by Folate Conjugated pH Sensitive Polymeric Micelles. J Control Release. 2011; 152: 84–9. doi: 10.1016/j.jconrel.2011.01.021.

109. Luk BT, Fang RH, Zhang L. Lipid- and Polymer-Based Nanostructures for Cancer Theranostics. Theranostics. Sydney: Ivyspring International Publisher; 2012; 2: 1117–26. doi: 10.7150/thno.4381.

110. Dai W, Yang F, Ma L, Fan Y, He B, He Q, Wang X, Zhang H, Zhang Q. Combined mTOR inhibitor rapamycin and doxorubicin-loaded cyclic octapeptide modified liposomes for targeting integrin α3 in triple-negative breast cancer. Biomaterials. 2014; 35: 5347–58. doi: 10.1016/j.biomaterials.2014.03.036.

111. Li S, Goins B, Hrycushko BA, Phillips WT, Bao A. Feasibility of Eradication of Breast Cancer Cells Remaining in Post-Lumpectomy Cavity and Draining Lymph

Nodes Following Intracavitary Injection of Radioactive Immunoliposomes. Mol Pharm. 2012; 9: 2513–22. doi: 10.1021/mp300132f.

112. Sepehri N, Rouhani H, Tavassolian F, Montazeri H, Khoshayand MR, Ghahremani MH, Ostad SN, Atyabi F, Dinarvand R. SN38 polymeric nanoparticles: In vitro cytotoxicity and in vivo antitumor efficacy in xenograft balb/c model with breast cancer versus irinotecan. Int J Pharm. 2014; 471: 485–97. doi: http://dx.doi.org/10.1016/j.ijpharm.2014.05.046.

113. Schluep T, Hwang J, Cheng J, Heidel JD, Bartlett DW, Hollister B, Davis ME. Preclinical Efficacy of the Camptothecin-Polymer Conjugate IT-101 in Multiple Cancer Models. Clin Cancer Res. 2006; 12: 1606 LP-1614.

114. Young C, Schluep T, Hwang J, Eliasof S. CRLX101 (formerly IT-101)–A Novel Nanopharmaceutical of Camptothecin in Clinical Development. Curr Bioact Compd. Bentham Science Publishers Ltd; 2011; 7: 8–14. doi: 10.2174/157340711795163866.

115. Li Y, Jin M, Shao S, Huang W, Yang F, Chen W, Zhang S, Xia G, Gao Z. Small-sized polymeric micelles incorporating docetaxel suppress distant metastases in the clinically-relevant 4T1 mouse breast cancer model. BMC Cancer. BioMed Central; 2014; 14: 329. doi: 10.1186/1471-2407-14-329.

116. Johnstone TC, Kulak N, Pridgen EM, Farokhzad OC, Langer R, Lippard SJ. Nanoparticle Encapsulation of Mitaplatin and the Effect Thereof on In Vivo Properties. ACS Nano. 2013; 7: 5675–83. doi: 10.1021/nn401905g.

117. Lee S-M, Ahn RW, Chen F, Fought AJ, O'Halloran T V, Cryns VL, Nguyen ST. Biological Evaluation of pH-Responsive Polymer-Caged Nanobins for Breast Cancer Therapy. ACS Nano. 2010; 4: 4971–8. doi: 10.1021/nn100560p.

118. Deng X, Cao M, Zhang J, Hu K, Yin Z, Zhou Z, Xiao X, Yang Y, Sheng W, Wu Y, Zeng Y. Hyaluronic acid-chitosan nanoparticles for co-delivery of MiR-34a and doxorubicin in therapy against triple negative breast cancer. Biomaterials. 2014; 35: 4333–44. doi: http://dx.doi.org/10.1016/j.biomaterials.2014.02.006.

119. Swaminathan SK, Roger E, Toti U, Niu L, Ohlfest JR, Panyam J. CD133-targeted paclitaxel delivery inhibits local tumor recurrence in a mouse model of breast cancer. J Control Release. 2013; 171: 280–7. doi: http://dx.doi.org/10.1016/j.jconrel.2013.07.014.

120. Zhou W, Zhou Y, Wu J, Liu Z, Zhao H, Liu J, Ding J. Aptamer-nanoparticle bioconjugates enhance intracellular delivery of vinorelbine to breast cancer cells. J Drug Target. Taylor & Francis; 2014; 22: 57–66. doi: 10.3109/1061186X.2013.839683.

121. Kulhari H, Pooja D, Shrivastava S, V.G.M N, Sistla R. Peptide conjugated polymeric nanoparticles as a carrier for targeted delivery of docetaxel. Colloids

Surfaces B Biointerfaces. 2014; 117: 166–73. doi: http://dx.doi.org/10.1016/j.colsurfb.2014.02.026.

122. Milane L, Duan Z, Amiji M. Therapeutic Efficacy and Safety of Paclitaxel/Lonidamine Loaded EGFR-Targeted Nanoparticles for the Treatment of Multi-Drug Resistant Cancer. Fatouros D, editor. PLoS One. San Francisco, USA: Public Library of Science; 2011; 6: e24075. doi: 10.1371/journal.pone.0024075.

123. Milane L, Duan Z, Amiji M. Biodistribution and Pharmacokinetic Analysis of Combination Lonidamine and Paclitaxel Delivery in an Orthotopic Animal Model of Multi-drug Resistant Breast Cancer Using EGFR-Targeted Polymeric Nanoparticles. Nanomedicine. 2011; 7: 435–44. doi: 10.1016/j.nano.2010.12.009.

124. Dreaden EC, Morton SW, Shopsowitz KE, Choi J-H, Deng ZJ, Cho N-J, Hammond PT. Bimodal Tumor-Targeting from Microenvironment Responsive Hyaluronan Layer-by-Layer (LbL) Nanoparticles. ACS Nano. 2014; 8: 8374–82. doi: 10.1021/nn502861t.

125. Huang J, Zhang H, Yu Y, Chen Y, Wang D, Zhang G, Zhou G, Liu J, Sun Z, Sun D, Lu Y, Zhong Y. Biodegradable self-assembled nanoparticles of poly (d,l-lactide-co-glycolide)/hyaluronic acid block copolymers for target delivery of docetaxel to breast cancer. Biomaterials. 2014; 35: 550–66. doi: http://dx.doi.org/10.1016/j.biomaterials.2013.09.089.

126. Geng J, Sun C, Liu J, Liao L-D, Yuan Y, Thakor N, Wang J, Liu B. Biocompatible Conjugated Polymer Nanoparticles for Efficient Photothermal Tumor Therapy. Small. 2015; 11: 1603–10. doi: 10.1002/smll.201402092.

127. Guo J, Hong H, Chen G, Shi S, Zheng Q, Zhang Y, Theuer CP, Barnhart TE, Cai W, Gong S. Image-guided and tumor-targeted drug delivery with radiolabeled unimolecular micelles. Biomaterials. 2013; 34: 8323–32. doi: 10.1016/j.biomaterials.2013.07.085.

128. Liu Z, Chen K, Davis C, Sherlock S, Cao Q, Chen X, Dai H. Drug delivery with carbon nanotubes for in vivo cancer treatment. Cancer Res. 2008; 68: 6652–60. doi: 10.1158/0008-5472.CAN-08-1468.

129. Robinson JT, Welsher K, Tabakman SM, Sherlock SP, Wang H, Luong R, Dai H. High Performance In Vivo Near-IR (>1 μm) Imaging and Photothermal Cancer Therapy with Carbon Nanotubes. Nano Res. 2010; 3: 779–93. doi: 10.1007/s12274-010-0045-1.

130. Liu Z, Tabakman S, Sherlock S, Li X, Chen Z, Jiang K, Fan S, Dai H. Multiplexed Five-Color Molecular Imaging of Cancer Cells and Tumor Tissues with Carbon Nanotube Raman Tags in the Near-Infrared. Nano Res. 2010; 3: 222–33. doi: 10.1007/s12274-010-1025-1.

131. DE LA ZERDA A, ZAVALETA C, KEREN S, VAITHILINGAM S, BODAPATI

S, LIU Z, LEVI J, SMITH BR, MA T-J, ORALKAN O, CHENG Z, CHEN X, DAI H, et al. Carbon nanotubes as photoacoustic molecular imaging agents in living mice. Nat Nanotechnol. 2008; 3: 557–62. doi: 10.1038/nnano.2008.231.

132. Ayala-Orozco C, Urban C, Bishnoi S, Urban A, Charron H, Mitchell T, Shea M, Nanda S, Schiff R, Halas N, Joshi A. Sub-100 nm Gold Nanomatryoshkas Improve Photo-thermal Therapy Efficacy in Large and Highly Aggressive Triple Negative Breast Tumors. J Control Release. 2014; 191: 90–7. doi: 10.1016/j.jconrel.2014.07.038.

133. Wang D, Xu Z, Yu H, Chen X, Feng B, Cui Z, Lin B, Yin Q, Zhang Z, Chen C, Wang J, Zhang W, Li Y. Treatment of metastatic breast cancer by combination of chemotherapy and photothermal ablation using doxorubicin-loaded DNA wrapped gold nanorods. Biomaterials. 2014; 35: 8374–84. doi: http://dx.doi.org/10.1016/j.biomaterials.2014.05.094.

134. You J, Zhang G, Li C. Exceptionally High Payload of Doxorubicin in Hollow Gold Nanospheres for Near-Infrared Light-Triggered Drug Release. ACS Nano. 2010; 4: 1033–41. doi: 10.1021/nn901181c.

135. Bulte JWM, Kraitchman DL. Iron oxide MR contrast agents for molecular and cellular imaging. NMR Biomed. 2004; 17: 484–99. doi: 10.1002/nbm.924.

136. Schultz JF, Bell JD, Goldstein RM, Kuhn JA, McCarty TM. Hepatic Tumor Imaging Using Iron Oxide MRI: Comparison With Computed Tomography, Clinical Impact, and Cost Analysis. Ann Surg Oncol. 1999; 6: 691–8. doi: 10.1007/PL00021736.

137. Harisinghani MG, Barentsz J, Hahn PF, Deserno WM, Tabatabaei S, van de Kaa CH, de la Rosette J, Weissleder R. Noninvasive Detection of Clinically Occult Lymph-Node Metastases in Prostate Cancer. N Engl J Med. Massachusetts Medical Society; 2003; 348: 2491–9. doi: 10.1056/NEJMoa022749.

138. McCarthy JR, Weissleder R. Multifunctional magnetic nanoparticles for targeted imaging and therapy. Adv Drug Deliv Rev. 2008; 60: 1241–51. doi: 10.1016/j.addr.2008.03.014.

139. Medarova Z, Rashkovetsky L, Pantazopoulos P, Moore A. Multi-Parametric Monitoring of Tumor Response to Chemotherapy by Non-Invasive Imaging. Cancer Res. 2009; 69: 1182–9. doi: 10.1158/0008-5472.CAN-08-2001.

140. Yang L, Cao Z, Sajja HK, Mao H, Wang L, Geng H, Xu H, Jiang T, Wood WC, Nie S, Wang YA. Development of Receptor Targeted Magnetic Iron Oxide Nanoparticles for Efficient Drug Delivery and Tumor Imaging. J Biomed Nanotechnol. 2008; 4: 439–49. doi: 10.1166/jbn.2008.007.

141. Wang L, Zhong X, Qian W, Huang J, Cao Z, Yu Q, Lipowska M, Lin R, Wang A, Yang L, Mao H. Ultrashort Echo Time (UTE) Imaging of Receptor Targeted

Magnetic Iron Oxide Nanoparticles in Mouse Tumor Models. J Magn Reson Imaging. 2014; 40: 1071–81.

142. He Y, Zhang L, Zhu D, Song C. Design of multifunctional magnetic iron oxide nanoparticles/mitoxantrone-loaded liposomes for both magnetic resonance imaging and targeted cancer therapy. Int J Nanomedicine. Dove Medical Press; 2014; 9: 4055–66. doi: 10.2147/IJN.S61880.

143. Xi L, Zhou G, Gao N, Yang L, Gonzalo DA, Hughes SJ, Jiang H. Photoacoustic and Fluorescence Image-Guided Surgery Using a Multifunctional Targeted Nanoprobe. Ann Surg Oncol. 2014; 21: 1602–9. doi: 10.1245/s10434-014-3541-9.

144. Cao Z, Lee G, Wang YA, Sajja HK, Wang L, Long R, Barwick BG, Leyland-Jones B, Wood WC, Nie S, Mao H, Yang L. Abstract 5482: Theranostic nanoparticles for targeted therapy of triple negative breast cancer and for monitoring therapeutic response by MRI. Cancer Res [Internet]. 2014; 70: 5482 LP-5482. Available from http://cancerres.aacrjournals.org/content/70/8_Supplement/5482.abstract

145. Guo P, Huang J, Wang L, Jia D, Yang J, Dillon DA, Zurakowski D, Mao H, Moses MA, Auguste DT. ICAM-1 as a molecular target for triple negative breast cancer. Proc Natl Acad Sci U S A. National Academy of Sciences; 2014; 111: 14710–5. doi: 10.1073/pnas.1408556111.

146. Perou CM, Sùrlie T, Eisen MB, Rijn M Van De, Jeffrey SS, Rees CA, Pollack JR, Ross DT, Johnsen H, Akslen LA, Fluge I, Pergamenschikov A, Williams C, et al. Molecular portraits of human breast tumours. 2000; 533: 747–52.

147. Banerjee, Sanjeev, Reis-Filho JS, Ashley S, Steele D, Ashworth A, Lakhani SR SI. Basal-like breast carcinomas: clinical outcome and response to chemotherapy. J Clin Pathol. 2006; : 729–36. doi: 10.1136/jcp.2005.033043.

148. Dent R, Trudeau M, Pritchard KI, Dent R, Trudeau M, Pritchard KI, Hanna WM, Kahn HK, Sawka CA, Lickley LA, Rawlinson E, Sun P, Narod SA. Triple-Negative Breast Cancer : Clinical Features and Patterns of Recurrence. Clin Cancer Res. 2007; 13: 4429–34. doi: 10.1158/1078-0432.CCR-06-3045.

149. Lehmann BDB, Bauer J a J, Chen X, Sanders ME, Chakravarthy a B, Shyr Y, Pietenpol J a. Identification of human triple-negative breast cancer subtypes and preclinical models for selection of targeted therapies. J Clin Invest [Internet]. 2011; 121: 2750–67. doi: 10.1172/JCI45014DS1.

150. Lehmann BD, Pietenpol JA. Clinical implications of molecular heterogeneity in triple negative breast cancer. The Breast [Internet]. Elsevier Ltd; 2015; 24: S36–40. doi: 10.1016/j.breast.2015.07.009.

151. Balko JM, Giltnane JM, Wang K, Schwarz LJ, Young CD, Cook RS, Owens P, Sanders ME, Kuba MG, Sánchez V, Kurupi R, Moore PD, Pinto JA, et al.

Molecular Profi ling of the Residual Disease of Triple-Negative Breast Cancers after Neoadjuvant Chemotherapy Identifi es Actionable Therapeutic Targets. 2014; . doi: 10.1158/2159-8290.CD-13-0286.

152. Lehmann BD, Pietenpol JA. Identification and use of biomarkers in treatment strategies for triple-negative breast cancer subtypes. 2014; : 142–50. doi: 10.1002/path.4280.

153. Tang L, Han X. The urokinase plasminogen activator system in breast cancer invasion and metastasis. Biomed Pharmacother [Internet]. 2013; 67: 179–82. doi: https://doi.org/10.1016/j.biopha.2012.10.003.

154. Pyke C, Grsem N, Ralfkiaer E, Brunner N, Dane K. Receptor for Urokinase Is Present in T \ imor-associated Breast Carcinoma1 Macrophages in Ductal. 1993; : 1911–6.

155. Sidenius N, Blasi F. The urokinase plasminogen activator system in cancer: Recent advances and implication for prognosis and therapy. Cancer Metastasis Rev [Internet]. 2003; 22: 205–22. doi: 10.1023/A:1023099415940.

156. Huber MC, Mall R, Braselmann H, Feuchtinger A, Molatore S, Lindner K, Walch A, Gross E, Schmitt M, Falkenberg N, Aubele M. uPAR enhances malignant potential of triple-negative breast cancer by directly interacting with uPA and IGF1R. BMC Cancer. BMC Cancer; 2016; 16: 615. doi: 10.1186/s12885-016-2663-9.

157. Jo M, Eastman BM, Webb DL, Stoletov K, Klemke R, Gonias SL. Cell Signaling by Urokinase-type Plasminogen Activator Receptor Induces Stem Cell – like Properties in Breast Cancer Cells. 2010; 70: 8948–59. doi: 10.1158/0008-5472.CAN-10-1936.

158. Foekens JA, Peters HA, Look MP, Portengen H, Schmitt M, Kramer MD, Ja F, Gelder MEM, Henzen-logmans SC, Putten WLJ Van, Klijn JGM. The Urokinase System of Plasminogen Activation and Prognosis in 2780 Breast Cancer Patients 1. J Cancer Res. 2000; : 636–43.

159. Gelder MEM, Look MP, Peters HA, Schmitt M, Bru N, Harbeck N, Klijn JGM, Foekens JA. Urokinase-Type Plasminogen Activator System in Breast Cancer : Association with Tamoxifen Therapy in Recurrent Disease. 2004; : 4563–8.

160. Hao W, Friedman A. Serum uPAR as Biomarker in Breast Cancer Recurrence : A Mathematical Model. PLoS One. 2016; 11: e0153508. doi: 10.1371/journal.pone.0153508.

161. Lebeau AM, Sevillano N, King ML, Duriseti S, Murphy ST, Charles S, Murphy LL, Vanbrocklin HF. T h e r a n o s t i c s Imaging the Urokinase Plasminongen Activator Receptor in Preclinical Breast Cancer Models of Acquired Drug Resistance. 2014; 4. doi: 10.7150/thno.7323.

162. Jingmei Zhang, Zhirong Yang, Pengfei Li, Grant Bledsoe, Lee Chao and JC. Kallistatin anatagonizes Wnt//β-catenin signaling and cancer cell motility via binding to low-density lipoprotein receptor-related protein6. Mol Cell Biochem. 2013; 379: 295–301. doi: 10.1038/jid.2014.371.

163. Kawaguchi T, Foster BA, Young J, Takabe K, Foster BA. Current Update of Patient-Derived Xenograft Model for Translational Breast Cancer Research. Journal of Mammary Gland Biology and Neoplasia; 2017; : 131–9. doi: 10.1007/s10911-017-9378-7.

164. Yu WW, Falkner JC, Yavuz CT, Colvin VL. Synthesis of monodisperse iron oxide nanocrystals by thermal decomposition of iron carboxylate salts. Chem Commun [Internet]. The Royal Society of Chemistry; 2004; : 2306–7. doi: 10.1039/B409601K.

165. Gao X, Cui Y, Levenson RM, Chung LWK, Nie S. In vivo cancer targeting and imaging with semiconductor quantum dots. Nat Biotech [Internet]. Nature Publishing Group; 2004; 22: 969–76. Available from http://dx.doi.org/10.1038/nbt994

166. Dobrolecki LE, Airhart SD, Alferez DG, Aparicio S, Behbod F, Bentires-alj M, Brisken C, Bult CJ, Cai S, Clarke RB, Dowst H, Ellis MJ, Meric-bernstam F, et al. Patient-derived xenograft (PDX) models in basic and translational breast cancer research. Cancer Metastasis Rev [Internet]. Cancer and Metastasis Reviews; 2016; : 547–73. doi: 10.1007/s10555-016-9653-x.

167. Gerlinger M, Rowan AJ, Sc B, Horswell S, Math M, Larkin J, Ph D, Endesfelder D, Math D, Gronroos E, Ph D, Martinez P, Ph D. Europe PMC Funders Group Intratumor Heterogeneity and Branched Evolution Revealed by Multiregion Sequencing. 2016; 366: 883–92. doi: 10.1056/NEJMoa1113205.Intratumor.

168. Torre LA, Bray F, Siegel RL, Ferlay J, Lortet-Tieulent J, Jemal A. Global cancer statistics, 2012. CA Cancer J Clin [Internet]. 2015 [cited 2017 Oct 3]; 65: 87–108. doi: 10.3322/caac.21262.

169. Symmans WF, Peintinger F, Hatzis C, Rajan R, Kuerer H, Valero V, Assad L, Poniecka A, Hennessy B, Green M, Buzdar AU, Singletary SE, Hortobagyi GN, et al. Measurement of residual breast cancer burden to predict survival after neoadjuvant chemotherapy. J Clin Oncol. 2007; 25: 4414–22. doi: 10.1200/JCO.2007.10.6823.

170. Davison Z, Blacquière GE De, Westley BR, May FEB. Insulin-like Growth Factor – Dependent Proliferation and Survival of Triple-Negative Breast Cancer Cells : Implications for Therapy 1. Neoplasia. 2011; 13: 504–15. doi: 10.1593/neo.101590.

171. Zeng X, Huang H, Tamai K, Zhang X, Harada Y, Yokota C, Almeida K, Wang J, Doble B, Woodgett J, Wynshaw-boris A, Hsieh J, He X. Initiation of Wnt

signaling : control of Wnt coreceptor Lrp6 phosphorylation / activation via frizzled , dishevelled and axin functions. Development. 2008; 375: 367–75. doi: 10.1242/dev.013540.

172. Bahrami A, Amerizadeh F, Shahidsales S, Khazaei M, Ghayour-mobarhan M, Sadeghnia HR, Maftouh M, Hassanian SM, Avan A. Therapeutic Potential of Targeting Wnt/B-Catenin Pathway in Treatment of Colorectal Cancer: Rational and Progress. J Cell Biochem. 2017; 118: 1979–83. doi: 10.1002/jcb.25903.

173. Blagodatski A, Poteryaev D, Katanaev VL. Targeting the Wnt pathways for therapies. Mol Cell Ther. 2014; 2: 28. doi: 10.1186/2052-8426-2-28.

174. Liu C-C, Prior J, Piwnica-Worms D, Bu G. LRP6 overexpression defines a class of breast cancer subtype and is a target for therapy. Proc Natl Acad Sci U S A. 2010; 107: 5136–41. doi: 10.1073/pnas.0911220107.

175. Tung EKK, Wong BYC, Yau TO, Ng IOL. Upregulation of the Wnt co-receptor LRP6 promotes hepatocarcinogenesis and enhances cell invasion. PLoS One. 2012; 7: 1–10. doi: 10.1371/journal.pone.0036565.

176. Lin C, Lu W, Zhai L, Bethea T, Berry K, Qu Z, Waud WR, Li Y. Mesd is a general inhibitor of different Wnt ligands in Wnt/LRP signaling and inhibits PC-3 tumor growth in vivo. FEBS Lett. 2011; 585: 3120–5. doi: 10.1016/j.febslet.2011.08.046.

177. DiMeo TA, Anderson K, Phadke P, Feng C, Perou CM, Naber S, Kuperwasser C. A novel lung metastasis signature links Wnt signaling with cancer cell self-renewal and epithelial-mesenchymal transition in basal-like breast cancer. Cancer Res. 2009; 69: 5364–73. doi: 10.1158/0008-5472.CAN-08-4135.

178. Lu W, Lin C, King TD, Chen H, Reynolds RC, Li Y. Silibinin inhibits Wnt/β-catenin signaling by suppressing Wnt co-receptor LRP6 expression in human prostate and breast cancer cells. Cell Signal. 2012; 24: 2291–6. doi: 10.1016/j.cellsig.2012.07.009.

179. Zhang X, Hao J. Development of anticancer agents targeting the Wnt/β-catenin signaling. Am J Cancer Res. 2015; 5: 2344–60.

180. Jo M, Eastman BM, Webb DL, Stoletov K, Klemke R, Gonias SL. Cell Signaling by Urokinase-type Plasminogen Activator Receptor Induces Stem Cell–like Properties in Breast Cancer Cells. Cancer Res. 2011; 70: 8948–58. doi: 10.1158/0008-5472.CAN-10-1936.Cell.

181. Asuthkar S, Gondi CS, Nalla AK, Velpula KK, Gorantla B, Rao JS. Urokinase-type plasminogen activator receptor (uPAR)-mediated regulation of WNT/β-catenin signaling is enhanced in irradiated medulloblastoma cells. J Biol Chem. 2012; 287: 20576–89. doi: 10.1074/jbc.M112.348888.

182. Mann B, Gelos M, Siedow A, Hanski ML, Gratchev A, Bodmer WF, Moyer MP, Riecken EO, Buhr HJ, Hanski AC. Target genes of β-catenin–T cell-factor/lymphoid-enhancer-factor signaling in human colorectal carcinomas. Med Sci. 1999; 96: 1603–8. doi: 10.1073/pnas.96.4.1603.

183. Bafico A, Liu GZ, Yaniv A, Gazit A, Aaronson SA. Novel mechanism of Wnt signalling inhibition mediated by Dickkopf-1 interaction with LRP6/Arrow. Nat Cell Biol. 2001; 3: 683–6. doi: 10.1038/35083081.

184. Mao B, Wu W, Davidson G, Marhold J, Li M, Mechler BM, Delius H, Hoppe D, Stannek P, Walter C, Glinka A, Niehrs C. Kremen proteins are Dickkopf receptors that regulate Wnt / b -catenin signalling. Nat Lett. 2002; 417: 6–9.

185. Jiang N, Huang J, Edwards LJ, Liu B, Zhang Y, Beal CD, Evavold BD, Zhu C. Two-Stage Cooperative T Cell Receptor-Peptide Major Histocompatibility Complex-CD8 Trimolecular Interactions Amplify Antigen Discrimination. Immunity [Internet]. 2011; 34: 13–23. doi: 10.1016/j.immuni.2010.12.017.

186. Wend P, Runke S, Wend K, Anchondo B, Yesayan M, Jardon M, Hardie N, Loddenkemper C, Ulasov I, Lesniak MS, Wolsky R, Bentolila LA, Grant SG, et al. WNT10B / β-catenin signalling induces HMGA2 and proliferation in metastatic triple-negative breast cancer. EMBO Mol Med. 2013; 5: 264–79. doi: 10.1002/emmm.201201320.

187. Bourhis E, Wang W, Tam C, Hwang J, Zhang Y, Spittler D, Huang OW, Gong Y, Estevez A, Zilberleyb I, Rouge L, Chiu C, Wu Y, et al. Wnt antagonists bind through a short peptide to the first β-propeller domain of LRP5/6. Structure. Elsevier Ltd; 2011; 19: 1433–42. doi: 10.1016/j.str.2011.07.005.

188. Zhang Y. I-TASSER server for protein 3D structure prediction. BMC Bioinformatics. 2008; 9: 40. doi: 10.1186/1471-2105-9-40.

189. Roy A, Kucukural A, Zhang Y. I-TASSER : a unified platform for automated protein structure and function prediction. Nat Protoc. 2010; 5: 725–38. doi: 10.1038/nprot.2010.5.

190. Yang L, Cao Z, Sajja HK, Mao H, Wang L, Geng H, Xu H, Jiang T, Wood WC, Nie S, Wang YA. Development of Receptor Targeted Magnetic Iron Oxide Nanoparticles for Efficient Drug Delivery and Tumor Imaging. J Biomed Nanotechnol. 2008; 4: 439–49. doi: 10.1166/jbn.2008.007.Development.

191. Iozzi S, Remelli R, Lelli B, Diamanti D, Pileri S, Bracci L, Roncarati R, Caricasole A, Bernocco S. Functional Characterization of a Small-Molecule Inhibitor of the DKK1-LRP6 Interaction. ISRN Mol Biol. 2012; 2012: 1–9. doi: 10.5402/2012/823875.

192. Mbalaviele G, Dunstan CR, Sasaki A, Williams PJ, Mundy GR, Yoneda T. E-Cadherin Expression in Human Breast Cancer Cells Suppresses the Development

of Osteolytic Bone Metastases in an Experimental Metastasis Model. Cancer Res. 1996; 56: 4063–70.

193. Khramtsov AI, Khramtsova GF, Tretiakova M, Huo D, Olopade OI, Goss KH. Wnt/β-Catenin Pathway Activation Is Enriched in Basal-Like Breast Cancers and Predicts Poor Outcome. Am J Pathol [Internet]. 2010; 176: 2911–20. doi: 10.2353/ajpath.2010.091125.

194. Vishnoi M, Peddibhotla S, Yin W, T Scamardo A, George GC, Hong DS, Marchetti D. The isolation and characterization of CTC subsets related to breast cancer dormancy. Sci Rep. Nature Publishing Group; 2015; 5: 17533. doi: 10.1038/srep17533.

195. Shima H, Yamada A, Ishikawa T, Endo I. Are breast cancer stem cells the key to resolving clinical issues in breast cancer therapy? Gland Surg. 2017; 6: 82–8. doi: 10.21037/gs.2016.08.03.

196. Xu H, Tian Y, Yuan X, Liu Y, Wu H, Liu Q, Wu GS, Wu K. Enrichment of CD44 in basal-type breast cancer correlates with EMT , cancer stem cell gene profile , and prognosis. Onco Targets Ther. 2016; 9: 431–44.

197. Lester RD, Jo M, Montel V, Takimoto S, Gonias SL. uPAR induces epithelial–mesenchymal transition in hypoxic breast cancer cells. J Cell Biol. 2007; 178: 425–36. doi: 10.1083/jcb.200701092.

198. Yook JI, Li X, Ota I, Hu C, Kim HS, Kim NH, Cha SY, Ryu JK, Choi YJ, Kim J, Fearon ER, Weiss SJ. A Wnt – Axin2 – GSK3 β cascade regulates Snail1 activity in breast cancer cells. Nat Cell Biol. 2006; 8: 1398–406. doi: 10.1038/ncb1508.

199. Cano A, Pérez-moreno MA, Rodrigo I, Locascio A, Blanco MJ, Barrio MG, Portillo F, Nieto MA. The transcription factor Snail controls epithelial – mesenchymal transitions by repressing E-cadherin expression. Nat Cell Biol. 2000; 2: 76–83.

200. Batlle E, Sancho E, Francí C, Domínguez D, Monfar M, Baulida J, Herreros AG De. The transcription factor Snail is a repressor of E-cadherin gene expression in epithelial tumour cells. Nat Cell Biol. 2000; 2: 84–9.

201. Lin S-Y, Xia W, Wang JC, Kwong KY, Spohn B, Wen Y, Pestell RG, Hung M-C. β-Catenin, a novel prognostic marker for breast cancer: Its roles in cyclin D1 expression and cancer progression. Proc Natl Acad Sci [Internet]. 2000; 97: 4262–6. Available from http://www.pnas.org/content/97/8/4262.abstract

202. Lamb R, Ablett MP, Spence K, Landberg G, Sims AH, Clarke RB. Wnt Pathway Activity in Breast Cancer Sub-Types and Stem-Like Cells. PLoS One [Internet]. Public Library of Science; 2013; 8: e67811. Available from https://doi.org/10.1371/journal.pone.0067811

203. Ponnusamy L, Mahalingaiah PKS, Singh KP. Treatment schedule and estrogen receptor-status influence acquisition of doxorubicin resistance in breast cancer cells. Eur J Pharm Sci [Internet]. 2017; 104: 424–33. doi: https://doi.org/10.1016/j.ejps.2017.04.020.

204. Wang Z, Tacchelly-Benites O, Yang E, Thorne CA, Nojima H, Lee E, Ahmed Y. Wnt/Wingless Pathway Activation Is Promoted by a Critical Threshold of Axin Maintained by the Tumor Suppressor APC and the ADP-Ribose Polymerase Tankyrase. Genetics [Internet]. 2016; 203: 269 LP-281. Available from http://www.genetics.org/content/203/1/269.abstract

205. Lee E, Salic A, Krüger R, Heinrich R, Kirschner MW. The Roles of APC and Axin Derived from Experimental and Theoretical Analysis of the Wnt Pathway. PLOS Biol [Internet]. Public Library of Science; 2003; 1: e10. Available from https://doi.org/10.1371/journal.pbio.0000010

206. Zhang Y, Morris JP, Yan W, Schofield HK, Gurney A, Simeone DM, Millar SE, Hoey T, Hebrok M, Pasca di Magliano M. Canonical Wnt Signaling Is Required for Pancreatic Carcinogenesis. Cancer Res [Internet]. 2013; 73: 4909 LP-4922. Available from http://cancerres.aacrjournals.org/content/73/15/4909.abstract

207. Zhan T, Rindtorff N, Boutros M. Wnt signaling in cancer [Internet]. Oncogene. The Author(s); 2017. p. 1461–73. Available from http://dx.doi.org/10.1038/onc.2016.304

208. Yardy GW, Brewster SF. Wnt signalling and prostate cancer. Prostate Cancer Prostatic Dis [Internet]. 2005; 8: 119–26. Available from http://dx.doi.org/10.1038/sj.pcan.4500794

209. Arend RC, Londoño-Joshi AI, Straughn JM, Buchsbaum DJ. The Wnt/β-catenin pathway in ovarian cancer: A review. Gynecol Oncol [Internet]. 2013 [cited 2017 Aug 10]; 131: 772–9. doi: 10.1016/j.ygyno.2013.09.034.

210. Dass K, Ahmad A, Azmi AS, Sarkar SH, Sarkar FH. Evolving role of uPA/uPAR system in human cancers. Cancer Treat Rev [Internet]. 2008 [cited 2017 Aug 10]; 34: 122–36. doi: 10.1016/j.ctrv.2007.10.005.

211. Zhou H, Qian W, Uckun FM, Wang L, Wang YA, Chen H, Kooby D, Yu Q, Lipowska M, Staley CA, Mao H, Yang L. IGF1 Receptor Targeted Theranostic Nanoparticles for Targeted and Image- Guided Therapy of Pancreatic Cancer. 2015; : 7976–91. doi: 10.1021/acsnano.5b01288.